COMPUTATIONAL EVOLUTION OF FLOW CHARACTERSTICS AND EROSION WEAR OF PIPELINE AND BEND

A Thesis Report Submitted
in partial fulfillment of the requirements for
the award of degree of

MASTER OF ENGINEERING
IN
PRODUCTION AND INDUSTRIAL ENGINEERING

Submitted by

Mani Kanwar Singh
Roll No.: 800982011

Under the Guidance of

Mr. Satish Kumar
Department of Mechanical Engineering
Thapar University, Patiala.

Dr. Dwarika Nath Ratha
Department of Civil Engineering
Thapar University, Patiala.

DEPARTMENT OF MECHANICAL ENGINEERING
THAPAR UNIVERSITY
PATIALA-147004, INDIA.

June 2011

DECLARATION

I hereby declare that the work which is being presented in the dissertation work entitled, **"COMPUTATIONAL EVOLUTION OF FLOW CHARACTERSTICS AND EROSION WEAR OF PIPELINE AND BEND"**, in partial fulfillment of the requirements for the award of degree of Master of Engineering in Mechanical Engineering with specialization in **PRODUCTION & INDUSTRIAL ENGINEERING** submitted in Mechanical Engineering Department of Thapar University, Patiala, is an authentic record of my own work carried out under the supervision of **Dr. Dwarika Nath Ratha and Mr. Satish Kumar** refers other researcher's works which are duly listed in the reference section.

The matter presented in this thesis has not been submitted for the award of any other degree of this or any other university.

Date: - 8/7/11
Place: - Patiala

(MANI KANWAR SINGH)

.....

This is to certify that the above statement made by the candidate is correct and true to the best of my knowledge.

Supervisor:

Mr. Satish Kumar
Assistant Professor
Mechanical Engineering Department
Thapar University, Patiala

Dr .Dwarika Nath Ratha
Assistant Professor
Civil Engineering Department
Thapar University, Patiala

Dr. Ajay Batish
Professor & Head
Mechanical Engineering Department
Thapar University, Patiala

Dr. S.K Mohapatra
Dean of Academic Affairs
Thapar University, Patiala

ACKNOWLEDGEMENTS

Words are often less to revels one's deep regards. With an understanding that work like this can never be the outcome of a single person, I take this opportunity to express my profound sense of gratitude and respect to all those who helped me through the duration of this work.

This work would not have been possible without the encouragement and able guidance of supervisor Mr. Satish Kumar and Dr. Dwarika Nath Ratha. Their enthusiasm and optimism made this experience both rewarding and enjoyable. Most of the novel ideas and solutions in this work are the result of our numerous stimulating discussions. Their feedback and editorial comments were also invaluable for the writing of this thesis. I am grateful to Dr. Maneek Kumar, Head of Department of Civil Engineering Department for providing me the facilities in the Department for the completion of my work.

I take pride of myself being son of ideal parents for their everlasting desire, sacrifice, affectionate blessings, and help, without which it would not have been possible for me to complete my studies.

I am also very grateful to my all friends and colleague (Dalbir Singh Dhindsa and Randeep Singh Grewal) for accompanying me during the most outstanding year of my life and standing by me in every situation.

I would like to thank to all the faculty members and employees of Mechanical Engineering Department, Thapar Univeristy, Patiala for their everlasting support.

Last but not least, I would like to thank God for all good deeds.

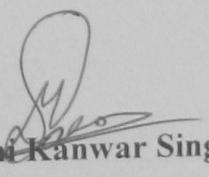

(Mani Kanwar Singh)

ABSTRACT

Transportation through slurry pipeline bend is a complex process and it involves the optimization of pressure drop & erosion wear. The bottom ash for the present investigation was collected from the Guru Gobind Singh thermal power plant, Ropar. Physical properties like specific gravity, particle size distribution (PSD), pH value & static settling characteristics of bottom ash are determined by various bench scale tests Rheological behaviour of bottom ash is measured by using rheometer. The flow characteristics of the pipe bend evaluated experimentally and numerically by using the computational dynamic code FLUET 6.3.

Modeling of slurry pipeline is performed with the help of CFD code GAMBIT. The pressure drop in pipeline with 90^0 bend calculated with water and at different concentrations of bottom ash 10% and 20% using CFD code FLUENT6.3. The result indicates that the pressure is more on the outer side of the curvature as compared to the inner side of the bend. This can be attributed to the change in the rheological characteristics of the slurries with efflux concentration, and the density and viscosity of the slurries also increase with increase in the efflux concentration. The pressure drop across the bend at a given flow velocity increases with increasing slurry concentrations of bottom ash. At higher concentration, there is significant increase in pressure drop even at low velocities, which could be attributed to increase in viscosity of the slurry.

CONTENTS

LIST OF FIGURES

LIST OF TABLES

ABBREVATIONS

CFD	Computational Fluid Dynamics
DSRW	Dry sand rubber wheel
PSD	Particle size distribution
SVR	Support vector regression
SVR-GA	Support vector regression and genetic algorithm technique
rpm	Revolution per minute

NOMENCLATURE AND SYMBOLS

Symbol	Description
cP	centipoises
t	Time, seconds
T	Temperature, °C
%	Percentage
°C	Degree Celsius
mm	Millimeter
µm	Micro meter
H_2SO_4	Sulphuric acid
W_b	Weight of beaker
W_{bs}	Weight of beaker and solid
W_{bw}	Weight of beaker and water
W_{bsw}	Weight of beaker, solid and water

CHAPTER 1

INTRODUCTION

Slurry pipelines are used in many industrial applications to transport solid materials with the help of water or any other carrier fluid. These pipelines are used in thermal power plants for disposal of waste materials like bottom ash, tailings materials etc. to the disposal sites. Slurry pipeline is most reliable and safe mode of solid transportation because of its low maintenance, low traffic congestion, air and noise pollution and its eco-friendly nature. Slurry pipelines are more energy efficient at appropriate operating conditions.

1.1 SLURRY

The mixture of solids and liquids is known as slurry. The physical characteristics of slurry are dependent on many factors such as particle size and distribution, solid concentration in the liquid phase, turbulence level, temperature, conduit size, and viscosity of the carrier. Slurry is a mixture of a solid particles and fluid held in suspension. Water is the most commonly used fluid. Theoretically, for laminar to a turbulent flow a single-phase liquid of low absolute (or dynamic) viscosity can be allowed to flow at slow speeds. However, slurry which is two-phase mixture must overcome a deposition critical velocity or a viscous transition critical velocity. The speed of slurry flow is sufficiently high to maintain the particles in suspension. The mixture resists the flow in highly viscous mixtures because of excessively low shear rate in the pipeline.

1.1.1 Types of Slurry Flows

There are two types of slurry flows:

i. Homogeneous flow
ii. Heterogeneous flow

Homogeneous Flows

The solids are uniformly distributed in the liquid carrier in homogeneous flow. The Particle size is less than 60-100μm. For example copper concentrate slurry after undergoing a process of grinding and thickening. Drilling mud, sewage sludge, and fine limestone behave as homogeneous flows.

Figure 1.1: Homogeneous mixture

Heterogeneous flows

The solids are not uniformly mixed in the horizontal plane in heterogeneous flow. The Particle size is greater than 100μm. Heavier particles settle down at the bottom and lighter particles float in suspension in heterogeneous flow. This forms the Sliding bed in the pipe. Heterogeneous slurries are encountered in many places like mining and dredging applications. Minimum carrier velocity is required for heterogeneous flow.

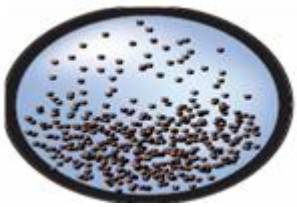

Figure 1.2: Heterogeneous mixture, partly stratified

1.1.2 Basic slurry transportation system

Slurry Pipelines are used for the transportation of solids either pneumatically and hydraulically. The basic different between the two systems is the nature of fluid used for transportation of solid particles. The slurry pipeline is the most important part in hydraulic transportation system.

Solid material is first mixed with carrier fluid before the transportation. For different solid materials the design of pipeline system is different and the design of pipeline system depends upon the solid material to be transported. The layout of system remains the same for all materials.

Slurry pipeline transportation system is divided into three sub-systems:

i. Preparation of slurry.
ii. Pipeline and centrifugal pumps.
iii. End facility.

Preparation of slurry

In this stage solid materials are crushed to appropriate size by using crusher and grinders for easy and economical transportation of material. Solids are mixed with carrier fluid to get the optimum value of concentration. The slurry is than stored in storage tank provided with an agitator. Chemical treatment is done during the storage to control the corrosion before pumping the slurry.

Pipeline and centrifugal pumps

The pumping requirements are determined by the effective distance of transportation. This requirement is provided at one or more points along with length of pipeline. Intermediate pumping require some other facilities like intermediate storage and quality control at lesser extent than starting point.

End Facility

Slurry is received in storage tanks at the utilization point. Slurry is then filtered, dewatered and dried according to the requirements. For hydraulic transportation special processing is not required for some cases where solids are required to be processed in wet form. Therefore additional cost dewatering and drying are avoided in hydraulic transportation system.

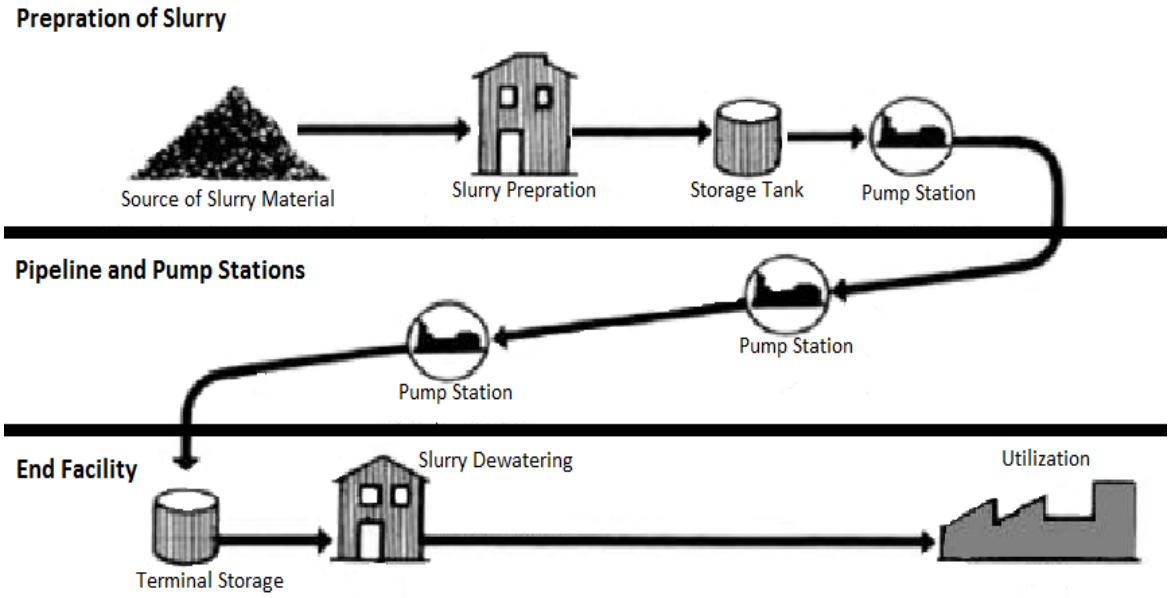

Figure 1.3: Basic Slurry Transportation System

1.1.3 Advantageous features of slurry pipeline in transportation

i. Operating cost decreases as the volume of transportation and distance increases.
ii. Pipeline transportation is highly efficient and reliable.
iii. Simple in installation and space requirement for installation is less.
iv. Low manpower is required for operation and maintenance.
v. Reduces the storage cost and assures continuous supply.
vi. Reduces the air pollution and noise pollution.
vii. Minimizes the ecological and environmental disturbances.
viii. Easy to operate and can be readily automated.
ix. Pipeline transportation is extremely safe and easily passes the roads, rivers and railways etc.

Besides above advantages there are some limitations in slurry pipeline transportation system

i. High initial capital investment in installation.
ii. Pipeline transportation requires water or any other carrier fluid which is easily available.
iii. Pipeline transportation is only beneficial for slurry transportation whereas rail and roads are multipurpose.

The advantageous features of slurry pipeline transportation system provides the future scope for transporting minerals from sea beds and mountains, this increases the need of data required for designing the slurry pipeline transportation system, so that the system is made reliable and more realistic.

1.2 PIPELINE

Pipeline is a long tubular conduit or series of pipes, often ground with pumps and valves for flow control, used to transport crude oil, natural gas, water, etc especially over great distances or it is also defined as a route, channel or process along which something passes.

1.2.1 Different types of losses in pipeline

Losses due to the local disturbances of the flow in the conduits such as changes in cross-section, projecting gaskets, elbows, valves and similar items are called minor losses. So, minor losses can be defined as the losses that occur in pipelines due to bends, elbows, joints, valves, etc. In case of a very long pipe, these losses are usually insignificant in comparison to the fluid friction in the length considered.

1.2.1.1 Head loss at entrance

The entrance loss is caused primarily by the turbulence created by the enlargement of the stream after it passes through the section of vena contraction, which is formed immediately after the edge of the entering mouth. Values of the entrance loss coefficients have been determined experimentally. If the entrance to the pipe is well rounded, then there is no contraction of the stream entering and the coefficient of loss is correspondingly small.

The loss of head at the entrance is given by:

$$h_e = k_e V^2/2g$$

Where, v = mean velocity of the pipe, k_e = loss coefficient whose value depends on the condition at the entrance of the pipe.

For a square edged entrance, as shown in fig.1.4 k_e has a value of around 0.5. Reentrant tube produces maximum contraction of the entering stream because streamlines come from around the wall of the pipe as well as directly from fluid in front of the entrance. The loss coefficients for reentrant tubes vary depending upon thickness of pipe wall and how far pipe is projected, for very thin tubes k_e

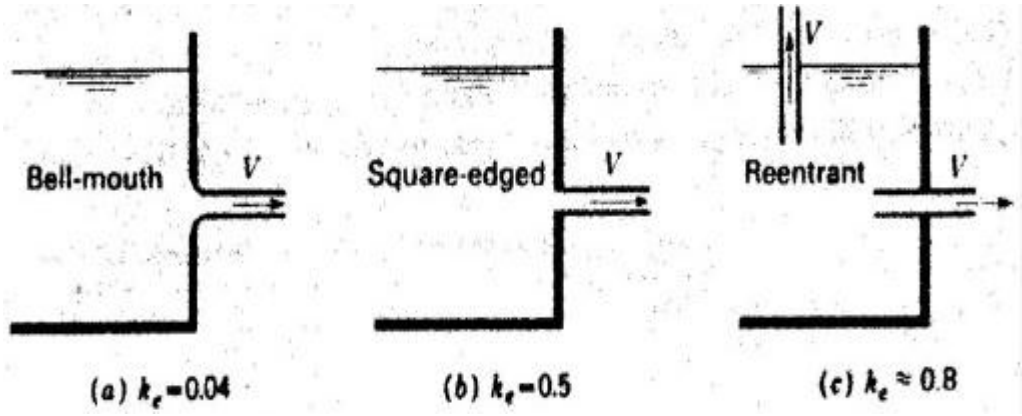

Figure 1.4: Entrance loss coefficient

1.2.1.2 Loss of head due to gradual contraction

Losses due to the abrupt changes in cross section area of the pipe can be reduced by means of smoothly curved transition. With smoothly curved transition a loss coefficient Kc is as small as 0.05 is possible. For conical reducters a minimum kc of about 0.10 is obtained with a total cone angle of 20 to 40 degrees. Larger cone angle results in higher value of Kc.

1.2.1.3 Loss of head at submerged discharge

When a fluid with a velocity V is discharged from the end of a pipe into a closed tank which is so large that the velocity within it is negligible, the entire kinetic energy is dissipated. Hence the discharge loss is

$$h'_d = V^2/2g$$

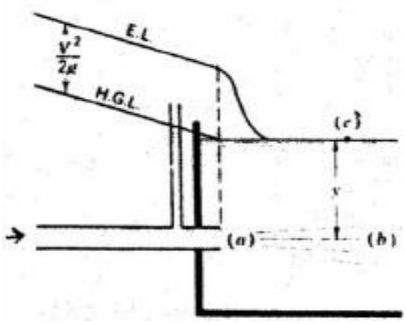

Figure 1.5: Submerged discharge loss

The discharge loss coefficient is 1.0 under all conditions. Only way to reduce this loss is to reduce the value of V by means of diverging tube as in the case of draft tube in reaction turbine. As contrasted with entrance loss, it must be noted that discharge loss occurs after the fluid leaves the pipe, while entrance loss occurs after fluid enters the pipe.

1.2.1.4 Loss of head due to sudden contraction

There is a drop in pressure due to the increase in velocity and loss of energy in turbulence. The loss of head for sudden contraction is given by

$$h_e = k_e V_2^2/2g$$

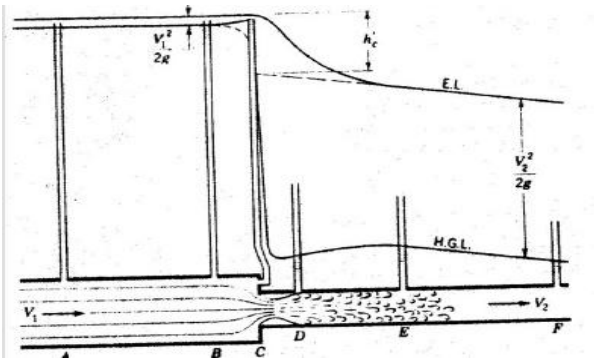

Figure 1.6: Loss due to sudden contraction

1.2.1.5 Loss due to sudden expansion

The loss due to sudden expansion is greater than the loss due to a corresponding contraction. This is because diverging paths of the flow tend to encourage the formation of eddies with the flow. Moreover, separation of the flow from the wall of the pipe induces pockets of eddying turbulence outside the flow region. In converging glow there is a dampening effect on eddy formation and the conversion from pressure energy to kinetic energy is quite efficient. The head loss due to suddent enlargement is given by

$$h'_x = (V_1 - V_2)^2/2g$$

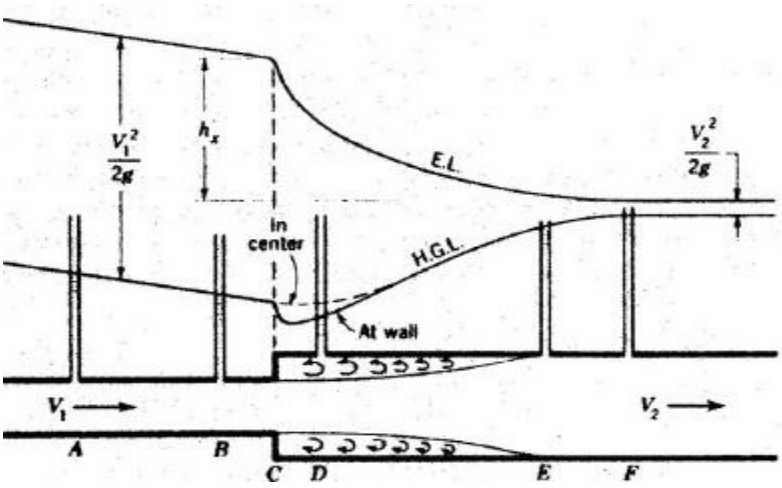

Figure 1.7: Loss due to sudden expansion

1.2.1.6 Loss in pipe fitting

The loss of head in pipe fittings may be expressed as

$$h = kV^2/2g$$

where, V is the velocity of water in a pipe of nominal size of the fitting.

1.2.1.7 Loss due to gradual expansion

Loss due to sudden expansion accompanying a reduction is velocity can be reduced by using diffuser. The loss of head is the function of the angle of divergence and the ratio of two areas. The length of the diffuser is determined by these two variables.

The loss due to a gradual enlargement is expressed as:

$$h' = k' (V_1 - V_2)^2/2g$$

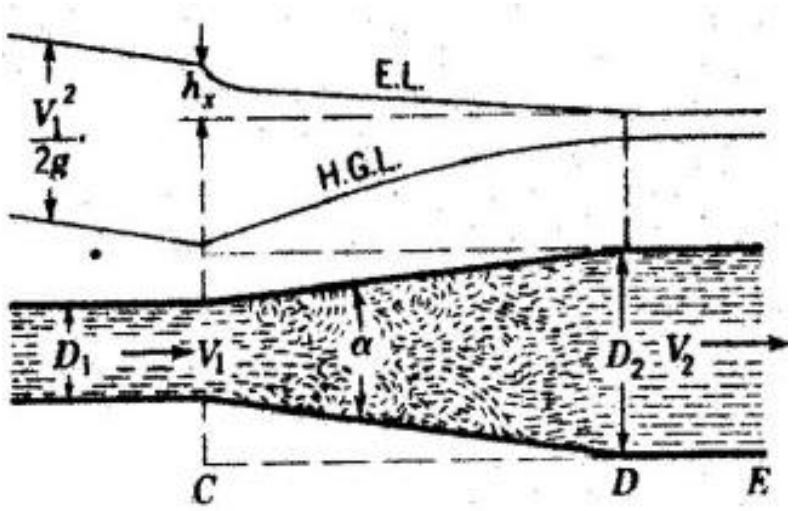

Figure 1.8: Loss due to gradual enlargement

1.2.1.8 Loss in bends and elbows

In flow around a bend or elbow, because of centrifugal effects, there is an increase in pressure along the outer wall and decrease in pressure along the inner wall. The centrifugal force on the particle near the center of the pipe, where the velocities are high, is larger than the centrifugal force on the particles near the walls of the pipe, where the velocities are low and because of this unbalanced condition a secondary flow develops as show in fig 1.9. This combines with the axial velocity for form a double spiral flow which persists for some distance.

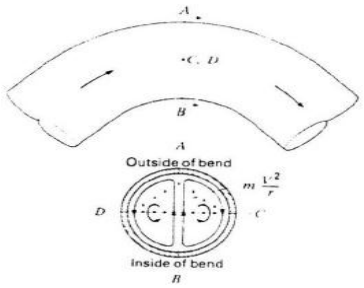

Figure 1.9: Secondary flow in bend

The head loss produced by bend ($h_b = k_b(V_1 - V_2)^2/2g$) is dependent upon the ratio of the radius of the curvature r to the diameter of the pipe D. For rough pipes k_b depends on both r/D and e/D. Bend loss is not proportional to the angle of bend; for 22.5 and 45 degree bends the losses are respectively about 40 and 80% of loss in a 90 degree bend.

1.3 WEAR

Wear is defined as the progressive volume loss of material from target surface. Due to erosion or corrosion, there may be progressive degradation of materials with time leading to failure of material. The wear due to erosion can be prevented by controlling the affecting parameters whereas the wear due to corrosion is caused by chemical reactions, which can be minimized by adopting suitable measures.

1.3.1 Types of wear

1.3.1.1 Corrosive wear

When a sliding surface is in a corrosive environment it causes corrosive wear, and the sliding action continuously removes the protective corrosion layer, and thus it exposed the fresh surface to further corrosive attack. Corrosive wear occurs due to chemical reaction on a wearing surface and main reactions occur between metal and oxygen. These oxides are wiped away with the flow and cause pitting of the surfaces. Corrosion is quicken as impacted surfaces are exposed to slurry chemistry.

1.3.1.2 Erosive wear

Erosive wear is the dominant process which can be defined as the removal of material from a solid surface. It is due to mechanical interaction between the surface and the impinging particles in a liquid stream. In Erosion process there is a transfer of kinetic energy to the surface. With the increase in kinetic energy of the particles impacting at the target surface, it leads to increase the material loss due to erosion. It depends on the predominant impact angle of particle impingement with the material surface and it will vary from 0 to 90 degrees. Impact angle depend on both fluid particle and particle- particle interaction. This type of wear can be found in slurry pumps, angled pipe bends, turbines, pipes and pipe fitting etc.

Types of erosion wear

Particle impingement is the major type of erosion wear in a slurry pipeline. Particles impacting directly onto a surface can generate very high specific contact pressures. As the particles with sharp edges having smaller contact area and higher stresses, so they wear the surface faster. By a process of ploughing and cutting, material is removed.

i. Cutting Erosion

If the particles are very sharp it causes cutting erosion and a micromachining action occurs when particles interacted with the material surface. Minimal plastic deformation of the surface region occurs in slurry pipeline because of two mechanisms namely, corrosion and erosion. These mechanisms are quite different in various manners.

Corrosion of metal is an electro-chemical phenomenon and this occurs in a slurry pipelines due to presence of dissolved oxygen in the slurry. This phenomenon can be controlled by passivating either the cathodic or the anodic reactions of the pipe wall. Corrosion rate can be reduced by the elimination of dissolved oxygen and the adjustment of slurry pH.

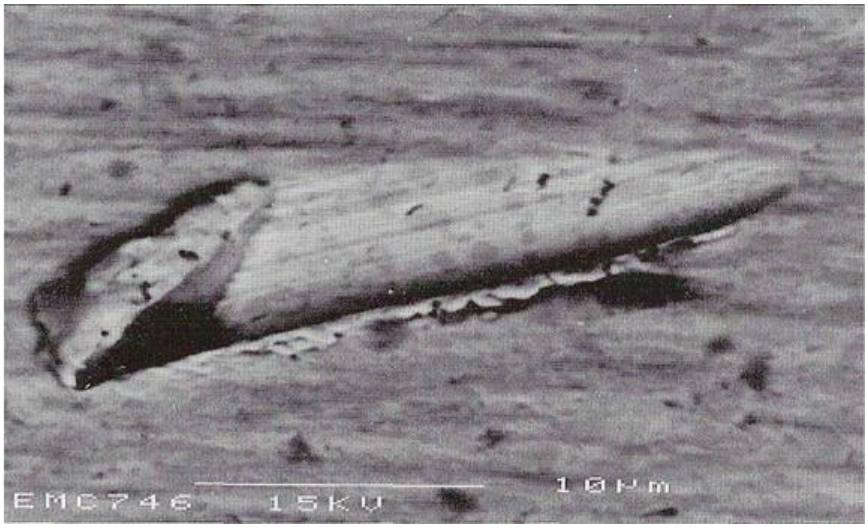

Figure 1.10: Cutting Erosion

Erosion of metals is more noticeable than corrosion in many slurry pipeline systems and it occurs due to dynamic action of the moving materials on the pipe wall. Erosion usually takes place through two mechanisms, namely "cutting wear" (sliding) and "deformation wear" (impact). A cutting wear (sliding) on the pipe surface is due to the oblique impact of the particles and the high kinetic energy of the impinging particles causes deformation wear (impact). The cutting wear dominates the overall wear in horizontal pipelines, whereas deformation wear is more significant in case of pipe bends, pumps etc. By the type of particle movement like sliding, and rolling along the pipe surface, erosion wear pattern get influenced. Hence, it is quite difficult to fore cast which form of erosion (sliding or impact) will be dominant for any given situation.

ii. Ploughing erosion

Ploughing Erosion is a two stage process involving localized plastic deformation of the surface from rounded particle impacts. In first stage process, particle impacts form surface craters with plastic flow of the surface occurring around the particle edges during impact. As a result of the particle collision, an extruded shear lip is formed. The second stage process involves repeated particle impacts causing fatigue of the extruded shear lip regions. The shear lips fail and are broken off.

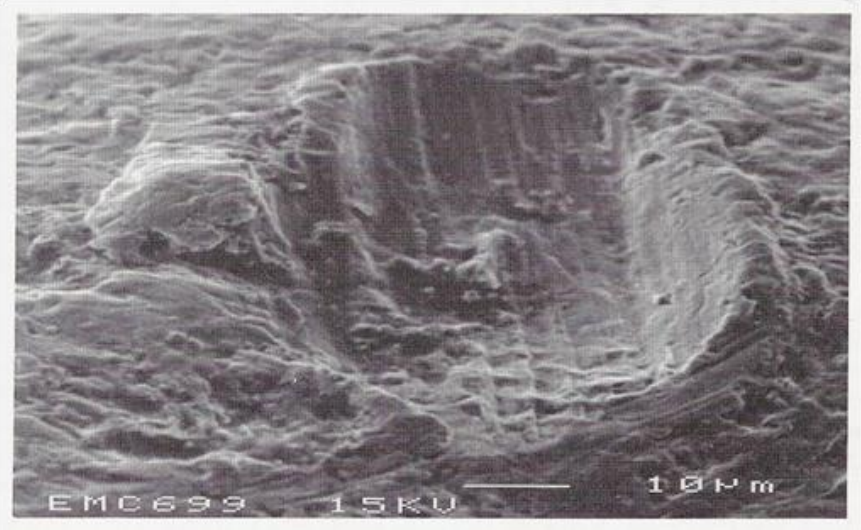

Figure 1.11: Ploughing Erosion

1.3.2 Parameters affecting erosion wear:

Erosion wear is a complex phenomenon and controlled experiments are required to identify the important parameters that affected the erosion wear. Those prominent parameters are as under:

Impact angle

Impact angle is the angle between the target surface and the direction striking velocity of the solid particle. Erosion wear with the impact angle can be varied and it depends on the characteristics of the target surface material i.e. brittle or ductile type.

Velocity of solid particles

Erosion wear can be strongly affected by velocity of solid particle. If the particle velocity increases there will be a significant increase in erosion rate. The erosion rate is related to the particle velocity by power law relationship in which the power index for velocity varies in the range of 2-4.

Hardness

Hardness is expressed as its resistance to permanent deformation and it is the characteristic of a solid material. Erosion wear mechanism is greatly affected by both surface hardness as well as hardness of solid particles. The ratio of hardness of target material to the hardness of solid particles is termed as hardness ratio.

Particle size and shape

Erosion wear can be affected by two main parameters i.e. Particle size and shape. From the various investigations it is found that solid particle size is important to erosion. With increase in particle size, erosion wear increased according to the power law relationship. Due to the difficulties in defining the different shape features, the effect of particle shape on the erosion is not very well established. Generally, roundness factor is taken into consideration and if roundness factor is having a lower values then it show the particle angularity but if roundness factor is one then the particles are perfectly spheres.

Effect of particle shape on wear

As particle shape is one of the most important variables in the erosion wear process so sharp particles erode at a much faster rate than rounded particles because of the high contact stresses at the point of impact. If rounded particles are significantly larger than the inter carbide spacing then the rounded particles are not able to erode between the carbides and the resulting wear rate is much more affected by the volume of carbides present than for sharp particles.

Solid concentration

Concentration is defined as the amount of solid particles by volume or by weight in the fluid. The concentration of slurries can vary from 2% to 50% depending upon the type of slurry. More particles will strike the surface of the impeller which increases the erosion rate by increasing the particle concentration. However, at very high concentrations the striking velocity of particle on the surface decreases and particle-particle interaction increases.

CHAPTER 2

LITERATURE REVIEW

Pipeline transportation of solids has been established as an attractive and reliable mode of transportation over the conventional modes of transportation. For better understanding of the flow characteristics of these pipelines, investigators have been analyzing the flow both experimentally and numerically. This chapter gives an insight into the present state of knowledge about the flow characteristics in these pipelines by exploring the available literature.

2.1.1 PRESSURE DROP STUDIES IN SOLID LIQUID FLOW THROUGH PIPELINE

Ahmad et al. (1994) have concluded that the presence of the particles reduces the additional pressure drop across the bends, an effect which they have attributed to the suppression of turbulence and secondary flow in bends. They measured the pressure drop across a 90^o bend in a horizontal plane using two multi-sized particulate slurries namely iron ore slurries and zinc tailings. The pressure measurements are made just across the bend.

Gupta et al. (1994) confirms the findings of Ahmad by carried the extensive measurements for pressure drop and concentration distribution in a 55mm ID 90^o horizontal bend having a radius ratio of 5.5. He also concluded that the additional pressure drop increases with solid concentration but is always less than that for clear water flows.

Panda et al. (1996) have reported that the pressure loss could be measured reasonably well using pressure loss models developed for Newtonian fluids in the range of 20-25% concentration by weight. They have also established the pressure loss in horizontal pipes for transportation of fly ash up to 60% concentration (by weight) by correlating it with the rheological behaviour of the slurry.

Mishra et al. (1998) have reported the pressure drop across the two diverging converging bends having an area ratio of 1.5 and 2.0 up to middle plane with inner curvature same as commercial bend using zinc tailing slurry and there 90^o bends in horizontal plane namely 90^o mild steel commercially available pipe bend (100mm NB diameter having a radius ratio of 4). They also observed the higher pressure drop for diverging-converging bends compared to the conventional

bends, but the extent of increase of pressure drop for bend with area ratio 2.0 over the conventional bend was only marginal.

Kaushal et al. (2002) have modified the Wasp model for calculating the pressure drop for homogeneous and suspended portions by modifying the particle diffusivity of the slurry flow based on the solid concentration in the range of 10 to 40% (by weight). The pressure drop thus predicted agreed reasonably well with the experimental data for straight pipe and 2-D channel for zinc tailing slurries.

Kaushal and Tomita (2002) studied the vertical concentration profiles for six particle sizes ranging from 38 to 739 μm for multisized particulate zinc tailings slurry flowing through 105 mm diameter pipe. Experiments were conducted at three flow velocities of 2, 2.75 and 3.5 m/s using five efflux concentrations ranging from 4% to 26% by volume for each velocity. Karabelas (1977) model for prediction of solids concentration profiles has been modified and then compared with experimental data which shows good agreement. Experimental data for pressure drop were collected for multisized zinc tailings slurry flowing through 105 mm diameter pipe at five efflux concentrations ranging from 4% to 26% using eight flow velocities in the range from 1.2 to 4.0 m/s for each efflux concentration. Wasp et al. (1977) model for pressure drop prediction has also been modified and then compared with experimental data which also shows good agreement.

Lei L et al (2002) studied the pipeline transportation of dense fly ash –water slurry. Rheological characteristics and sedimentation stability of the slurry were measured with the addition of four kinds of stabilizing additives. The relationship between flow rate and pressure drop has been estimated for the transportation of slurry by using thixotropy model. A feasibility study of new transport system was also performed.

Kaushal and Tomita (2003) concluded that solids concentration profiles were found to be a function of particle size, velocity of flow and efflux concentration of slurry. However, these solids concentration varied with the vertical position, except for particle size of 38 μm. It was also observed that pressure drop at different Reynolds number, due to the flow of slurry through rectangular duct having 200 mm x 50 mm cross-section was always less than that for the circular

pipe having diameter of 105 mm. Decrease in pressure drop, in case of rectangular duct reduces with increase in efflux concentration.

Kaushal et al. (2005) conducted the experiments in 54.9 mm diameter horizontal pipe on two sizes of glass beads of which mean diameter and geometric standard deviation are 440 μm & 1.2 and 125 μm & 1.15, respectively, and a mixture of the two sizes in equal fraction by mass. Flow velocity was up to 5 m/s and overall concentration up to 50% by volume for each velocity. Pressure drop and concentration profiles were obtained traversing isokinetic sampling probes in the horizontal, 45º inclined and vertical planes including the pipe axis. Slurry samples of the mixture collected in the vertical plane were analyzed for concentration profiles of each particle batch constituting the mixture. It was found that the pressure drop is decreased for the mixture at high concentrations except 5 m/s and a distinct change of concentration profiles was observed for 440 μm particles indicating a sliding bed regime, while the profiles in the horizontal plane remains almost constant irrespective of flow velocity, overall concentration and slurry type.

Kaushal and Tomita (2006) concluded that γ-ray densitometer and sampling probe give quite similar concentration profiles except for few cases of coarser (440 μm) particles at lower flow velocities. In case of 125 μm size particles, pressure gradients for equivalent fluid were almost the same to water data up to overall concentration of 40% due to no slip between particles and liquid phase, however for 50%; it has larger values at all flow velocities due to sudden increase in viscous sublayer thickness. For 440 μm size particles, pressure gradients for the equivalent fluid were found larger at lower velocities to accelerate the particles at the bottom of the pipe line and smaller at higher velocities due to the near-wall lift effect and thus have favorable implications for pipeline economics in transport of coarser particles at higher concentrations and flow velocities. It is observed that near-wall lift decreases with increase in flow velocity; however, the effect of slip velocity on pressure drop is greater at lower flow velocities and less at higher flow velocities than near-wall lift of coarser particles in slurry pipeline.

Cartigny et al. (2007) concluded that the pressure difference over a bend is dependent of the flow regime. It was observed that within the pseudo-homogeneous flow regime the mixture behaves like a single-phase flow. The hydraulic loss in this pseudo-homogeneous flow regime can be described by the loss coefficient model. It was also concluded that the asymmetric

velocity and concentration profile of the heterogeneous and stratified flow regime give rise to a single helical flow inside the bend. The two major processes to predict the total hydraulic loss are, first the flow separation and secondly the change of hydraulic gradient in the swirling flow section after the bend and by the combination of these to it is used to determine the overall pressure drop.

Knezevic et al. (2008) presents the influence of ash concentration on change of flow and pressure in slurry transportation. The results indicate that the transport should be accomplished with ash and bottom ash concentration below 50% but above 40% of solids. In this concentration range there is decrease of both flow (per volume) and pressure. However this decrease is considerably small regarding quantity of fly and bottom ash transported during the time limit.

Lahiri and Ghanta (2008) describe a robust support vector regression (SVR) methodology, which can offer superior performance for important process engineering problems. The method incorporates hybrid support vector regression and genetic algorithm technique (SVR-GA) for efficient tuning of SVR meta-parameters. A comparison with selected correlations in the literature showed that the developed SVR correlation noticeably improved the prediction of pressure drop over a wide range of operating conditions, physical properties, and pipe diameters. The proposed hybrid technique (SVR-GA) also relieves the non-expert users to choose the meta-parameters of SVR algorithm for his case study and find out optimum value of these meta-parameters on its own. The results indicate that SVR based technique with the GA based parameters tuning approach which can be advantageously employed for a large class of regression problems encountered in process engineering.

2.2 EXPERIMENTAL EVOLUTION OF EROSION WEAR IN SOLID LIQUID FLOW THROUGH PIPELINE

Ni (1996) experimentally evaluated the effect of high delivered volumetric concentration (c_{vd}) on characteristics of slurry. They performed extensive experiments by using three sorts of narrowly graded sands tested in the laboratory of DN150 mm pump loop of the Delft University of technology for the observation of pump and pipeline characteristics. They concluded that high solid concentration has a strong influence on the pump head, efficiency and power consumption

and this influence behaves differently with different sand size. When c_{vd} becomes 42% then the pump efficiency in coarse sand slurry service may drop almost 60% as compared to that of water service. Within the measured range of concentrations in each passages may experience similar stratification process occurred in pipelines. The mechanical friction regime in the impeller passages could be similar to that in pipelines. Therefore the delivered volumetric concentration and the size affect the head loss in the same way both in pumps and pipelines.

Clark et al. (2001) have distinguished between the erosion resistance of different steels (AISI 1045 and AISI 1020) by using coriolis erosion tester. This tester provides a low-angle scouring action that simulates the erosive conditions encountered in oil sands and tailings pipeline transport. Coriolis erosion tester operated at 5000 rpm. The slurry contains 10% silica sand particles by weight in tap water and silica sand density is 2650 kg/m^3. They also observed that the erosion resistance of AISI 1045 steel pipe was more than five times of AISI 1020 steel pipe and also obtained that steel of homogeneous microstructure gives best performance in both erosion and abrasion. They also made the comparison between the performance of the materials in the ASTM G65 dry sand rubber wheel (DSRW) sliding abrasion test and slurry erosion data.

Clark et al. (2002) has studied the effect of Particle velocity and particle size in slurry erosion. The various factors which affect the slurry erosion such are concentration of particles, particle impact speed, particle impact angle, particle size, particle density, hardness, nature of suspending liquid, nature of slurry flow (esp. local turbulence), nature of material. The loss of material must be measured by changes in surface profile rather than mass loss.

Ghanta et al. (2002) suggested two different solids namely coal and copper ore having different surface characteristics. They observed that coarse size coal-in-water slurries exhibit lower viscosities compared to fine size coal-in-water slurries, whereas due to its opposite surface characteristics, copper or coal behaves in a reverse way. The results have also shown that PSD has market influence on viscosity of suspension. For coal water system 60:40 weight proportion gave maximum reduction and for copper ore-water system 40:60 gave maximum reduction. From this it reveals that mixing fines particles with coarse slurry could reduce the viscosity of the suspension.

Heywood et al. (2002) has described three alternative methods for highly viscous, often non-Newtonian slurries to reduce pipe friction. In addition to frequent economic advantages to be had by employing one of these methods, other benefits also accrue. These include lower wear rates and reduced instances of pipe blockages and therefore maintenance costs for pumps. These methods also increase the flexibility of existing pipeline systems when there is a requirement to increase slurry concentrations, and therefore slurry viscosities. Each of these three methods is considered whenever an existing pipeline needs upgrading, or a new pipeline system is to be designed.

Korving et al. (2002) had done an experimental study on pipeline flow of fine sand slurry at various densities up to 1800 kg/$m^{3.}$ From this it has shown that the fine sand slurries above 1700 kg/m^3 density behave quite differently at high concentrations than for slurries at lower densities. For lower density slurries, the bed formation was observed at about 1.5 m/s velocity even at higher concentration whereas no bed formation was observed even at the lowest velocities tested (<.5m/s^2)for higher densities.

Kumar et al. (2002) have carried out the measurements for concentration profiles in mid-horizontal and mid-vertical planes at 6D, 25D and 50D downstream of a conventional 90^o horizontal circular pipe bend using equi-sized silica sand slurries in a 50 mm NB re-circulating pilot plant test loop having total length of 30m. For the flow to be fully developed (free from the effect of the bend to its downstream side), the re-adjustment length required for the slurry flow through the bend is of the order of 50 diameter from the bend exit as the concentration profile at 50D and thereafter showed no sign of effect of the bend. The concentration profile just downstream of the bend is more uniform in the mid vertical plane as compared to the mid horizontal plane because the effect of bend is more pronounced at the latter.

Rudman et al. (2002) performed extensive experiments to compare the behaviour of non-Newtonian fluids with the behaviour of Newtonian fluids and also to explore the behaviour of non-Newtonian fluids at transition to turbulence or in a weak turbulent pipe flow situation. Operating in the transitional regime may be advantageous for suspension transport with the intermittency of such flows being useful in re-suspending solids that have settled but still operating at lower pressure gradient than fully developed turbulent flow.

Clark et al. (2004) has observed the influence of the squeeze film in slurry erosion. A squeeze film may be of any liquid layer separate the two surfaces and prevents direct impact between wearing surfaces. The slurry pot tester is used for experiments. They also found that if the Reynolds number (i.e. velocity or mass) of the approaching particles is low enough, penetration of the squeeze film on rebound or even approach may not be possible, resulting in particle entrapment at the surface and a change in erosion mechanism. They observed that small particles (less then100 micron) and concentrated slurries were especially liable to behave in this way.

Eskin et al. (2004) explored the possibility of extending the Kolmogoroff's model of multi-scale turbulence structure to dense slurry flows in pipelines. The analysis is based on experimental data of slurry behaviour as a Newtonian liquid with some equivalent density and viscosity. A connection is made between the turbulence structure and the head losses in the pipeline that can be calculated by the known engineering methods. The latter, the total loss, is considered as comprising of viscous and turbulent components, and the turbulent component is associated with the turbulence structure. The lower turbulence scale for the dense slurries is also estimated. A modified application of the known two-layer model of slurry flow is proposed for the simulation of turbulence in stratified flows.

Gandhi et al. (2004) have suggested a methodology to determine the nominal particle size of multi-sized particulate slurry for estimation of mass loss due to the erosion wear. He observed the effect of presence of finer particles in relative to coarse particulate slurry. The size of finer particles is less than 75 micron. He also found that with the addition of particles finer than 75 micron in narrow-size or multi-sized slurries, it reduced the erosion wear. The weighted mass particle size seems to be a better choice for multi-sized particulate slurries whereas the effective particle size for narrow-size particulate slurries can be taken as the mean size. The reductions in erosion wear due to addition of fine particles decreases with increase in the concentration of coarse size particles.

Wood et al. (2004) performed experiments regarding erosion in an experimental setup consisted of an upstream straight section followed by a bend. The radius of curvature of the bend was of 1.2 bore diameters within a 78mm diameter pipe test loop of AISI 304 stainless steel handling water–sand mixture at 10% by volume. The mean velocity was 3 m/s. It shows wear is more at

the outside of the bend as compared to the inside, but also significant wear occurred at the base of the bend. Bend erodes 4.5 times that of the upstream straight pipe for the estimate of erosive wear.

Badr et al. (2005) have investigated the special case of two-phase turbulent flow with low particle concentration. They extensively discussed the problem of erosion in a vertical pipe with sudden contraction. Two mathematical models were used for the determination of fluid flow velocity field and calculation of motion of solid particles and an erosion model was used to predict the erosion rate using flow velocity ranging 1m/s-10m/s and the particle size ranging 10µm-400µm. Using these models shows that both particle size and flow velocity but the effect of flow direction was found to be significant only for large particle size (400lm) and moderate flow velocity (5 m/s).

Das et al. (2006) developed a mathematical model for the mechanisms of erosion to predict erosion rate of coal-fired boiler components at different temperatures. For the fabrication of boiler components various grades of steels were used and published data pertaining to boiler fly ash have been used for the modeling. The model incorporates high temperature tensile properties of the metal surface at room and elevated temperatures and to predict the erosion rates of various grades of steel, it has been implemented in a user-interactive in-house computer code. The model is calibrated with plant and experimental data generated from a high temperature air-jet erosion-testing facility.

Desale et al. (2007) have performed experiments on slurry pot tester to show the effect of slurry erosion under normal impact condition on ductile materials. This shows that wear depends upon hardness of material and hardness of solid particles. The erodent materials used were quartz, alumina, and silicon carbide. The ductile materials like copper, mild steel, brass etc were tested. The velocity of 3m/s and 10 % by weight concentration of 550 micron size particles at normal impact condition for combination of different erodent and materials was used for experiments.

Habib et al. (2007) studied erosion predictions with abrupt contraction of different contraction ratios for the case of two-phase (liquid and solid) turbulent flow with low particle concentration. For the calculations of the fluid velocity field, a mathematical model based on the time-averaged

governing equations of 2-D axi-symmetry turbulent flow was used. Lagrangian particle tracking approach was adopted for particle tracking. Developed the Correlations for total erosion rate in terms of inlet flow velocity and thickness and depth of the protruded pipe were measured and show that the erosion rate is proportional to V^2, to $T^{-0.25}$, and to $H^{-0.2}$. It was proved that erosion rate increased exponentially with the inlet velocity and erosion rate is inversely proportional to both protruded pipe depth and thickness.

Huang et al. (2008) developed a single particle erosion model based on the turbulent flow theory for erosion of material in slurry pipeline flow. This model captures the effects of particle shape, particle size, slurry mean velocity, pipe diameter, fluid viscosity and the properties of target material. The model shows that the erosion rate has a power-law relation with slurry mean velocity, particle size, pipe diameter, fluid viscosity and solid concentration. The erosion rate depends strongly on the slurry mean velocity and weakly on pipe diameter and fluid viscosity. Erosion rate slightly decreases as the pipe diameter increases. The exponent of slurry mean velocity varies in a range of 2–3.575.The model also explains that the effect of particle size on erosion rate depends on the particle shape, flow condition and erosion location on the periphery of a pipe.

Giguere et al. (2009) studied slurry flow regimes in horizontal pipe by using the electric resistance tomography by taking pipe loop of diameter 0.076m and 10m long. Slurry is a mixture of tap water and electric conductive glass beads having concentration 38% with a density of 2500 kg/m^3 and diameter of 100µm and the average velocity of slurry during testing is ranging 0.27–2.15 m/s. By using this technique, they observed the influence of solids concentration and the distance from the bend outlet by determining the transition velocity between homogeneous and heterogeneous slurry flow and transition velocity at the bottom of the pipe. Finally it was concluded that the transition velocities are also influenced by solids concentration at low slurry concentration, while for high concentrated slurry there are weak influenced by solids concentration.

Steward et al. (2009) tested the pipe flow behaviour of fly ash and water mixtures in a closed loop pipe system at solids concentrations ranging from 51% to 74% by mass, in three different pipe sizes, 40, 50 and 65 nominal bore. From this experiment, the

resulting flow behaviour has been presented on pipe flow curves and the laminar flow data which have been used to rheologically characterize the material as viscoplastic, using the Herschel-Bulkley rheological model. Anomalous transitional flow behaviour is reported in that the results appear to fit the Newtonian laminar to turbulent transition model as opposed to the more widely accepted Slatter transition model.

Tian et al. (2009) evaluated erosion wear rate using coriolis erosion pot tester of three high-chromium white iron alloys containing 25%, 30% and 40% of chromium. Three particle size range of silica sand with 10 micron, 148 micron and 660 micron had taken with clean water at varied temperature range of 32 °C and 47.5 ºC and then evaluate the corrosion wear of same material by using silica sand water slurry with addition of sulphuric acid (H_2SO_4,) and sodium chloride (NaCl). It was found that with increase of practical size erosion wear rate also increases and temperature rise play important role with corrosion wear.

2.3 COMPUTATIONAL STUDIES IN SOLID LIQUID FLOW THROUGH PIPELINE

Shah et al. (2007) have performed the experiments to show the effect of slurry flow rate on the erosion of coiled tubing. Erosion rate has been observed as a function of flow rate, slurry concentration, solid particles size and density, and fluid viscosity. This study utilizes both experimental tests and CFD simulations to investigate erosion by fracturing fluids. The fracturing fluid is pumped at high enough rates to overcome the tensile strength of the rock in hydraulic fracturing. The slurry is pumped through 6 cm coiled tubing at rates from 1.43 to 1.91 m^3/min. CFD simulations have been conducted by utilizing erosion prediction and particle tracking modules in a commercial CFD code FLUENT.

Kumar et al. (2008) evaluated experimental data for bend pressure drop were collected from a pilot plant test loop with a pipe diameter of 53 mm. The experiments were performed at three different efflux volumetric concentrations (0%, 3.94% and 8.82%) of 448.5 μm silica sand particles and for each concentration the flow velocity was varied from 1.78 to 3.56 m/s. It was observed that pressure drop along the pipe bend increases with flow velocity and particle concentration. The experimental data has also compared with three dimensional computational

fluid dynamics (CFD) modelling by running the commercial CFD code Fluent, and show good agreement (within a percentage deviation of *6*10%). These results indicate that the velocity and concentration distribution of solids become more uniform downstream, and the pressure at the outer wall is greater than that at the inner wall in the bend.

Lahiri and Ghanta (2008) developed a comprehensive computational fluid dynamics (CFD) model to predict the concentration profile of the solid liquid slurry flow in pipelines. In light of the shortcomings of the existing fluid solid exchange coefficient, an effort was made in the present study to modify the existing models to incorporate the effect of solid concentration at drag co-efficient. The proposed correlation was then incorporated in a two-fluid CFD model (Euler-Euler) along with the standard k-ε turbulence model with mixture properties to simulate the turbulent solid-liquid flow in a pipeline. It was observed that the computational model and results discussed in this work would be useful for extending the applications of CFD models for simulating large slurry pipelines.

Graham et al. (2009) measured the slurry erosion on two different geometries, a pipe elbow and a cylinder in pipe flow by using a coordinate measuring machine. Quantitative erosion measurements were compared with paint modelling, visual observations and CFD erosion modelling. The CMM data showed good agreement with the paint modelling and visual observations for a pipe elbow and a cylinder in pipe flow. Comparison with CFD erosion modelling for the cylinder in pipe flow showed good agreement with the Grant and Tabakoff erosion model considering that the default coefficients for an aluminium/silica sand system were used rather than values obtained experimentally for the exact sand and aluminium alloy used in the experiments. The CMM technique shows significant promise for obtaining quantitative data for comparison with CFD modelling of erosion.

CHAPTER 3

EXPERIMENTAL-SETUP

3.1 EXPERIMENTAION SET-UP FOR EROSION WEAR

3.1.1 Description of testing apparatus

The test rig consists of a centrifugal pump, conical tank, nozzle, specimen holder, valves and flow meter. Electric motor of 7.5 HP is used to drive Centrifugal pump has a capacity of max pressure 13.5 bar at a discharge of 240 L/min. Slurry available in conical tank as can be seen in Fig. 3.2, is sucked through a 100mm GI pipe with help of pump and delivered to the nozzle through 25 mm pipe having control valves and electromagnetic flow meter located upstream. Slurry is re-circulated during test. The main valve and bypass regulator valve between delivery side and nozzle is used to control the flow rate of the slurry. The rectangular tapered tank having 650×650 mm at top which converges to 100×100 mm at the bottom through a length of 700mm was used to store the slurry. A mesh is provided in the bottom of the tank to avoid the object from falling into the tank and get struck inside the pipeline.

Slurry flowing through the pump at high pressure is converted into high velocity stream while passing through the converging section of the 125mm long nozzle having diameter of 8 mm. the standoff distance between the nozzle and specimen can be varied from 25mm to 90mm. After striking the specimen slurry falls back into the tank. The electronic magnetic flow meter (Elmag-200M) arranged in between control valves and nozzle is equipped with digital display and contains PTEF coated liner through which the slurry flows and discharge is calculated, when a conductive fluid passes through magnetic field (applied) a voltage is induced in an electrically conductive body which is proportional to the mean flow velocity according to Faraday's law of induction.

3.1.2 Working of Jet Erosion Tester

In jet erosion testing a high velocity jet strikes a flat specimen at some adjustable angle. The amount of material removed is determined by the weight loss. The material which accumulates

on the specimen surface interferes with the incoming particle. The weight loss of the specimen corresponds to the average erosion over the surface.

Jet erosion tester investigate the effect of different parameters particularly the impact angle. A jet of solid–liquid mixture strikes the specimen fixed in a fixture, which can be changed at any angle with respect to the former. The pump supplies water at high pressure and the solid particles are being sucked through an injector. The slurry is mixed in the mixing chamber before the jet comes out through a nozzle

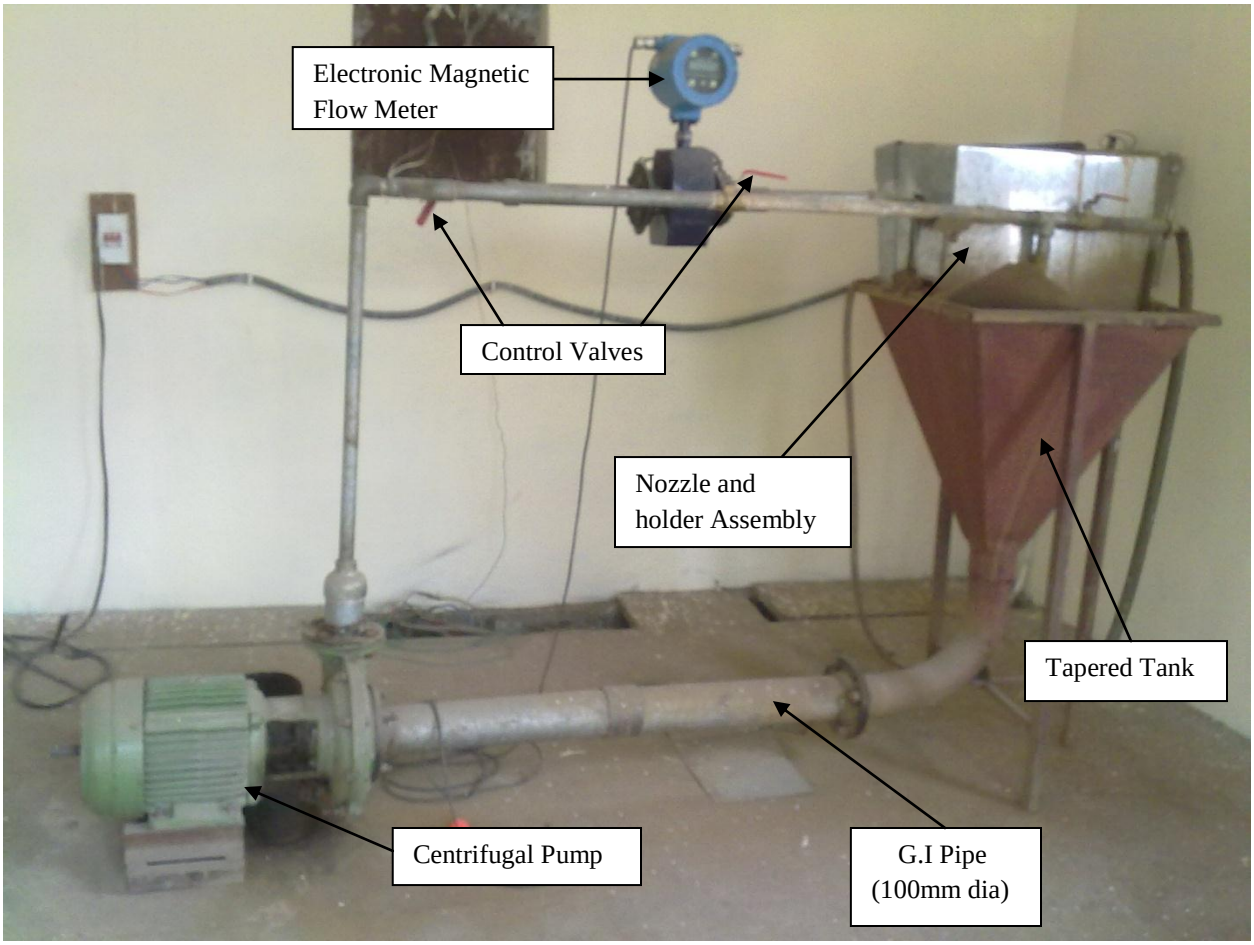

Figure3.1: Jet Erosion Tester

3.2 EXPERIMENTATION SET-UP FOR PRESSURE DROP

3.2.1 Description of Experimental Setup

The test setup consists of overhead tank, horizontal pipe bend with eight pressure tapings, exit valve and measuring tank. Overhead tank is connected to pipeline from the bottom. The horizontal pipe bend lying in the horizontal plane is connected to this pipeline. An over flow pipe is provided in overhead tank to maintain constant head. The horizontal pipe bend is 56mm diameter pipe having inlet side pipe length of 680 mm bend at 90 degree with radius of curvature is 390 mm and outlet side pipe length 650 mm. Pressure taping are provided on the inner and outer radii of the pipe bend at a given fixed distance from the inlet of horizontal pipe bend. All the pressure tapings are connected to piezometers which are fitted on a board having measuring scales for measurements. An exit valve is provided at the outlet of horizontal pipe bend for regulating the flow in the pipe bend. Measuring tank 915×395 mm is provided for measurement of discharge through pipe. Measuring tank is also fitted with piezometer to measure the level.

Pressure tapings	Distance from inlet
Pressure taping 1	690 mm
Pressure taping 2	770 mm
Pressure taping 3	820 mm
Pressure taping 4	870 mm
Pressure taping 5	960 mm
Pressure taping 6	990 mm
Pressure taping 7	1020 mm
Pressure taping 8	1050 mm

Plan Area of Measuring Tank, a = 915 X 395 mm

Diameter of Pipe = 56 mm

Cross-sectional Area of Pipe = 2461.76 mm^2

3.2.2 Working of Experimental Setup

Supply valve is open to fill the overhead tank, if there is any overflow it will discharge through the overflow valve. The exit valve is fully closed to remove the air bubbles. Than exit valve is partially open and supply valve is adjusted so that the water level in overhead tank is constant. Now the measurements are taken from the piezometer tubes connected to the pressure tapings provided on the inner and outer radii of the bend. After taking piezometer readings discharge is measured from the measuring tank by taking measurement from the piezometer fitted on tank for given time interval.

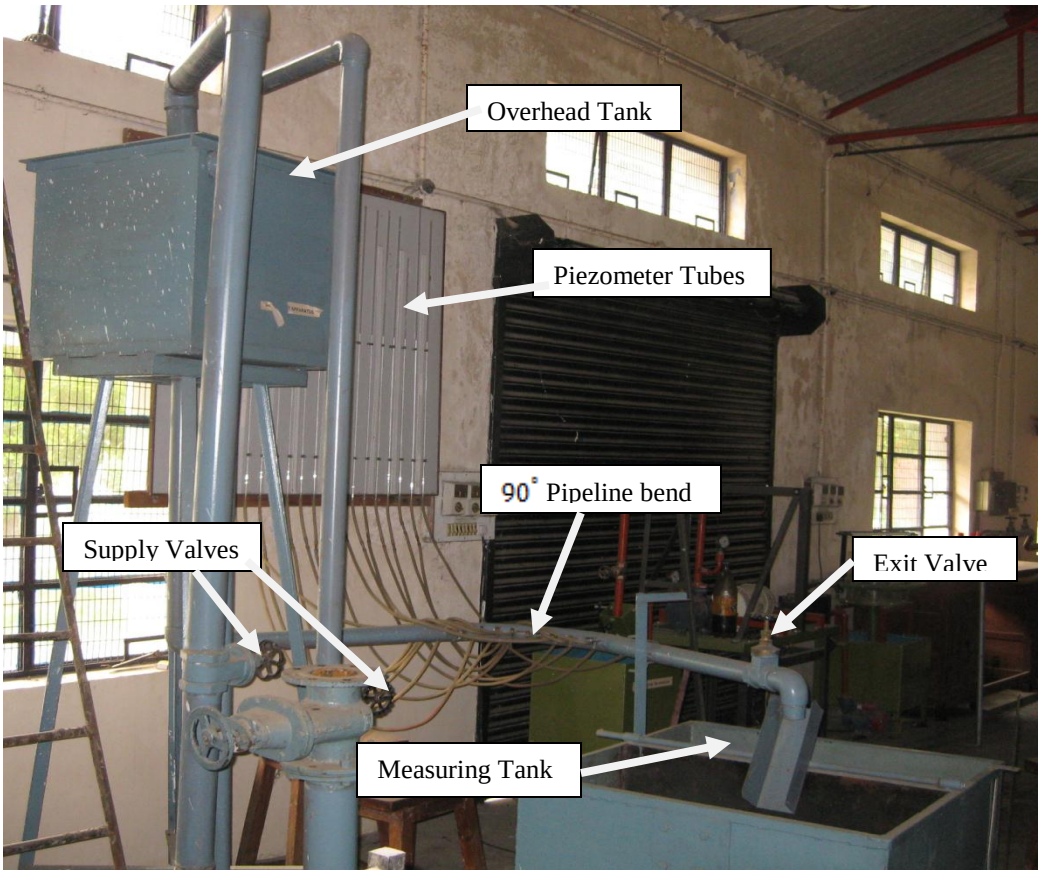

Figure3.2: Pipe Bend experimental setup

CHAPTER 4

PROPERTIES OF BOTTOM ASH

4.1 BENCH SCALE TEST

The material required for testing purpose was collected from Guru Govind Singh thermal power plant, Ropar, Punjab. Various bench scale tests were carried out on ash collected to determine the specific gravity, particle size distribution (PSD) of the solid materials. The pH value & static settling characteristics of bottom ash was determined in the laboratory at IIT Roorkee. A brief description of these tests is presented here.

4.1.1 Particle Size Distribution

The variation in the size of the particles in the solid sample and the percentage of particles present in different pre-selected size ranges are determined to establish the particle size distribution (PSD). Two methods namely sieve analysis and hydrometer analysis, can be employed to get this distribution. In the present study a known weight of sample of solid particles is taken and washed over a B.S. 200 mesh (75 mm). Particulate materials are dried in an oven. The dried material is sieved through a set of standard sieves. Special care is taken to ensure that the sample is properly dried. The sample retained on each sieve is collected and the percentage retained on each sieve is calculated using the standard procedure.

4.1.2. Specific gravity

In the present study, the specific gravity of solid particles is determined using fixed volume bottle. In this method first take 50 ml fix volume bottle and clean it thoroughly, keep it in the oven in order to remove moisture from bottle. After 2 hours, take out the bottle from an oven and allow it to cool down, and then take the weight of bottle (W_b). After weight put some solids (over dried) about 30 grams in it and weight it again and note down this weight (W_{bs}). After this slowly pour water (distilled) in the bottle so that no air is entrapped in it and shake it well, and keep on pouring the water. Shake it well each time till all the solid get wet. Fill $3/4^{th}$ of bottle with water and put the thumb on the mouth of the bottle and shake it well for 5 minutes. Keep it for at least 2 Hours, so that air bubbles get out from the bottle. Then fill the bottle of water and

cork it. Clean it with cloth/tissue paper and weight it. Note down the weight (W_{bsw}). Now remove the solids from the bottle and clean it, Thoroughly, Dry it and fill it with distilled water. Note down the weight (W_{bw}). Calculate the specific gravity of solids as given below.

Specific Gravity of solids= $(W_{bs}-W_b)/ \{W_{bw}-W_{bsw}+(W_{bs}-W_b)\}$

Where, W_b = Weight of beaker

W_{bs} = Weight of beaker and solid

W_{bw} = Weight of beaker and water

W_{bsw} = weight of beaker, solid and water

4.1.3 Static Settled Concentration

The static settled concentration is an important parameter as it decides the highest limit of solid concentration, which can be achieved by gravitational settling. The static settled concentration depends on a large number of parameters like specific gravity, shape and size distribution of solids, density and viscosity, of carrier fluid etc. It is well accepted that the optimum concentration for solids transportation is around 5 to 10% lower than the static settled value.

In the present study, the static settled concentration has been determined by preparing a slurry sample of intermediate concentration i.e. 20% (by weight) and allowing it to settle in a graduated measuring jar till the level of the solids become constant. This value of solid concentration in the settled portion of slurry is the static settled concentration. The slurry level at regular intervals of time was also recorded during the process of settling of the slurry to determine the setting rate of the slurry.

4.1.4 pH value

A pH meter was used for measurement of the pH value of the slurry of any given solid concentration. The electrode of the meter was first moistened with tap water and then calibrated with a buffer solution of a known pH value. It is cleaned by rinsing vigorously with distilled

water and then immersed in the slurry sample whose pH value was to be determined. The pH suspension was read on the digital display unit when equilibrium value was reached.

4.1.5 Rheological Behavior of Solid-Liquid Mixture

Rheological behavior of the slurry at various concentrations and flow conditions is one of the most important input data required to design of the slurry transportation system. The rheological characteristics of slurry depends on several parameters such as shape, size particle size distribution, solids concentration, carrier fluid properties etc. h

Preparation of the slurry sample: For rheological test 100 ml of the ash-water suspension is prepared by mixing the required quantity of ash with distilled water. The ash was accurately weighed in an electronic type single pan balance. The suspension was mixed gently by a glass rod taking care to avoid attrition of the particles.

Rheometer: The standard Rheolab Q-C is used to calculate the rheological characteristics of the slurries which is shown in figure 4.1. Co-axial concentric cylinder cup and bob geometry is used for measuring the rheological properties of fly ash. The bob and cup assembly is fixing using a locking device and slurry mixture is added into cup (cylinder) up to the particular mark before test. The shear stress value and viscosity measured at the shear rate range from 50-225 s^{-1} at the constant temperature condition 26 °C with wide range of concentrations varying from 0 to 40% (by weight) for ash and water slurries

Figure 4.1: Rheometer (Anton Paar, Germany)

4.2 PHYSICAL PROPERTIES OF BOTTOM ASH

Physical properties of bottom ash are given in table 4.1. The specific gravity of bottom ash was determined as2.25. Particle size distribution of bottom ash given in Table 4.1 shows that the largest particle is 2000μm and only 3% particles are finer than 75μm. Fig. 4.2 shows the Particle size distribution of bottom ash sample. Fig. 4.3 shows the static settled of bottom ash sample is 49.1% by weight. The pH values of bottom ash at various concentrations in the range of 0 to 50% (by weight) varies in the range of 7.62 to 7.75 which also represent that the sample of bottom ash is also non reactive nature.

(1) Specific gravity of Bottom Ash: **2.25**, particle size **d_{50} = 230 μm, d_{wn} = 162.139 μm**

(2) Rheological Properties of bottom ash at temperature 26°C

Table 4.1: Rheological Properties of bottom ash

Concentration (Cw) %	**Yield stress (Pascal)**	**Slurry viscosity(cP)**	**Water viscosity(cP)**	**Relative viscosity**	**Flow behaviour**
0	0	---	0.995	1	Newtonian
10	0	1.01	0.995	1.02	Newtonian
20	0	1.6	0.995	1.61	Newtonian
30	0	2.2	0.995	2.21	Newtonian
40	0	4.3	0.995	4.31	Newtonian
50	0	5.6	0.995	5.62	Newtonian

(3) pH value of slurry

Table 4.2: pH value of slurry

Cw, %	0	20	25	30	35	40	45	50
pH	7.75	7.67	7.66	7.66	7.64	7.63	7.62	7.62

(4) Static settled concentration of slurry = 49.1 % with Initial concentration= 20% (by weight)

Table 4.3: Settled concentration of bottom ash sample

Sr. No.	**Time(Minute)**	**Conc. (%C_w)**
1	0	20
2	1	28.12
3	2	33.16
4	3	42.37
5	4	45.25
6	5	47.39
7	15	47.39
8	30	47.39
9	60	48.54
10	120	48.54
11	180	48.54
12	240	49.01
13	480	49.01

(5) Particle size distribution

Table 4.4: Particle size distribution

Sr. No.	Particle size, μ	% finer
1	below 2000	100
2	1400	89.5
3	710	85.5
4	355	72.6
5	300	65
6	250	58.8
7	212	46.8
8	180	44.1
9	150	20.6
10	125	17.4
11	90	13.5
12	75	3

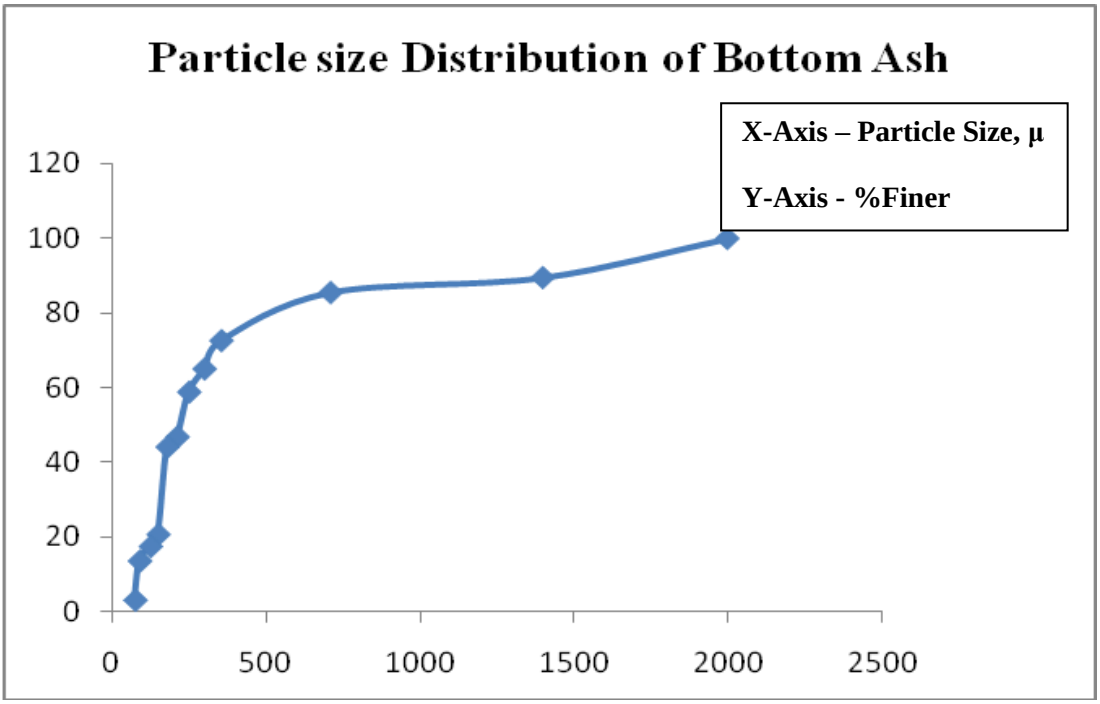

Figure 4.2: Particle size distribution curve of bottom ash sample

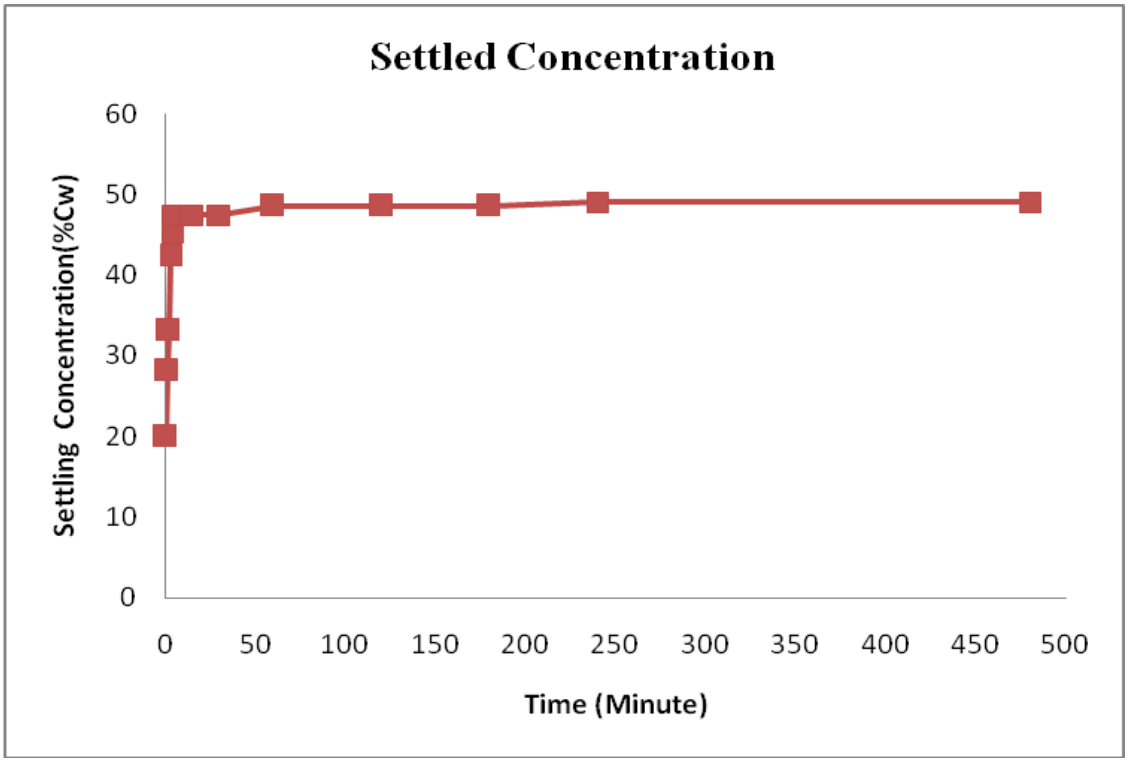

Figure4.3: Settled concentration curve of bottom ash sample

Graphical representation of the Rheology of bottom ash slurry sample with variation of concentration

(a)

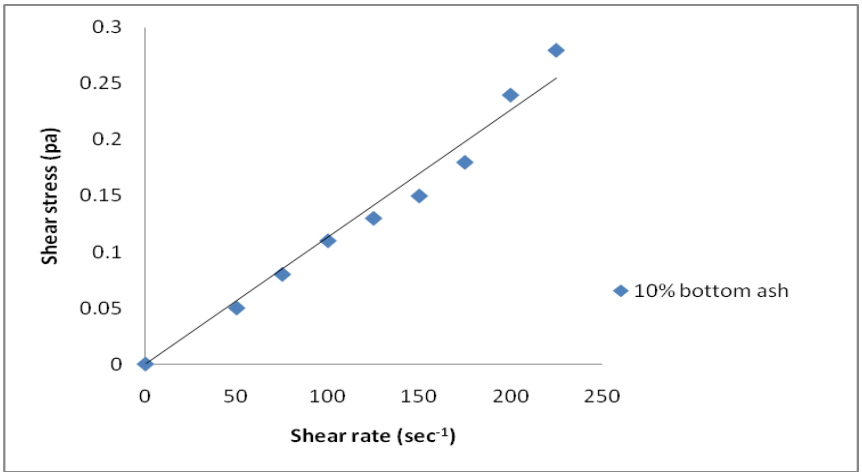

(b)

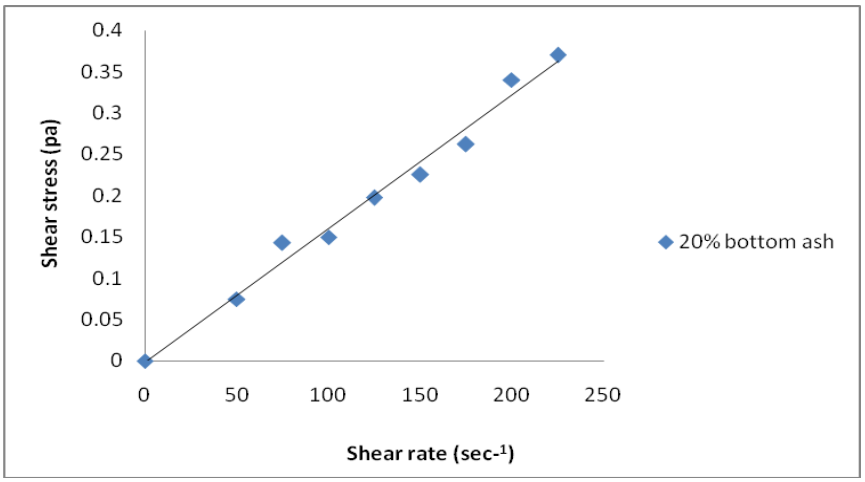

(c)

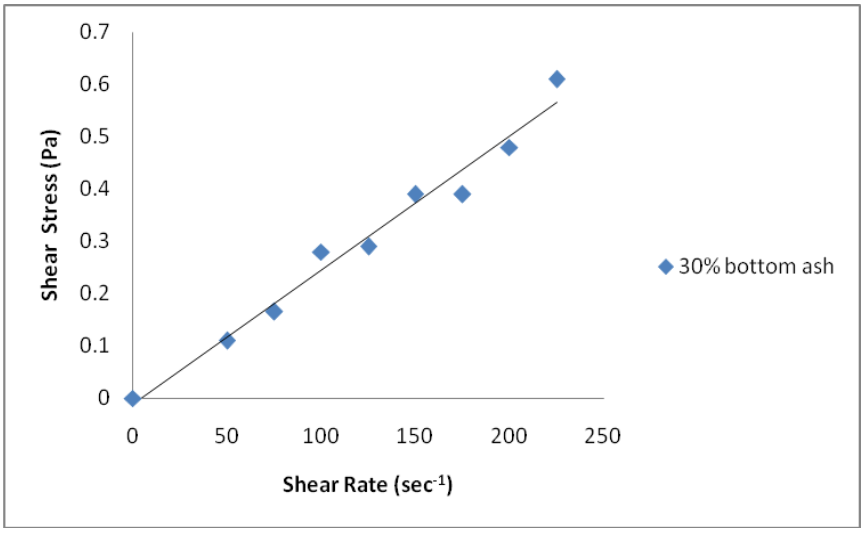

(d)

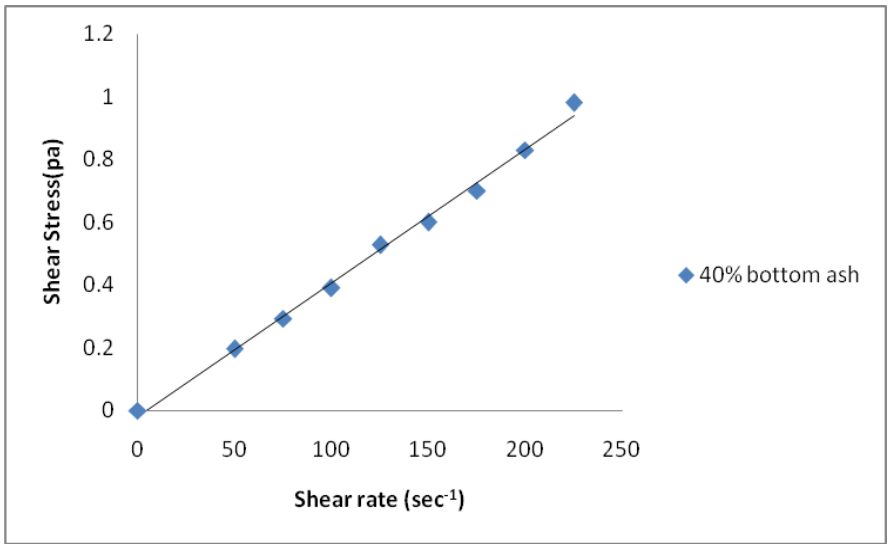

(e)

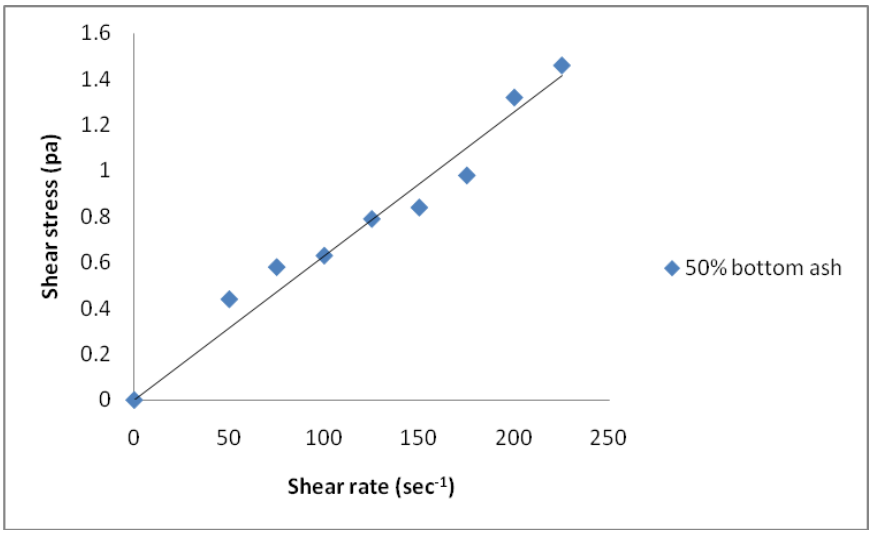

Figure 4.4: Rheology of bottom ash slurry sample with variation of concentration such as (a) 10% bottom ash (b) 20% bottom ash (c) 30% bottom ash (d) 40% bottom ash (e) 50% bottom ash

CHAPTER 5

NUMERICAL EVALUATION OF PIPELINE PERFORMANCE

In the recent years, Computational Fluid Dynamics (CFD) has been increasingly used for a wide range of engineering applications. Some examples of interesting applications of computational modeling are cooling of electronics systems, rotating and reciprocating machinery, furnaces and combustion chambers. CFD is finding its way into process, chemical, civil, and environmental engineering. Optimization in these areas can produce large savings in equipment and energy costs and in reduction of environmental pollution.

All CFD codes contain three main elements:

1. A **pre-processor**, which is used to input the problem geometry, generates the grid; define the flow parameter and the boundary conditions to the code.
2. A **flow solver**, which is used to solve the governing equations of the flow subject to the conditions provided. There are three different methods used as a flow solver:

    - Finite difference method
    - Finite element method
    - `Finite volume method

3. A **post-processor**, which is used to massage the data and show the results in graphical and easy to read format.

5.1 GOVERNING EQUATIONS OF CFD

The physical aspects of any fluid flow are governed by the following three fundamental principles:

1. Conservation of mass
2. Conservation of momentum (Newton's second law)
3. Conservation of energy (first law of thermodynamics)

5.1.1 Conservation of Mass equation

The equation for conservation of mass also called the continuity equation can be written as follows:

$$\frac{\partial \rho}{\partial t}.\nabla(\rho \vec{V}) = S_m \qquad (5.1)$$

The equation is the general form of the mass conservation equation and is valid for incompressible as well as compressible flows. The source S_m is the mass added the continuous phase from the dispersed second phase. For steady state compressible fluid flow the continuity equation is given by:

$$\rho(\nabla \vec{V}) = 0 \qquad (5.2)$$

Where, $\nabla = \frac{\partial}{\partial x_i}\hat{i} + \frac{\partial}{\partial x_i}\hat{j} + \frac{\partial}{\partial x_i}\hat{k}$ and $V = u_i\,\hat{i} + u_j\,\hat{j} + u_k\,\hat{k}$

5.1.2 Momentum conservation equation

Conservation of momentum in an inertial (non-accelerating) reference frame is described as:

$$\frac{\partial \rho}{\partial t}(\rho \vec{V}) + \nabla.(\rho \vec{V}\vec{V}) = -\nabla p + \nabla(\bar{\bar{\tau}}) + \rho \vec{g} + \vec{F} \qquad (5.3)$$

Where, $\rho \vec{g}$ = gravitational body force,

F = external body forces (e.g., that arise from interaction with the dispersed phase), respectively. F also contains other model-dependent source terms such as porous media and user-defined sources.

The stress tensor $\bar{\bar{\tau}}$ is given by;

$$\bar{\bar{\tau}} = \mu[(\nabla \vec{V} + \nabla \vec{V}^{T})] = -\frac{2}{3}\nabla.\vec{V} I \qquad (5.4)$$

Where, the second term on the right hand side is taken for consider the effect of volume dilation.

For steady state incompressible fluid flow, the momentum conservation equation is given by

$$\nabla.(\rho \vec{v} \vec{v}) = -\nabla p + \nabla.(\bar{\bar{\tau}}) + \rho \vec{g} + \vec{F} \qquad (5.5)$$

These fundamental principles can be expressed in terms of mathematical equations. CFD is the art of replacing the governing partial differential equations of fluid flow with numbers and advancing these numbers in space and / or time domain to obtain a final description of complete flow field of interest. With the development of high-speed digital computers, CFD has become a powerful tool to predict flow characteristics in varied problem, in an economical way.

5.2 MODELLING OF PIPELINE

To study the numerical analysis on the pipe, the dimension data of the pipe was required to generate a model in the software. In the present work, pipe line bend is taken for the simulation. For taking the dimensions of pipeline the test loop all the valves were closed to prevent any leakage of water or slurry. The dimensions of pipeline bend and various tapping's are taken by using measuring tape and pipeline bend is modelled by using Pro-E and imported in pre-processor Gambit. Three-dimensional modelling of the pipeline is shown in Figure 5.1:

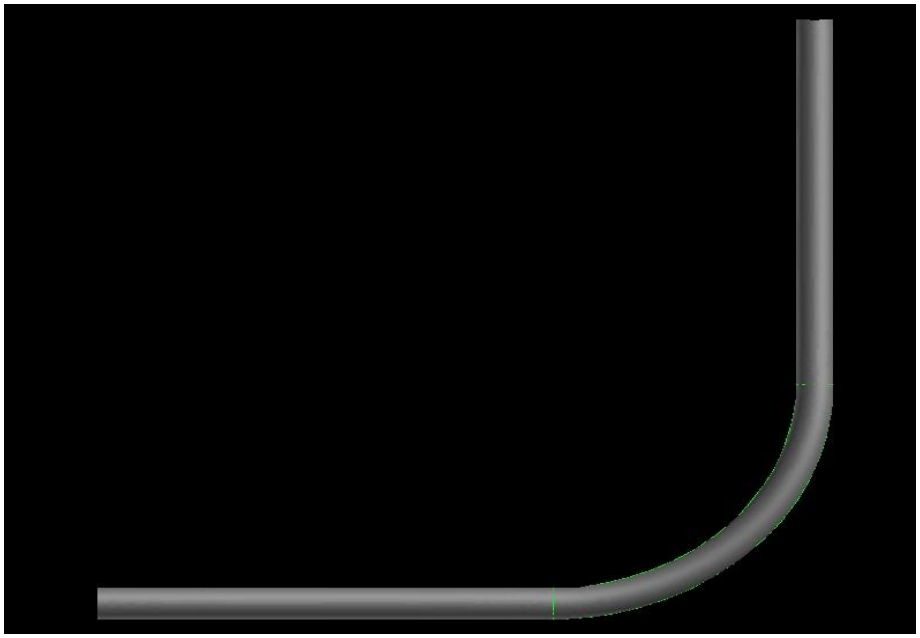

Figure 5.1: Modelling of Pipeline Bend

Grid Generation

The T-Grid tool is used for mashing the geometry of pipeline. T-Grid is highly efficient unstructured grid generation tool. It is consisting of triangular, tetrahedral, hexahedral, prismatic, or pyramidal cells. Pipeline bend geometry mesh generated using unstructured tetrahedral meshing using Gambit. Mesh quality parameter skewness and aspect ratio calculated 0.81 and 3.1.Total number of 267516 elements generated. Meshed pipe bend is shown in figure 5.2:

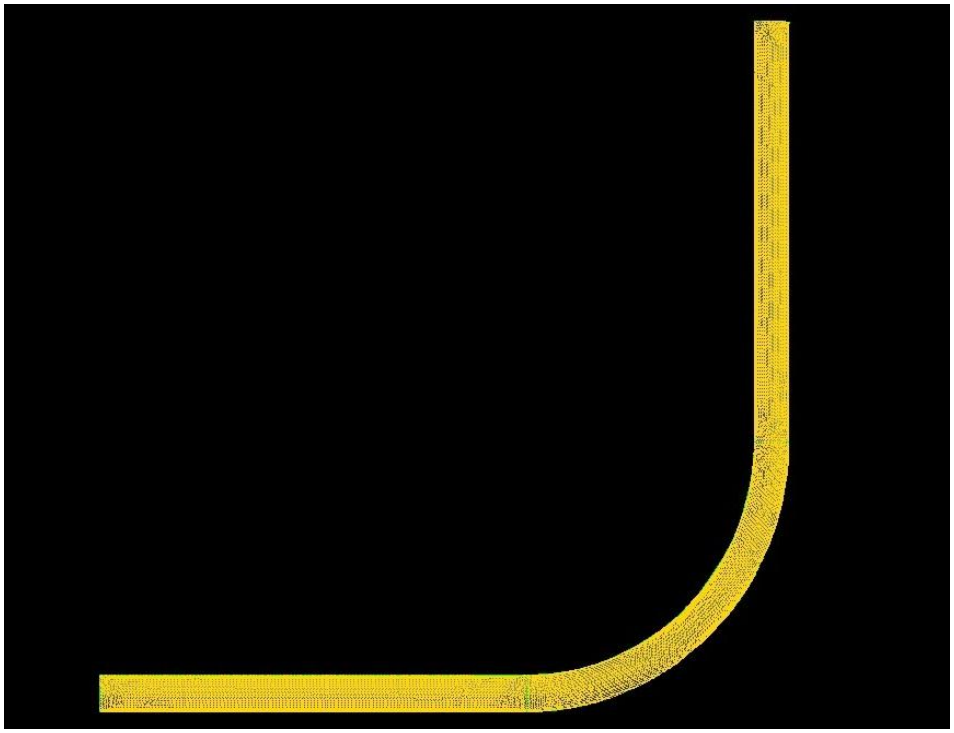

Figure 5.2: Meshed Pipeline Bend

5.2.1 Examine of Mesh

It is important to check the quality of mesh, because parameter such as skewness affects the accuracy of the CFD simulation. Each element has of value of skewness between 0 and 1. The skewness is classified in two ways, EquiAngle skew and EquiSize skew. The smaller value of equiAngle skew and equisize skew are more acceptable. It is also important to verify that all of the elements in mesh have positive area/volume otherwise the simulation in 'FLUENT' solver is not possible.

EquiAngle Skew

The EquiAngle Skew (Q_{EAS}) is the measure of skewness that is defined as follows:

$$Q_{EAS} = \max\left\{\frac{\theta_{\max} - \theta_{eq}}{180 - \theta_{eq}}, \frac{\theta_{eq} - \theta_{\min}}{\theta_{eq}}\right\} \quad (5.6)$$

Where,

θ_{max} & θ_{min} = maximum and minimum angles between the edges of the element, degrees

θ_{eq} = angle corresponding to an equilateral cell of similar form. For triangular and tetrahedral elements, $\theta_{eq} = 60^0$ for quadrilateral and $\theta_{eq} = 90^0$ for hexahedral elements.

By definition, $0 \leq Q_{EAS} \leq 1$

Where, Q_{EAS} = 0 describes an equilateral element, and Q_{EAS} =1 describes a completely degenerate (poorly shaped) element. In general, high-quality meshes contain elements that possess average Q_{EAS} values of 0.1 in two-dimensional case and 0.4 in three-dimensional case.

EquiSize Skew

The EquiSize Skew (Q_{EAS}) is a measure of skewness that is defined as follows:

$$Q_{EVS} = \frac{\left(S_{eq} - S\right)}{S_{eq}} \quad (5.7)$$

Where, S = area in 2-dimensional or volume in 3-dimensional case of the mesh element,

S_{eq} = maximum area in 2-dimensional or volume in 3-dimensional case of an equilateral cell the circumscribing radius of which is identical to that of the mesh element.

$0 \leq Q_{EVS} \leq 1$

5.2.2 Grid independency test

In the present work three types of mesh size taken for checking of the grid independent test. It is observed that a coarse of 7 mm mesh size in the pipeline bend generates 103545 tetrahedral elements, fine mesh of 6 mm cell size in the pipeline bend generates 151900 tetrahedral elements and a finer mesh of 5 mm cell size in the pipeline bend generates 267516 tetrahedral elements in

computational domain. Mesh quality of the pipeline bend is shown in table 5.1. The mesh size 5 shows the closer result with the experimental data. So the mesh size 5 is used for further simulation analysis.

Table 5.1 Mesh Quality

Sr. No.	Mesh type	Mesh size	No. of element	Quality parameter		
				Equi size skewness	Equi angle skewness	Aspect ratio
1	Tetrahedral Elements	7	103545	0.85	0.76	2.99
2	Tetrahedral Elements	6	151900	0.82	0.78	3.07
3.	Tetrahedral Elements	5	267516	0.81	0.78	3.1

Assumptions

The simulation of flow in pipeline bend is done on basis of following basic assumptions:

1. Steady state condition.
2. Incompressible fluid flow.
3. Constant fluid properties.

Boundary conditions

The boundary conditions are specified as follows:

1. Constant velocity is given in X-direction at velocity-inlet.
2. Turbulence intensity is 2% and Turbulence viscosity ratio is taken as 10 for intlet condition.

3. Pressure outlet at discharge end is given as gauge pressure and target mass flow rate is constant.
4. Backflow turbulence intensity is 2% and Backflow turbulence viscosity ration is taken as 10 for outlet condition.

Solution parameters

1. 3-D double precision solver used to solve for simulation
2. Clear water used is taken as working fluid
3. Standard K-€ model is used for turbulence modeling.
4. Convergence criteria for continuity, velocity and turbulence parameters was set to 10^{-4}
5. Second order scheme is used for pressure correction as well as for solving momentum, turbulent kinetic energy and turbulence dissipation rate.
6. A simple scheme is used for pressure velocity coupling
7. To achieve convergence is less time under relaxation factor applied are 0.3 for pressure, 0.7 for momentum equation, 0.8 for turbulence kinetic energy and 0.8 for turbulence dissipation rate.

CHAPTER 6

RESULTS AND DISCUSSION

6.1 PRESSURE DROP IN HORIZONTAL SLURRY PIPELINE BEND

The pressure loss across the 90^o horizontal bend of diameter 56mm is determined by incorporating the pipe bend in the bend pressure apparatus. The pressure taps are provided on the both inner and outer periphery of the curvature of the bend to measure the pressure drop across the bend for water and the slurry flow at different concentrations. The flow characteristics of the pipe bend evaluated experimentally and numerically by using the computational dynamic code FLUET 6.3. Table No.6.1, 6.2 and 6.3 represents the experiment and numerical values of head loss with water obtained at different pairs of pressure taps.

Table No. 6.1: Comparison of experimental and numerical values of pressure at different pressure tapping

Discharge= 45.4 X 10^{-4} m^3/sec Velocity=1.84 m/sec					
Sr. No.	Distance of pressure tapping from inlet (mm)	Experimental values of pressure at different pressure tapping (mm)		Numerical values of pressure at different pressure tapping (mm)	
		Inner side of bend	Outer side of bend	Inner side of bend	Outer side of bend
1	690	68.5	104	72.95	108.67
2	770	59	105	61.22	110.3
3	820	57.5	101.5	58.46	107.14
4	870	53	98	54.89	103.57
5	960	46	92	48.48	96.22
6	990	42	89	44.89	93.88
7	1020	41.5	86.5	43.36	90.51
8	1050	36	84	38.26	88.7

Table No. 6.2: Comparison of experimental and numerical values of pressure at different pressure tapping

Discharge= 35.7 X 10^{-4} m^3/sec Velocity=1.45 m/sec					
Sr. No.	Distance of pressure tapping from inlet	Experimental values of pressure at different pressure tapping		Numerical values of pressure at different pressure tapping	
		Inner side of bend	Outer side of bend	Inner side of bend	Outer side of bend
1	690	42	62	43.87	65.81
2	770	34	62.5	36.02	66.63
3	820	32	61	34.18	64.08
4	870	30	59	32.14	62.24
5	960	26	56	27.85	58.67
6	990	23.5	53	25.17	56.63
7	1020	22	51.5	24.18	53.77
8	1050	20	50	21.12	51.73

Table No. 6.3: Comparison of experimental and numerical values of pressure at different pressure tapping

Discharge = 25.7 X 10^{-4} m^3/sec Velocity=1.043 m/sec					
Sr. No.	Distance of pressure tapping from inlet	Experimental values of pressure at different pressure tapping		Numerical values of pressure at different pressure tapping	
		Inner side of bend	Outer side of bend	Inner side of bend	Outer side of bend
1	690	25	34	26.02	37.65
2	770	19	34.5	21.93	37.75
3	820	18	34	20.71	36.42
4	870	17.5	33	19.59	35.31
5	960	15	30	16.83	32.65
6	990	14	29	15.71	31.38
7	1020	12.5	27.5	14.79	30.31
8	1050	11	26	13.06	28.87

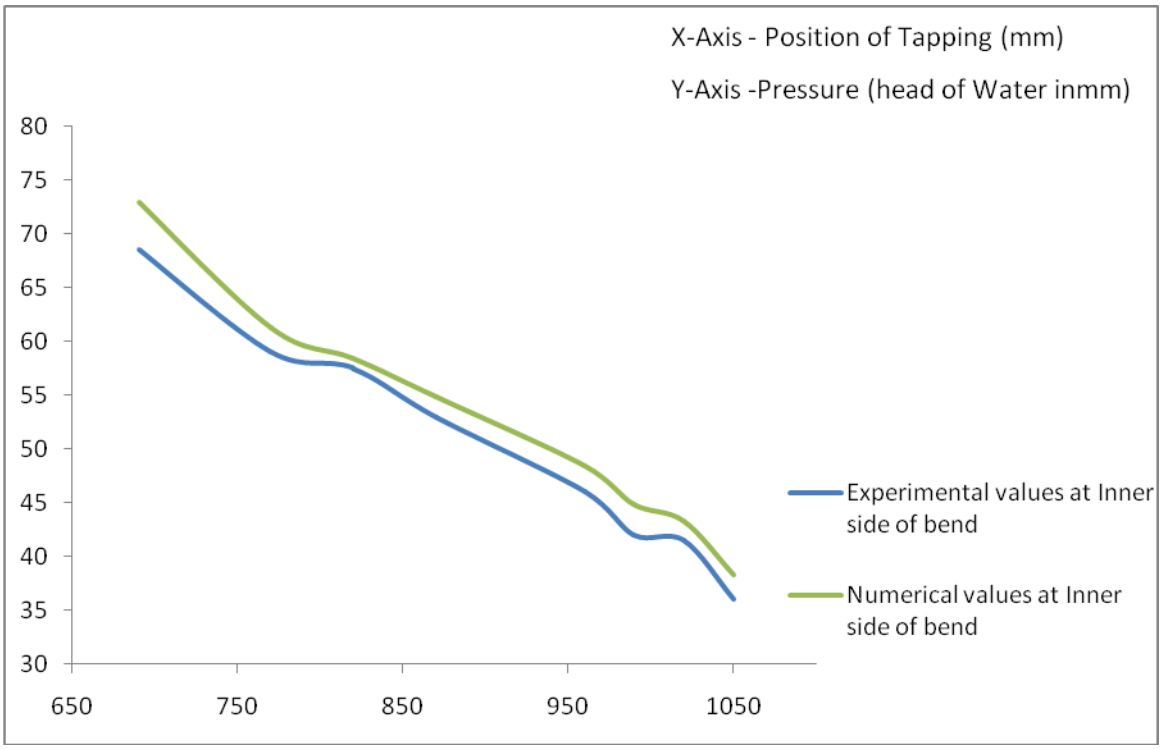

Figure No.6.1 (a): Pressure at inner side of pipe bend for 45.4 X 10^{-4} m^3/sec discharge

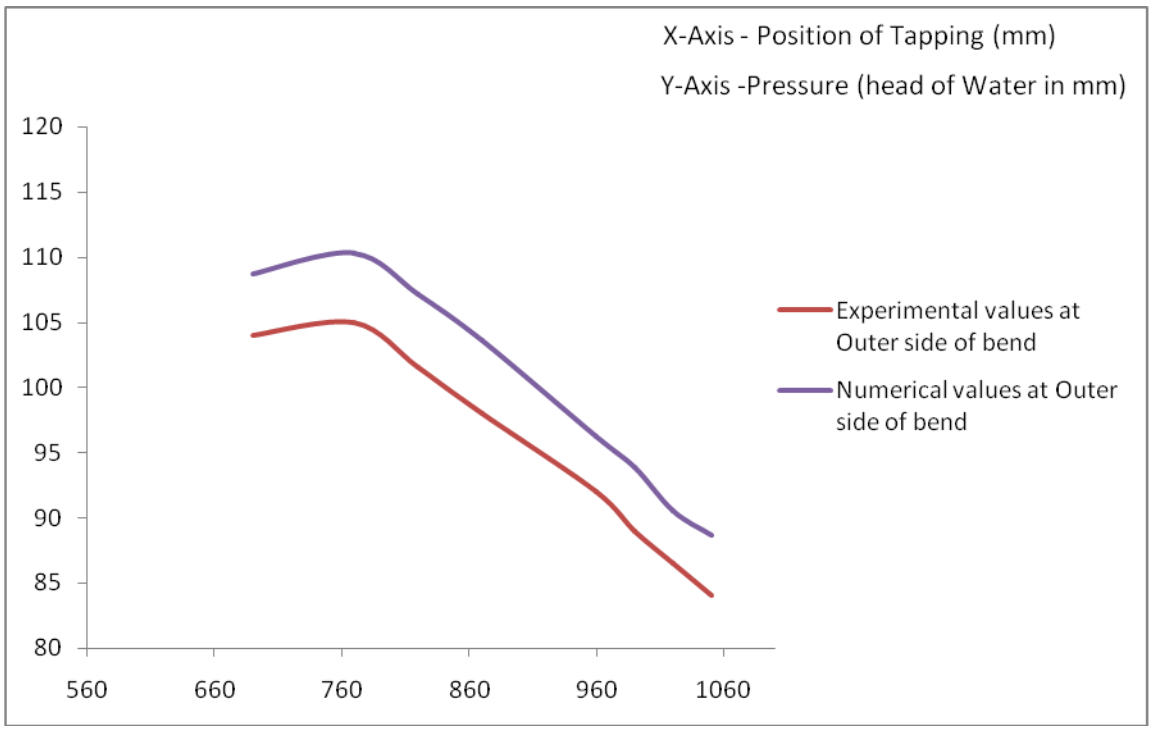

Figure No.6.1 (b): Pressure at outer side of pipe bend for 45.4 X 10^{-4} m^3/sec discharge

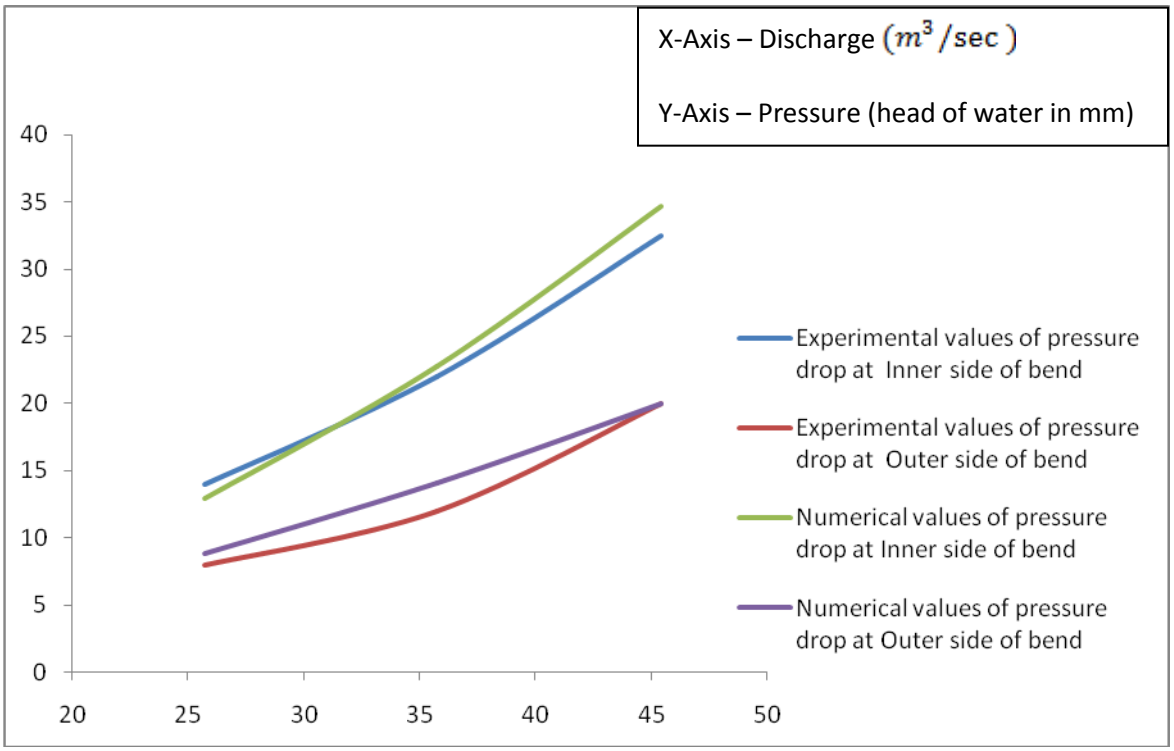

Figure No.6.1 (c): Pressure drop (inner & outer) at different discharges

Figure No. 6.1 (a) shows the variations of pressure at the inner side of the pipeline bend both experimentally and numerically. Figure No. 6.1 (b) shows the variations of pressure at the outer side of the pipeline bend. It is observed from the above figures that both the experimental and numerical values of pressure flows the same pattern of curve with 5% to 10% variation in values. Figure No. 6.1 (c) shows the variations of pressure drop experimentally and numerically for both inner and outer side of the pipeline bend for different discharges with 5% to 10% variation in values.

6.1.1 Pressure Drop with water in Pipeline Bend

The pressure drop across the bend is a function of flow velocity, solid concentration. The pressure drop is first measured with water and then with different concentrations of bottom ash 10% and 20% with different flow discharges. Figure No. 6.2 (a), (b) & (c) shows the pressure contours at three different discharges. These pressure contours shows that the pressure is maximum at starting of the bend and its decreases across the bend and it is minimum at the end of the bend. It is also observed that the pressure drop increases with the increase in flow velocity.

Figure No.6.3 (a), (b) & (c) shows the variation of pressure at the section of various pressure tapping. The pressure is more on the outer side of the curvature as compared to the inner side of the bend. When the fluid strikes the outer side the kinetic energy due to velocity is converted into the pressure this increases the pressure on outer side of bend. Figure No.6.4 (a), (b), (c) & (d) shows the comparison of velocity at the section of different pressure tapping for different discharges and it is found that the velocity is increased with the increases in discharge and is maximum at the centre of the pipe and minimum at the periphery of pipe. Figure No.6.5 (a), (b), (c), (d) shows the turbulent dissipation rate for different discharges at different sections and it is found that there is no turbulence dissipation rate at the centre of the pipe but the maximum dissipation occurs at the boundary of pipe. From these figures it can also be concluded that the turbulent dissipation rate at boundary increases with the increase in discharge. The maximum dissipation rate occurs at boundary as the kinetic energy of incoming water immediately transfers to the wall of pipe after striking to the bend. Figure No.6.6 (a), (b), (c) & (d) shows the turbulence intensity for different discharges at different sections of pipe bend. It is found that the turbulence intensity is maximum at the boundary of pipe but minimum at the center of the pipe.

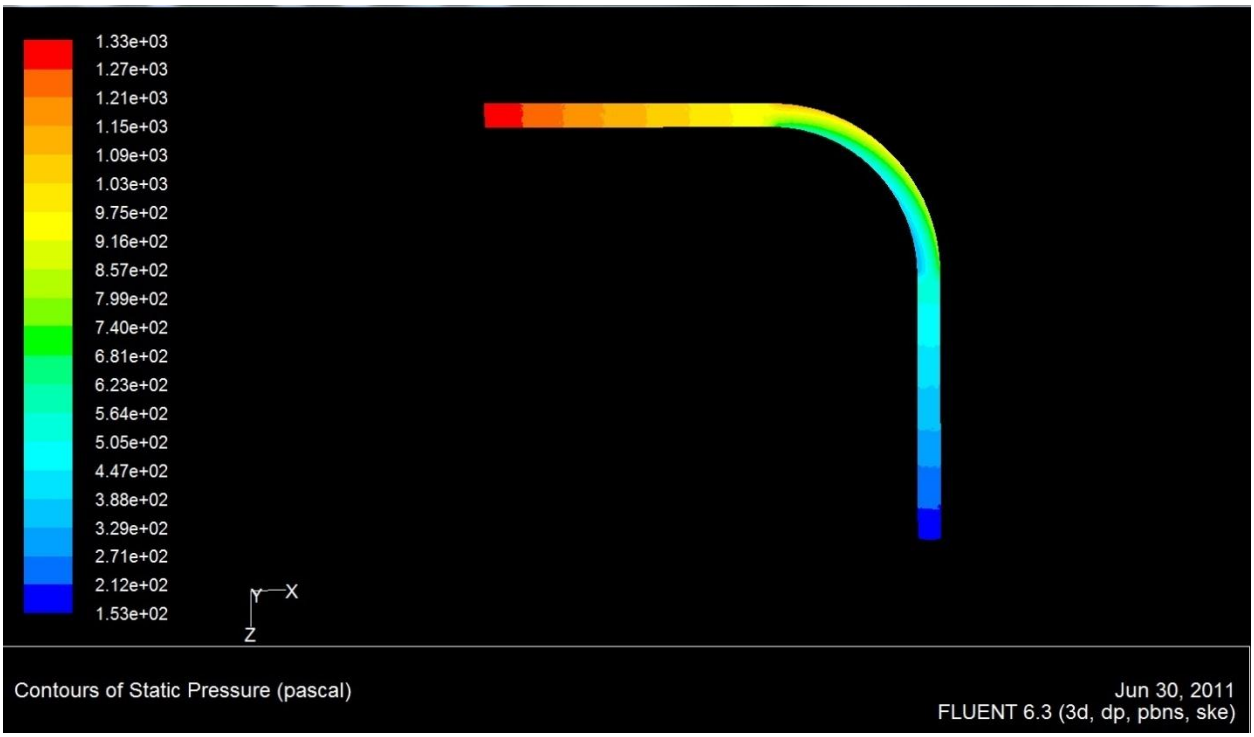

Figure No. 6.2(a): Pressure contour for 45.4 X 10^{-4} m^3/sec discharge with water

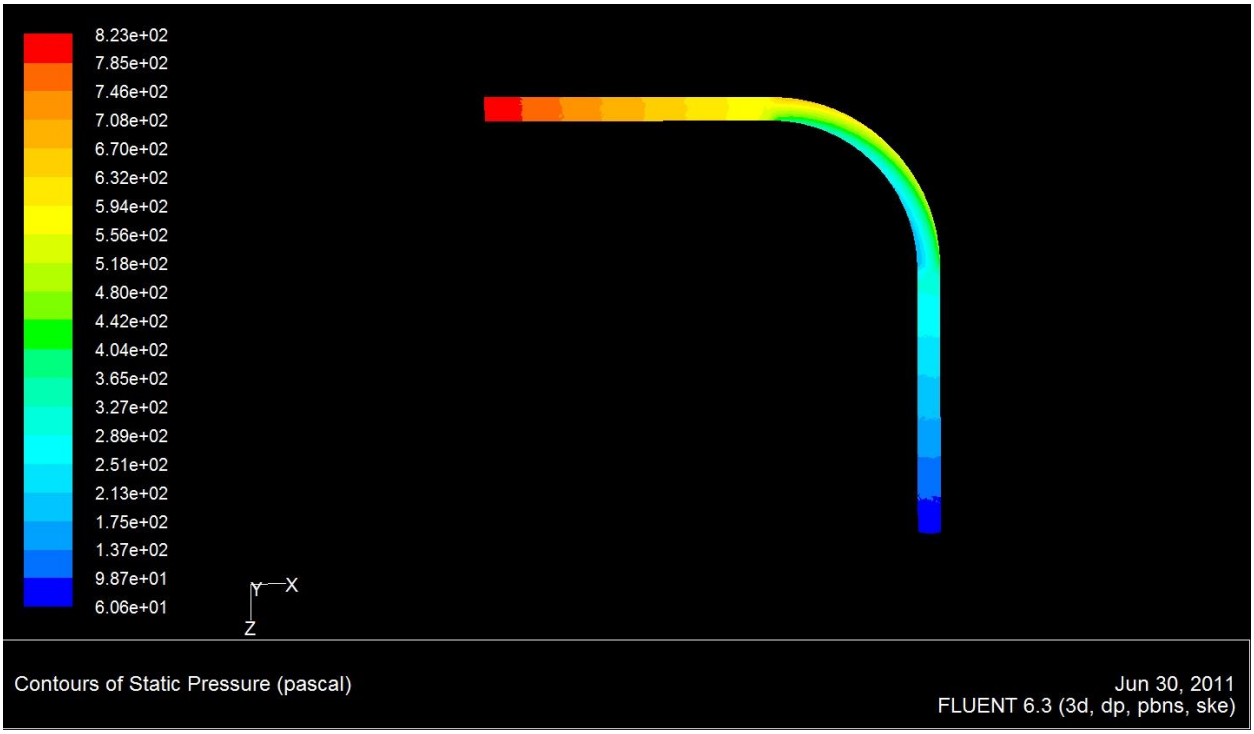

Figure No. 6.2 (b): Pressure contour for 35.7 X 10^{-4} m^3/sec discharge with water

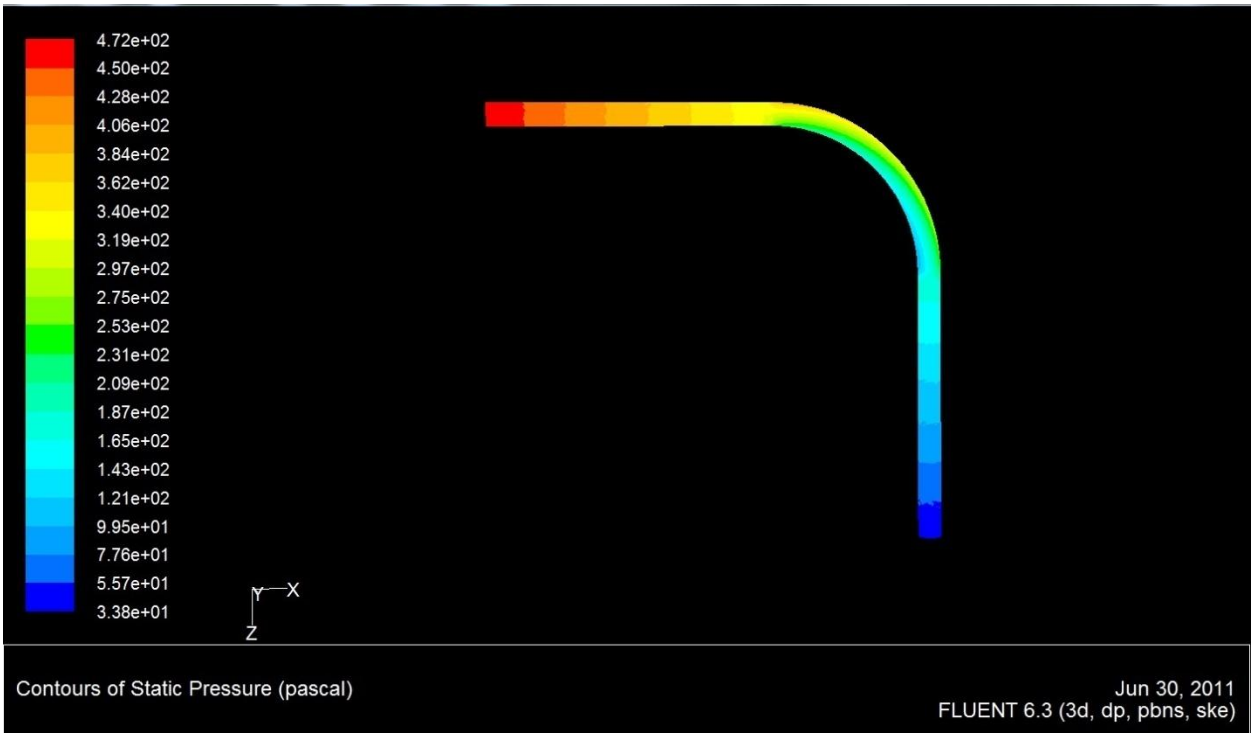

Figure No. 6.2 (c): Pressure contour for 25.7 X 10^{-4} m^3/sec discharge with water

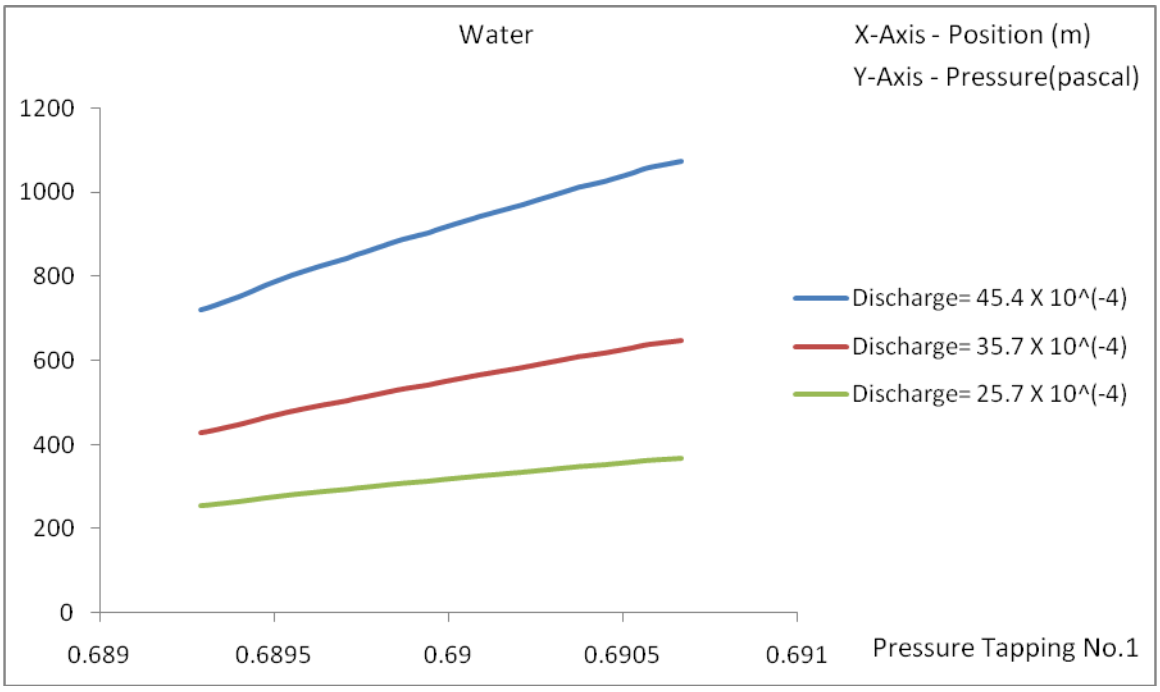

Figure No.6.3 (a): Variation of pressure at pressure tapping no. 1 for different discharges

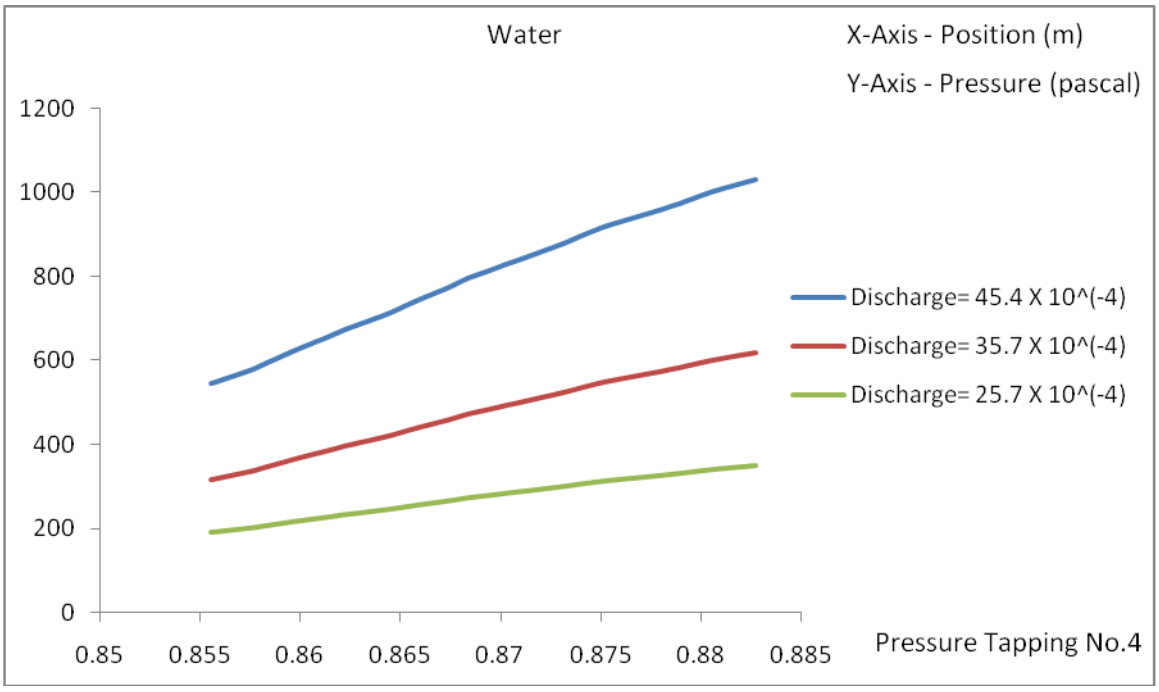

Figure No.6.3 (b): Variation of pressure at pressure tapping no. 4 for different discharges

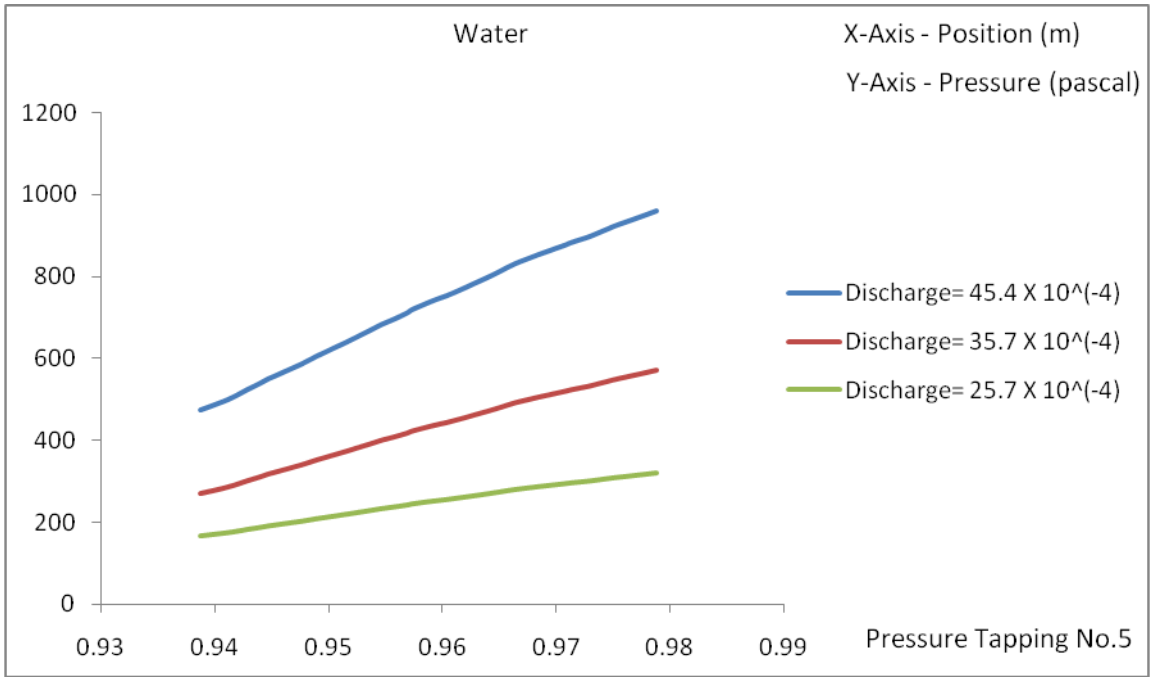

Figure No.6.3 (c): Variation of pressure at pressure tapping no. 5 for different discharges

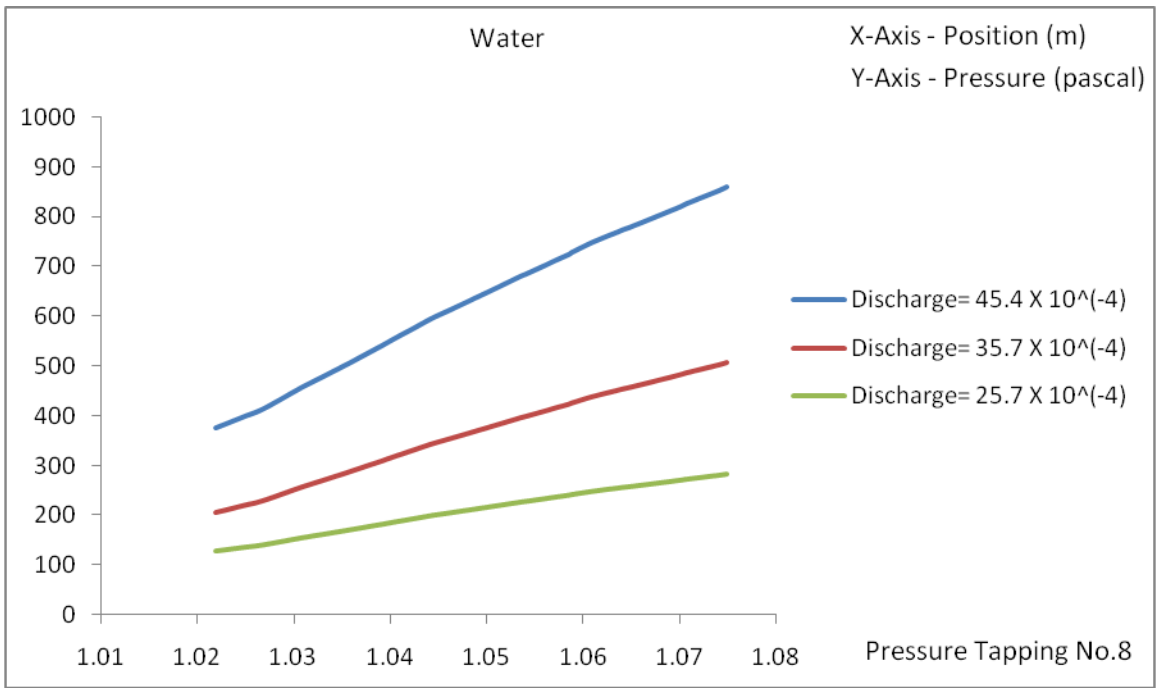

Figure No.6.3 (d): Variation of pressure at pressure tapping no. 8 for different discharges

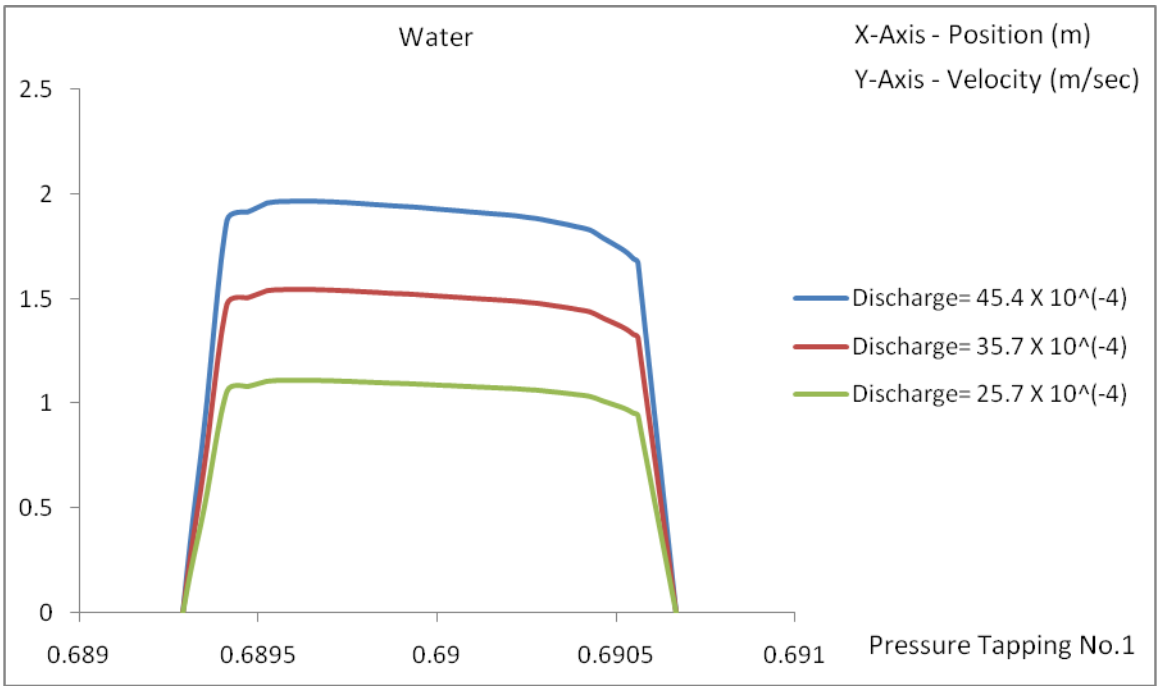

Figure No.6.4 (a): Variation of velocity at pressure tapping No. 1 for different discharges

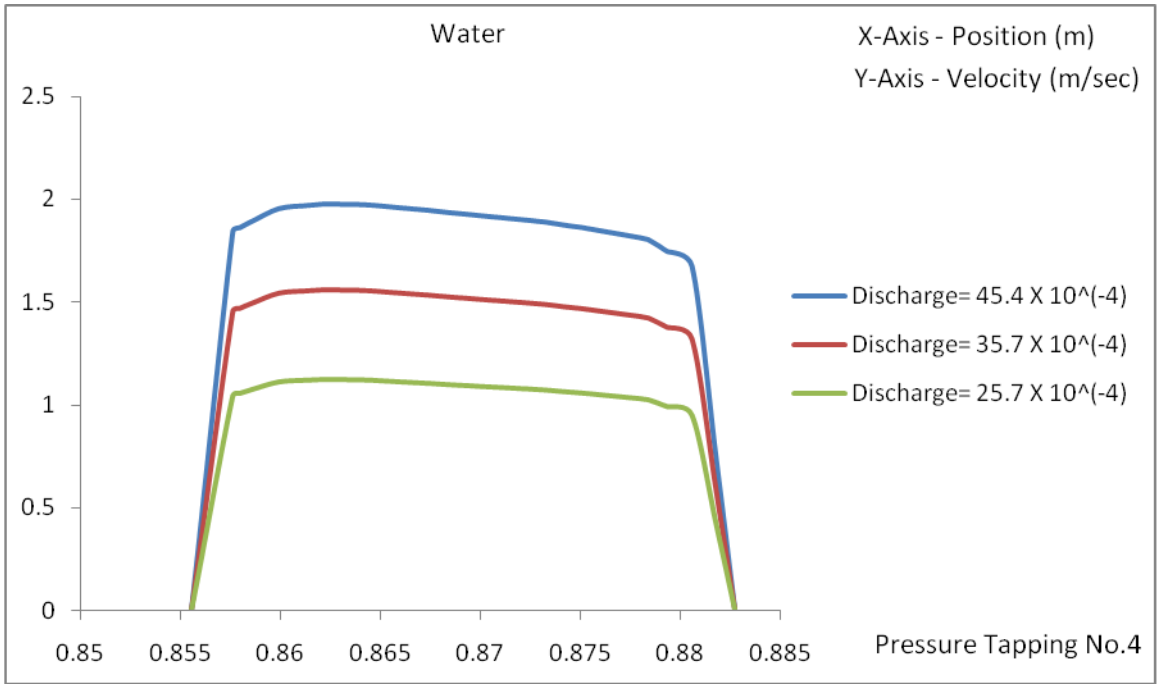

Figure No.6.4 (b): Variation of velocity at pressure tapping No. 4 for different discharges

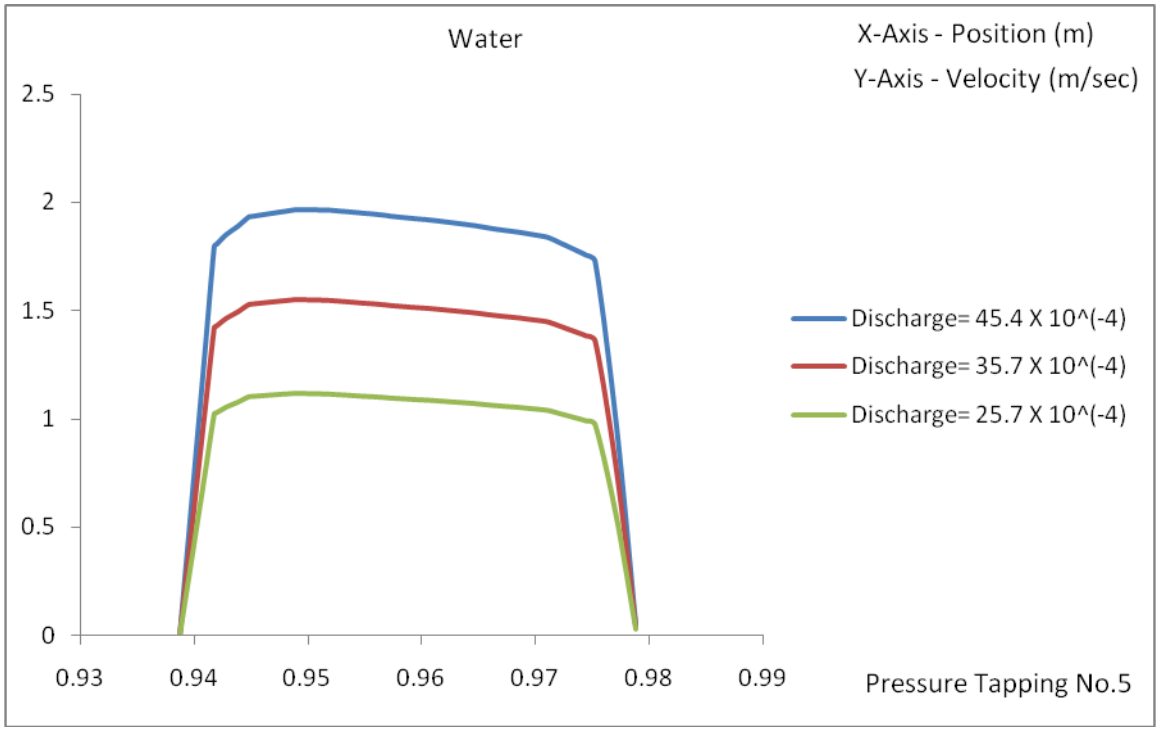

Figure No.6.4 (c): Variation of velocity at pressure tapping No. 5 for different discharges

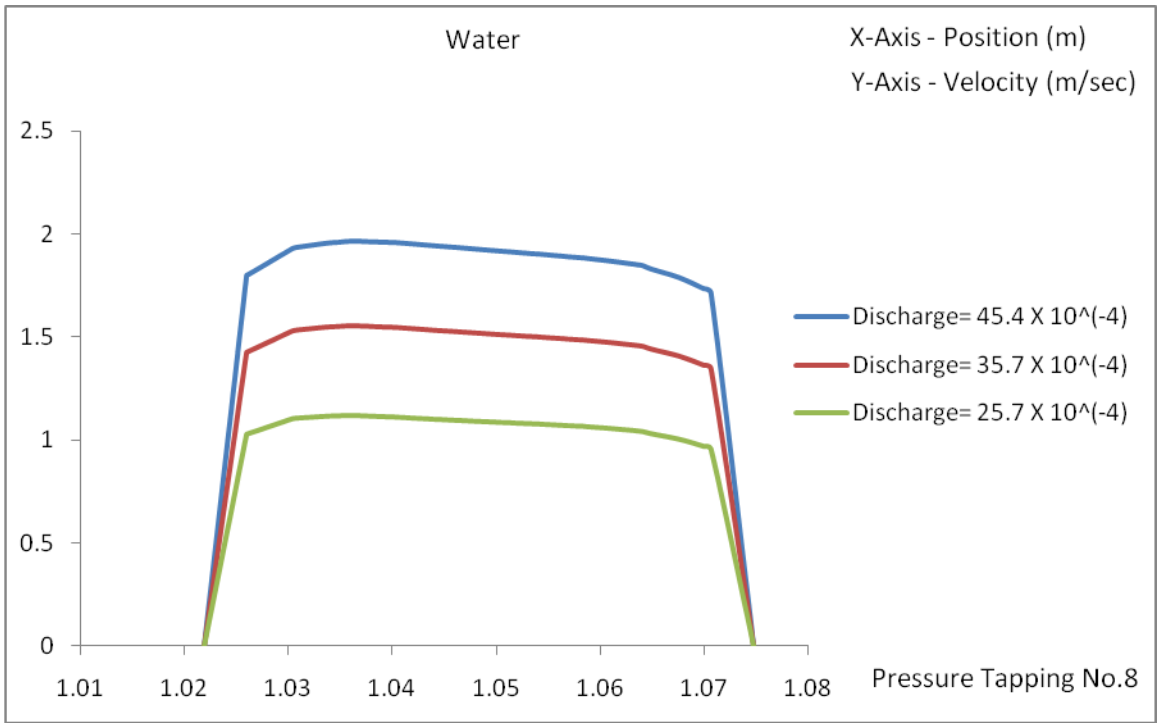

Figure No.6.4 (d): Variation of velocity at Pressure tapping No. 8 for different discharges

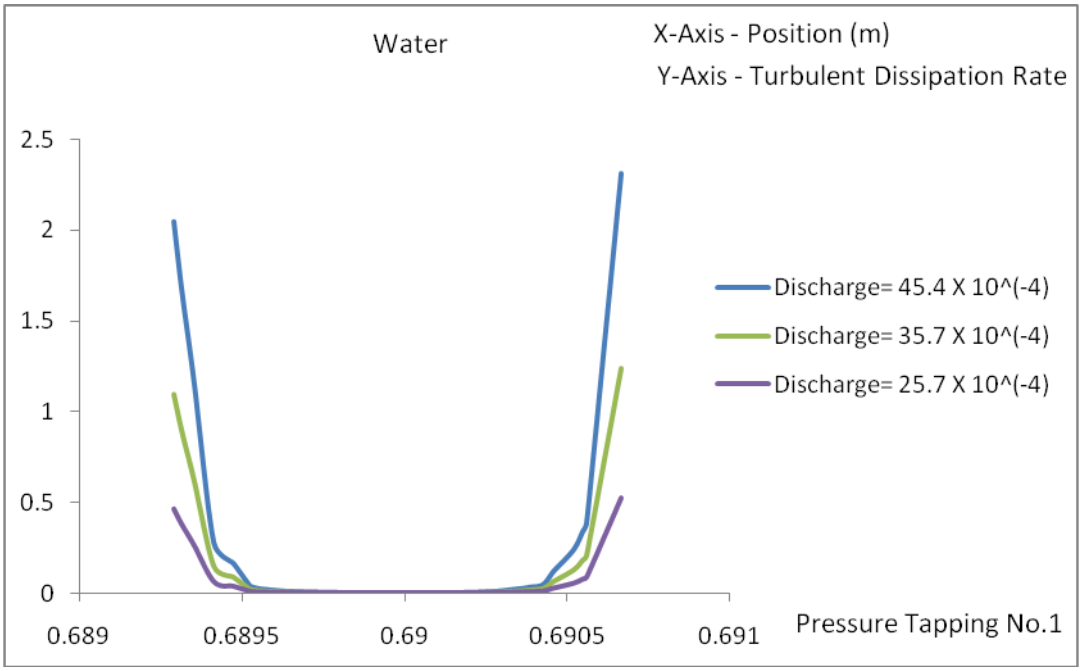

Figure No.6.5 (a): Turbulent dissipation rate at pressure tapping no. 1 for different discharges

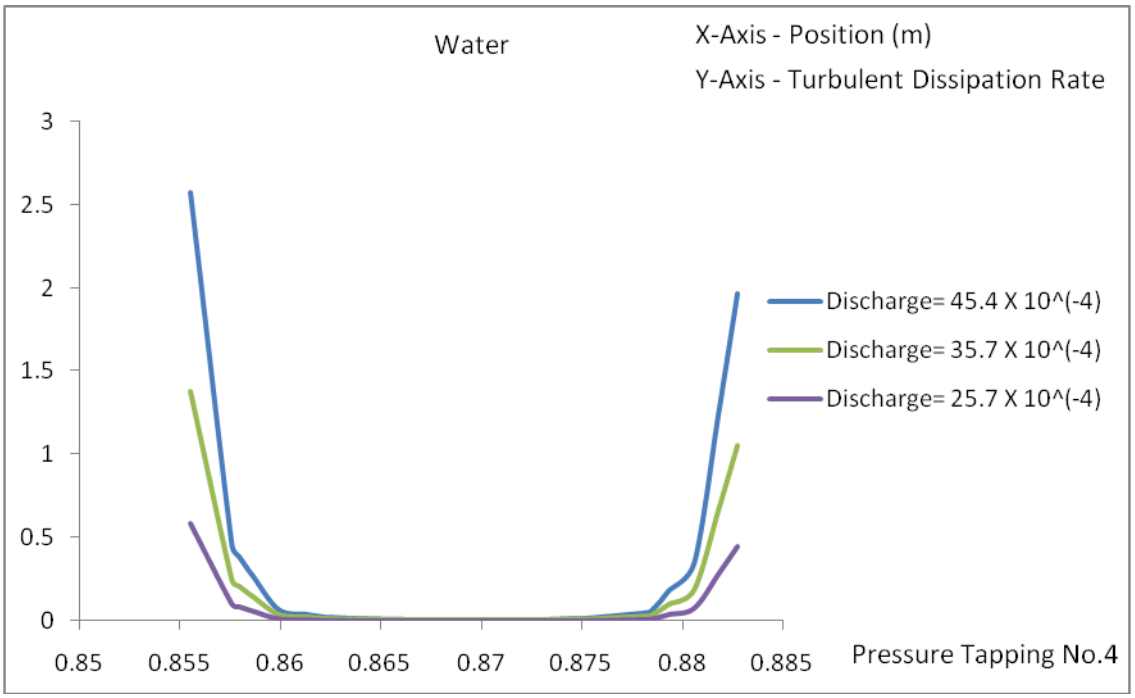

Figure No.6.5 (b): Turbulent dissipation rate at pressure tapping no. 4 for different discharges

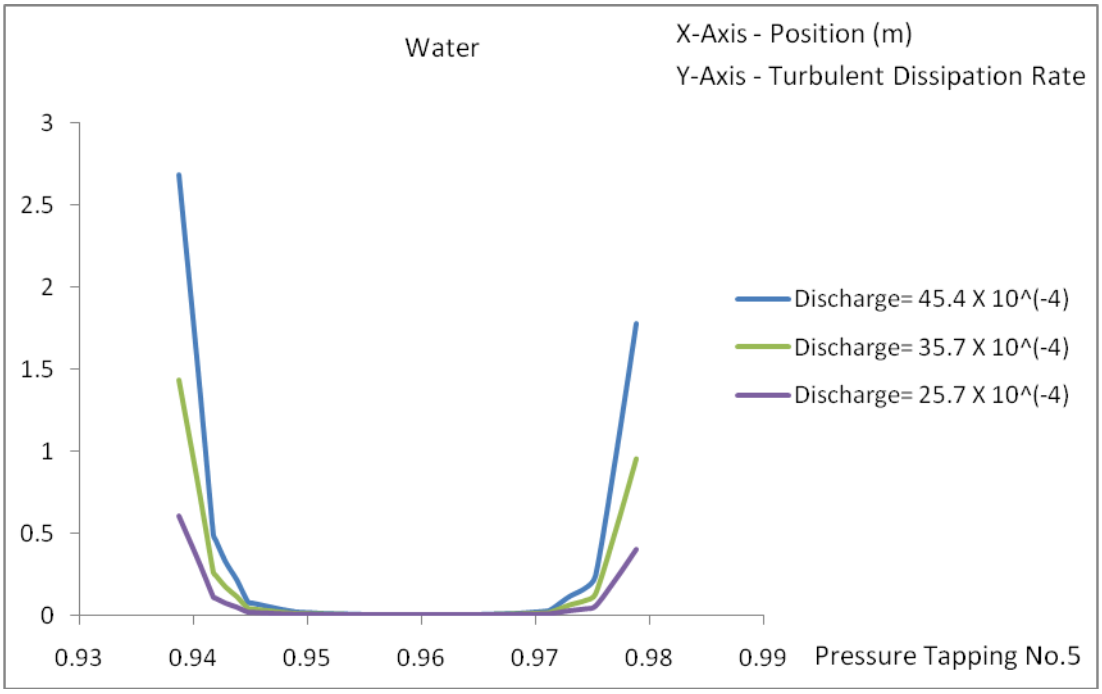

Figure No.6.5 (c): Turbulent dissipation rate at pressure tapping no.5 for different discharges

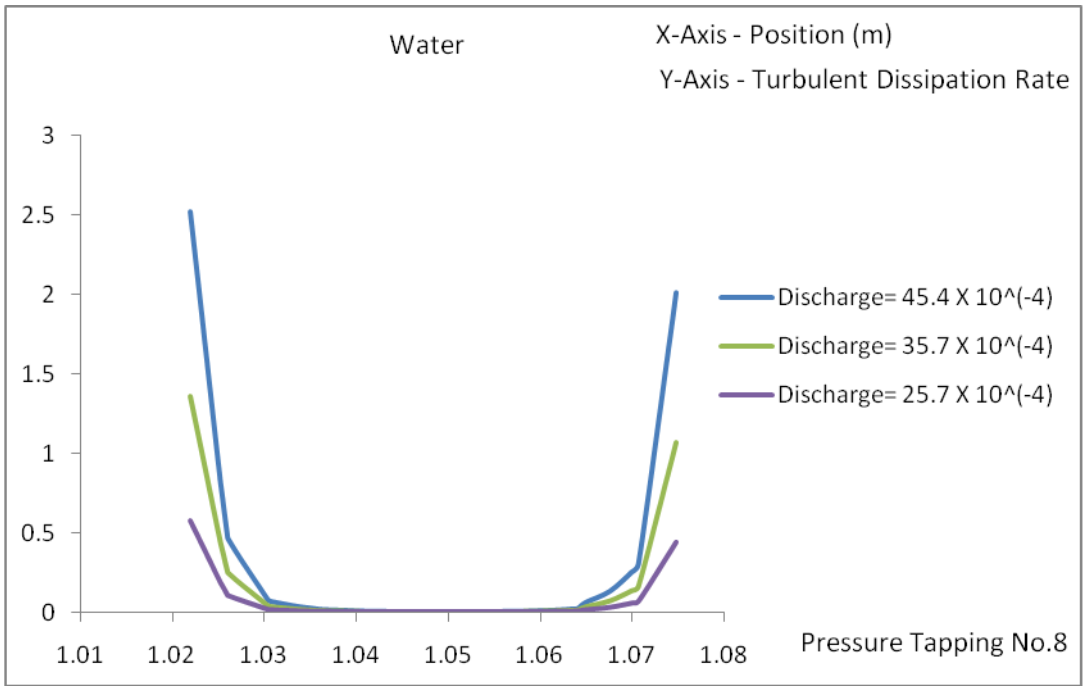

Figure No.6.5 (d): Turbulent dissipation rate at pressure tapping no. 8 for different discharges

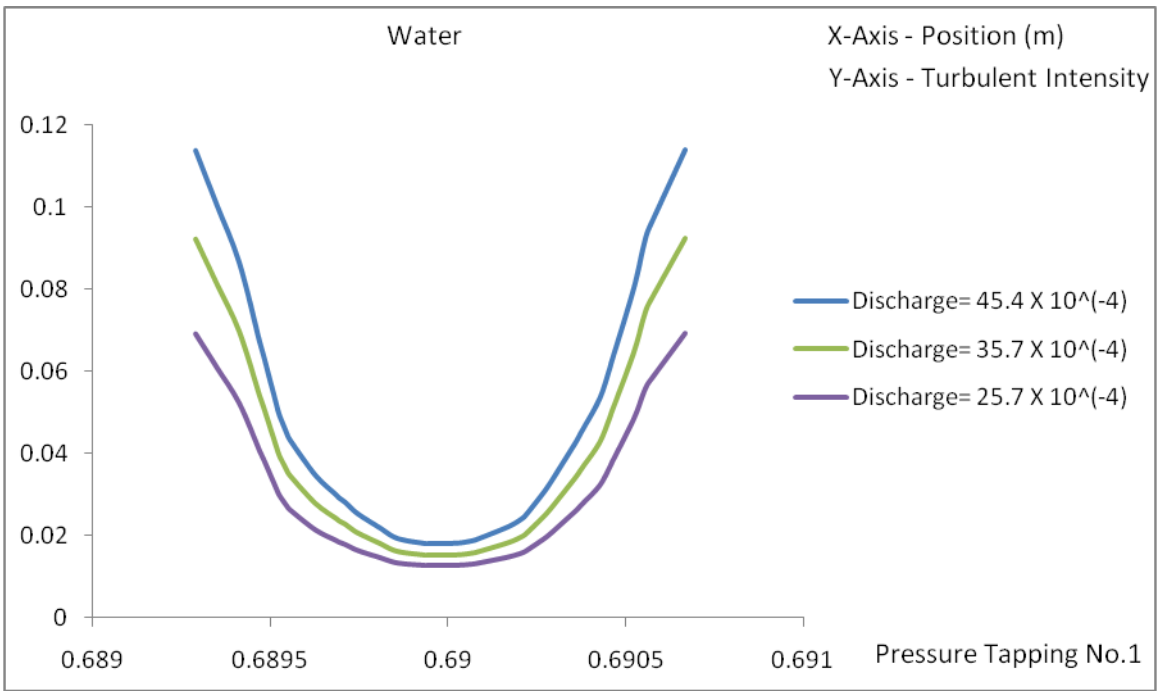

Figure No.6.6 (a): Turbulence intensity at pressure tapping no. 1 for different discharges

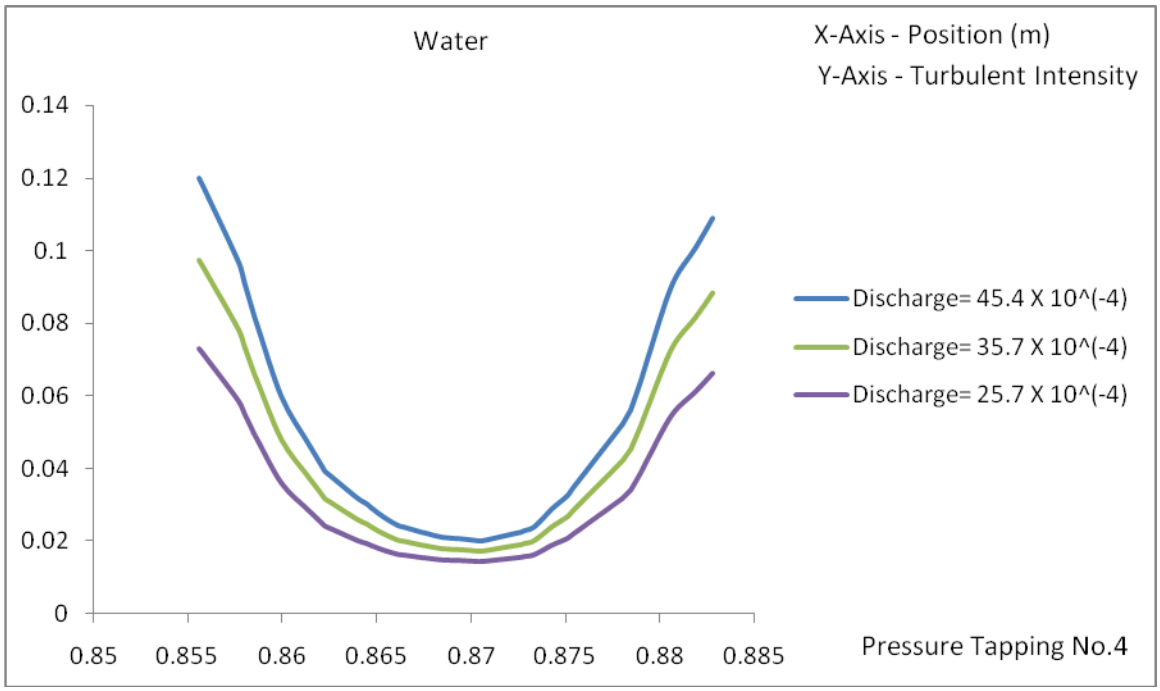

Figure No.6.6 (b): Turbulence intensity at pressure tapping no.4 for different discharges

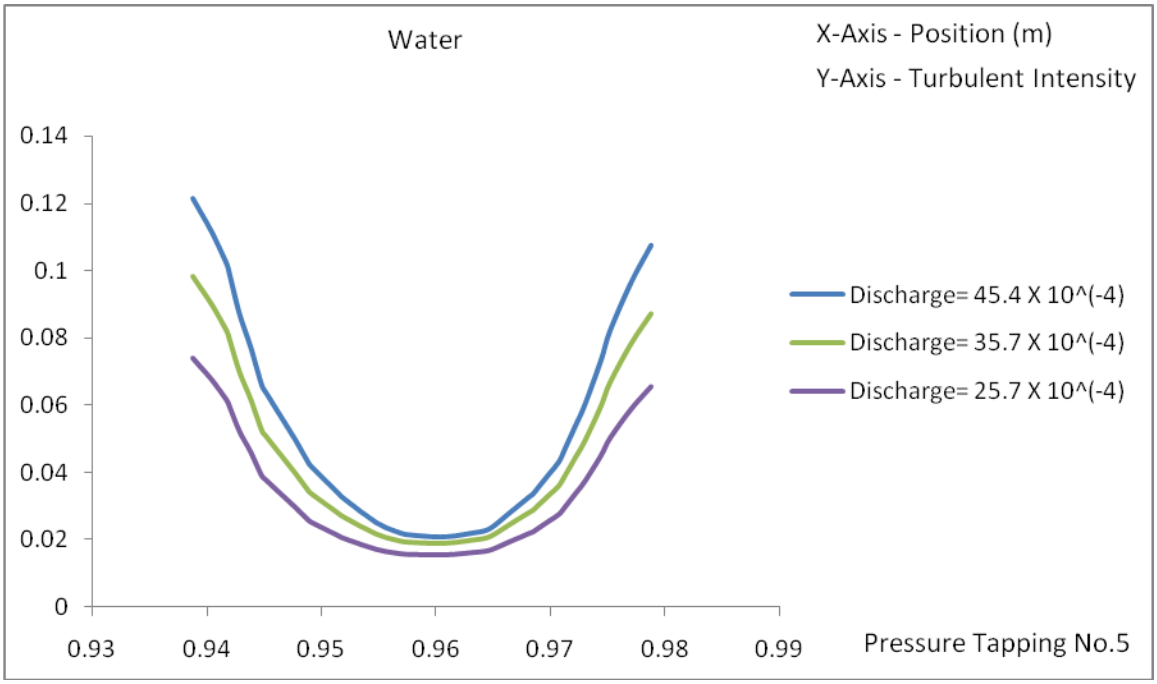

Figure No.6.6 (c): Turbulence intensity at pressure tapping no.5 for different discharges

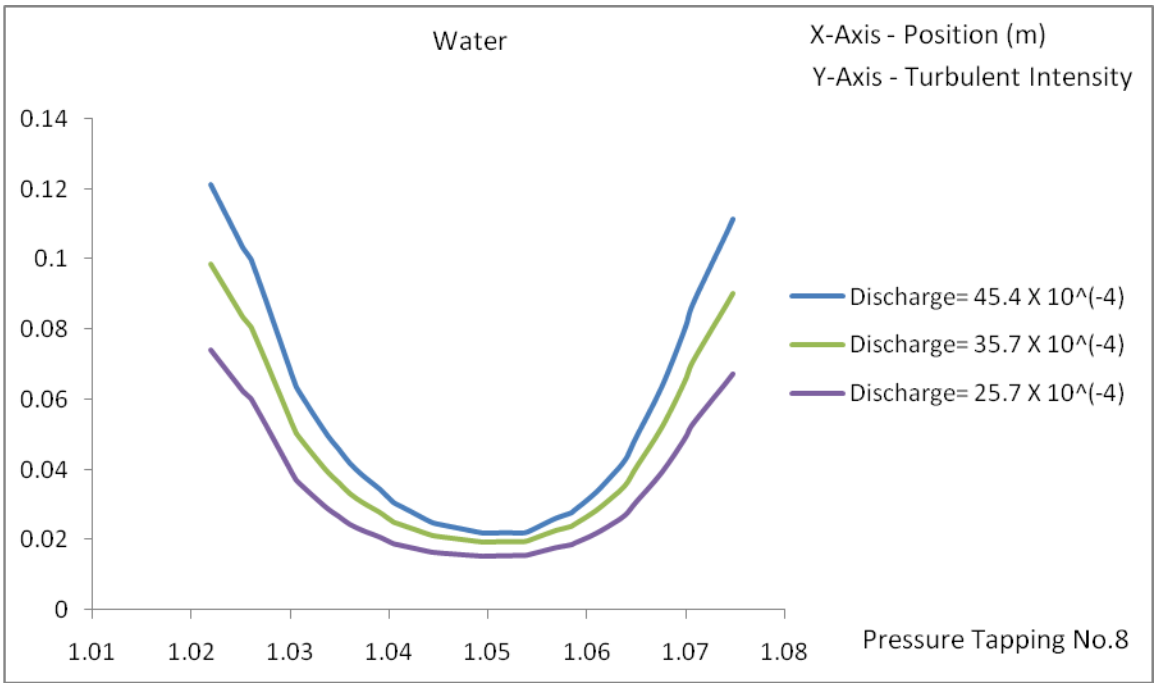

Figure No.6.6 (d): Turbulence intensity at pressure tapping no.8 for different discharges

6.1.2 Pressure drop with slurry (bottom ash) in pipe bend

The pressure drop is measured with different concentrations of bottom ash 10% and 20% with different flow discharges. Figure No. 6.7 (a), (b) & (c) shows the pressure contours at three different discharges for 10% bottom ash and Figure No. 6.8 (a), (b) & (c) shows the pressure contours for 20% bottom ash. These pressure contours shows that the pressure is maximum at starting of the bend and its decreases across the bend and it is minimum at the end of the bend. The pressure is increased with the increases in concentration. It is also observed that the pressure drop increases with the increase in flow velocity. Figure No.6.9 (a), (b), (c) & (d) shows the variation of pressure at the section of various pressure tapping for 10% bottom ash for different discharges and Figure No.6.10 (a), (b), (c) & (d) shows the variation of pressure at the section of various pressure tapping for 20% bottom ash The pressure is more on the outer side of the curvature as compared to the inner side of the bend and there magnitude increases with the increase in concentration. When the fluid strikes the outer side the kinetic energy due to velocity is converted into the pressure this increases the pressure on outer side of bend. Figure No.6.11 (a), (b), (c) & (d) shows the comparison of velocity at the section of different pressure tapping for 10% bottom ash for different discharges and Figure No.6.12 (a), (b), (c) & (d) shows the comparison of velocity at the section of different pressure tapping for 20% bottom ash. It is found that the velocity is increased with the increases in discharge and is maximum at the centre of the pipe and minimum at the periphery of pipe. Figure No.6.13 (a), (b), (c), (d) shows the turbulent dissipation rate for different discharges at different sections for 10% bottom ash and Figure No.6.14 (a), (b), (c), (d) shows the turbulent dissipation rate for 20% bottom ash. It is found that there is no turbulence dissipation rate at the centre of the pipe but the maximum dissipation occurs at the boundary of pipe. From these figures it can also be concluded that the turbulent dissipation rate at boundary increases with the increase in discharge and reduces with increase in concentration. The maximum dissipation rate occurs at boundary as the kinetic energy of incoming water immediately transfers to the wall of pipe after striking to the bend. Figure No.6.15 (a), (b), (c) & (d) shows the turbulence intensity for different discharges for 10% bottom ash at different sections of pipe bend and Figure No.6.16 (a), (b), (c) & (d) shows the turbulence intensity for 20% bottom ash. It is found that the turbulence intensity is maximum at the boundary of pipe but minimum at the center of the pipe.

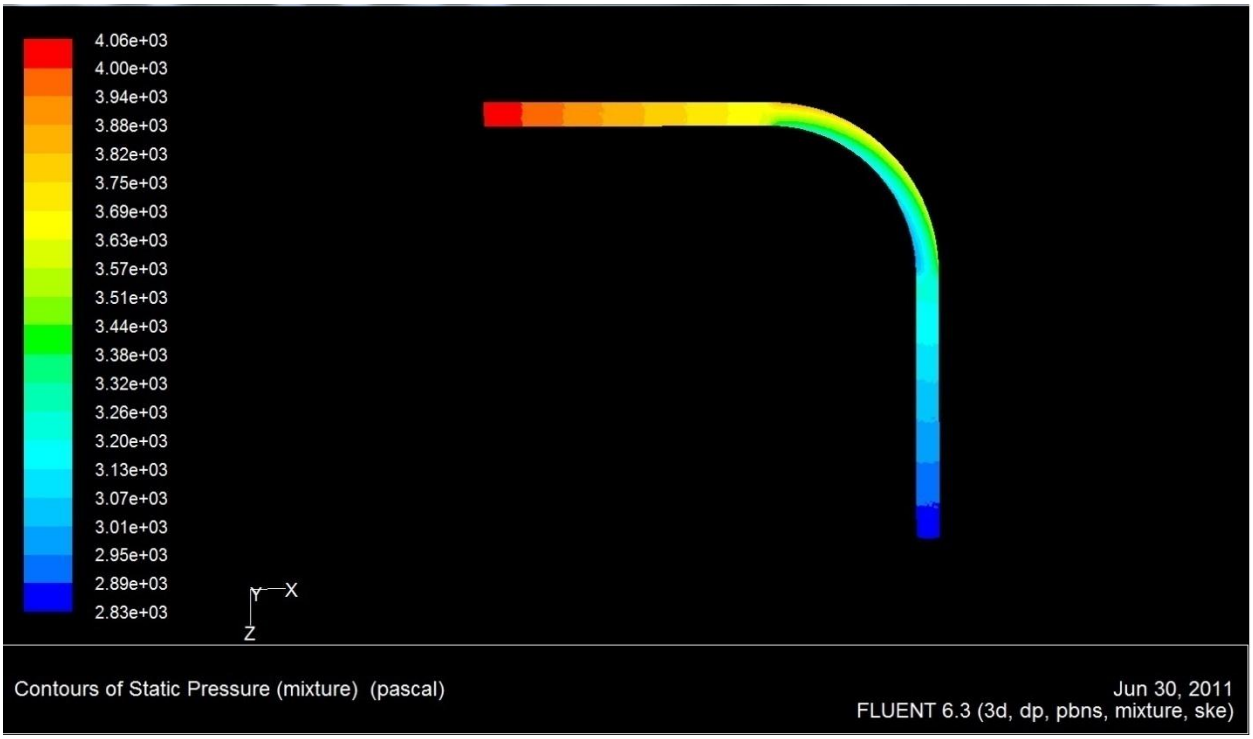

Figure No. 6.7(a): Pressure contour for 45.4 X 10^{-4} m^3/sec discharge with 10% bottom ash

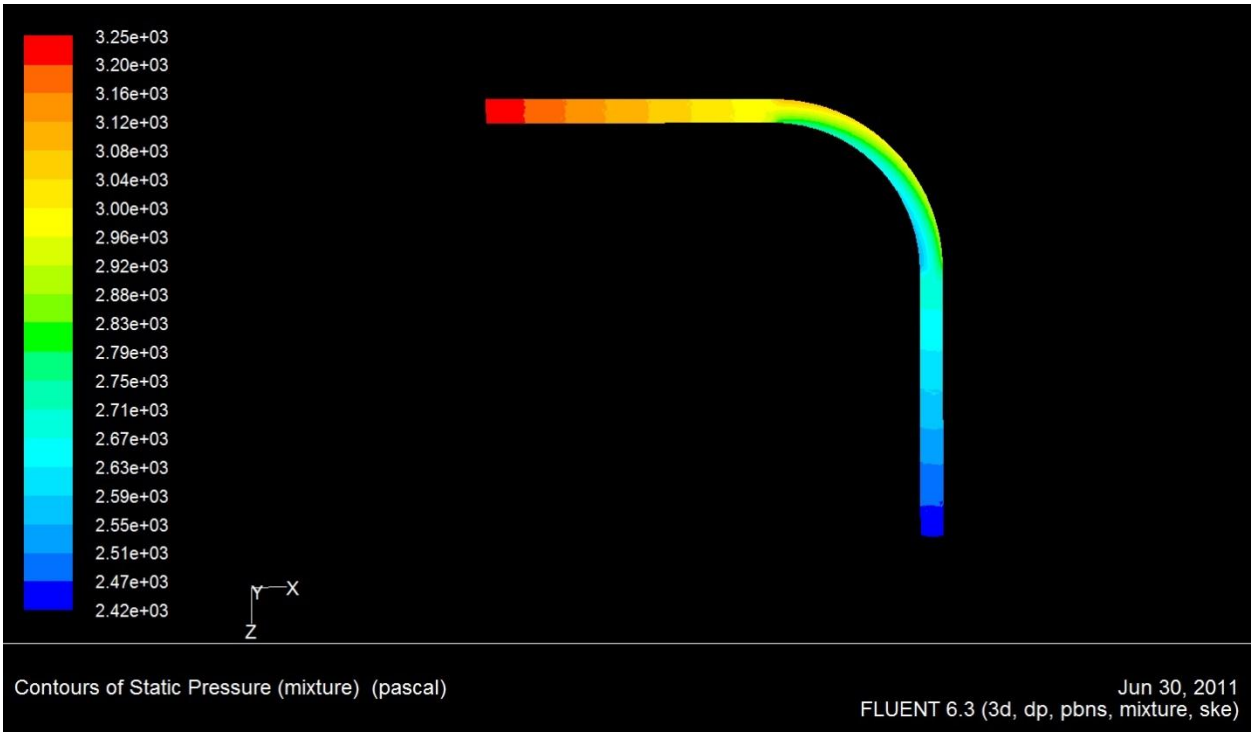

Figure No. 6.7(b): Pressure contour for 35.7 X 10^{-4} m^3/sec discharge with 10% bottom ash

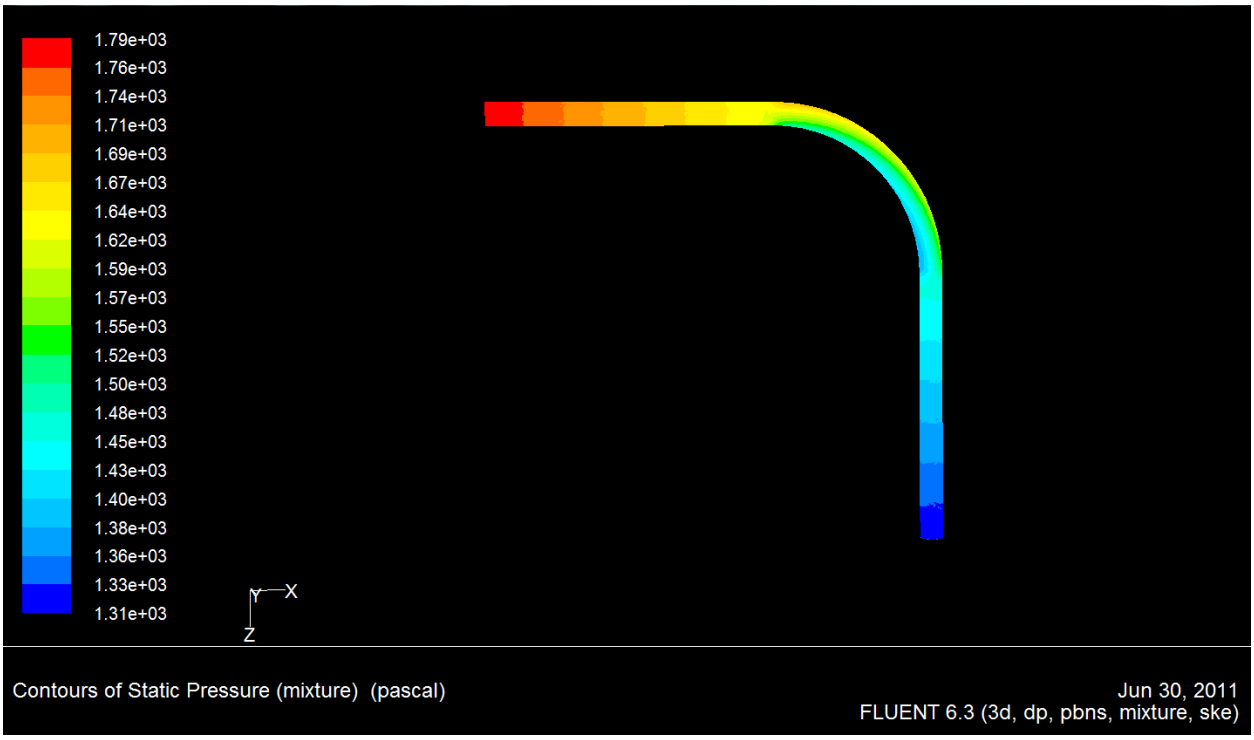

Figure No. 6.7(c): Pressure contour for 25.7 X 10^{-4} m^3/sec discharge with 10% bottom ash

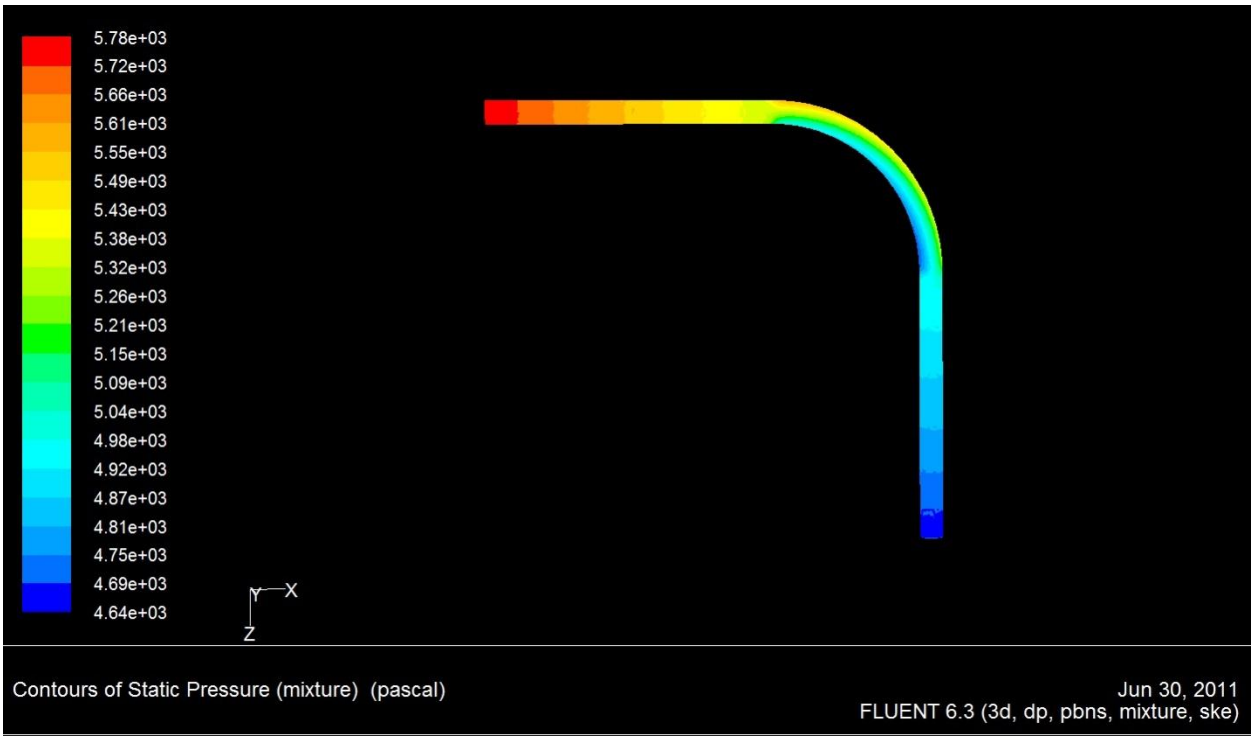

Figure No. 6.8(a): Pressure contour for 45.7 X 10^{-4} m^3/sec discharge with 20% bottom ash

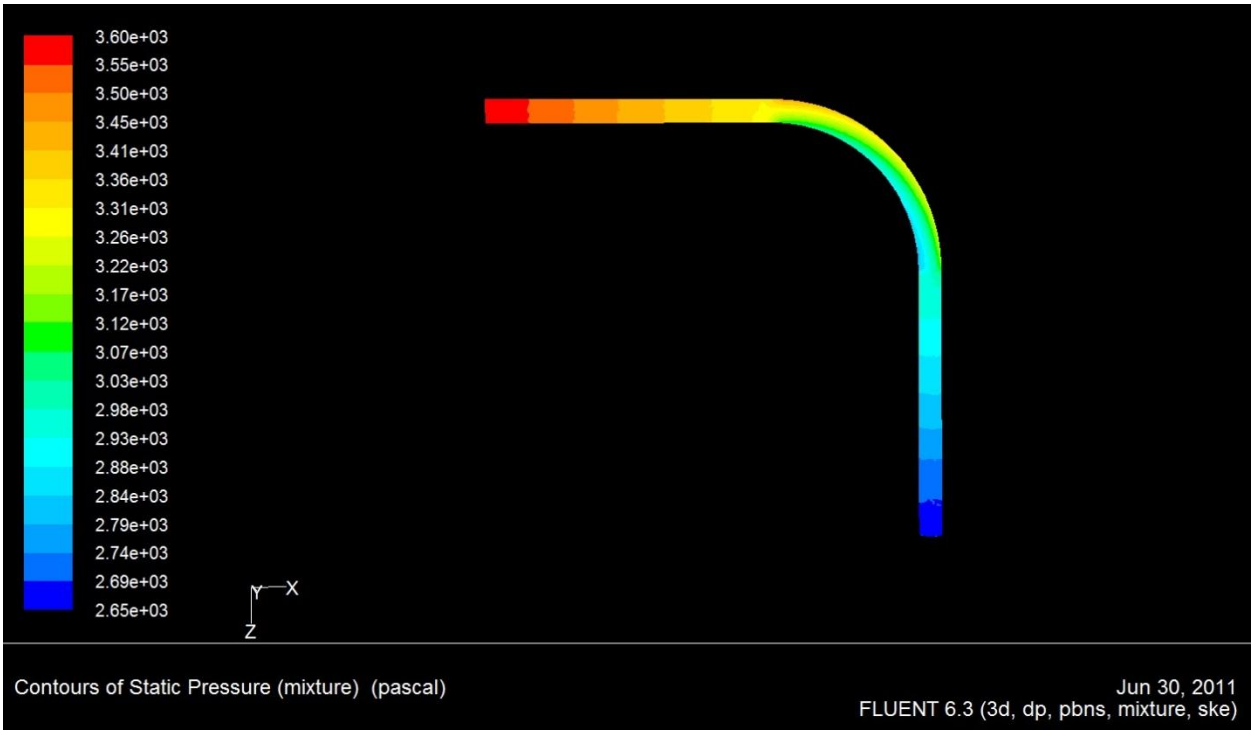

Figure No. 6.8(b): Pressure contour for 35.7 X $10^{-4}\ m^3/sec$ discharge with 20% bottom ash

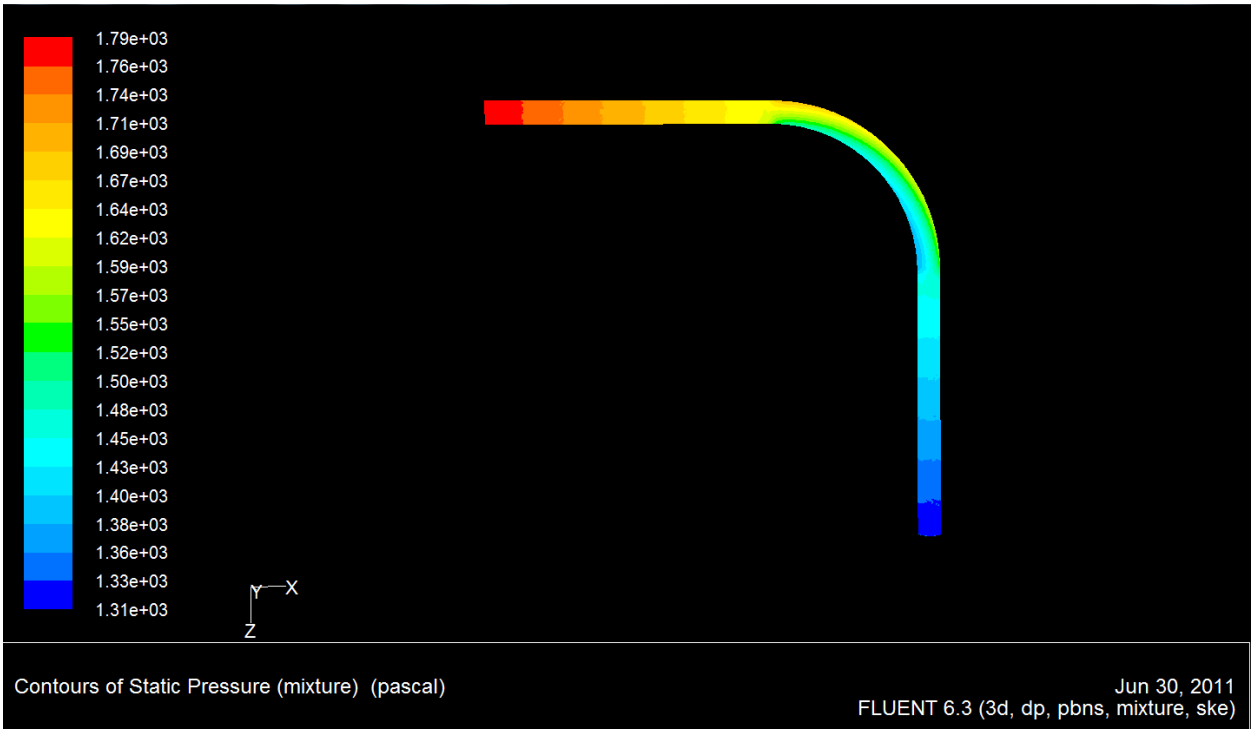

Figure No. 6.8(c): Pressure contour for 25.7 X $10^{-4}\ m^3/sec$ discharge with 20% bottom ash

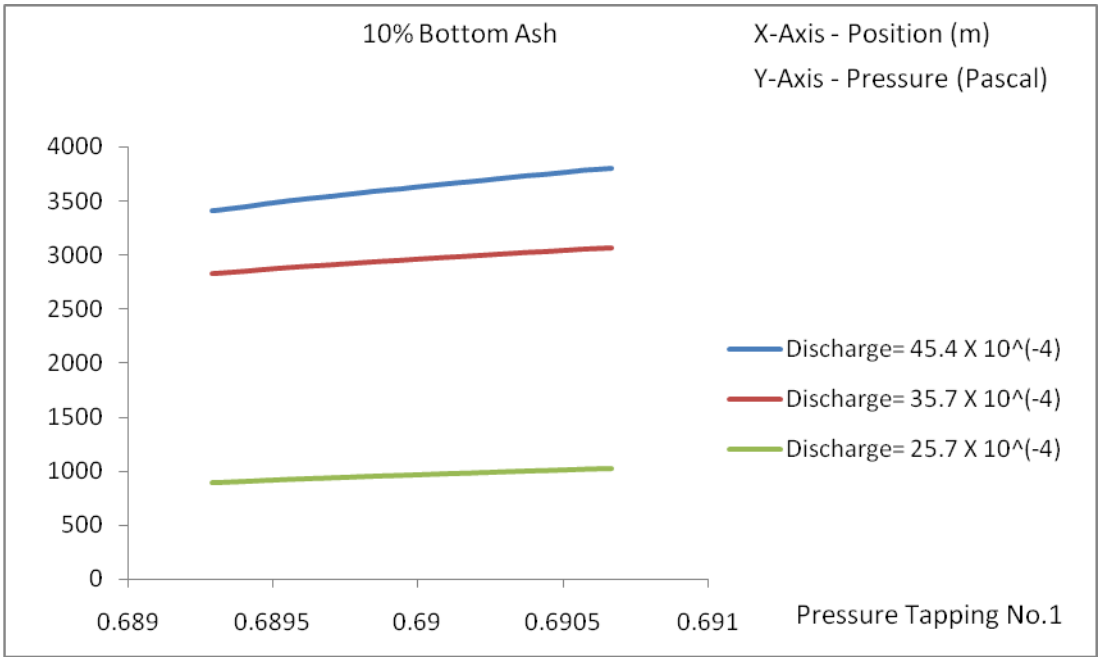

Figure No.6.9 (a): Variation of pressure at pressure tapping no.1 for different discharges with 10% bottom ash

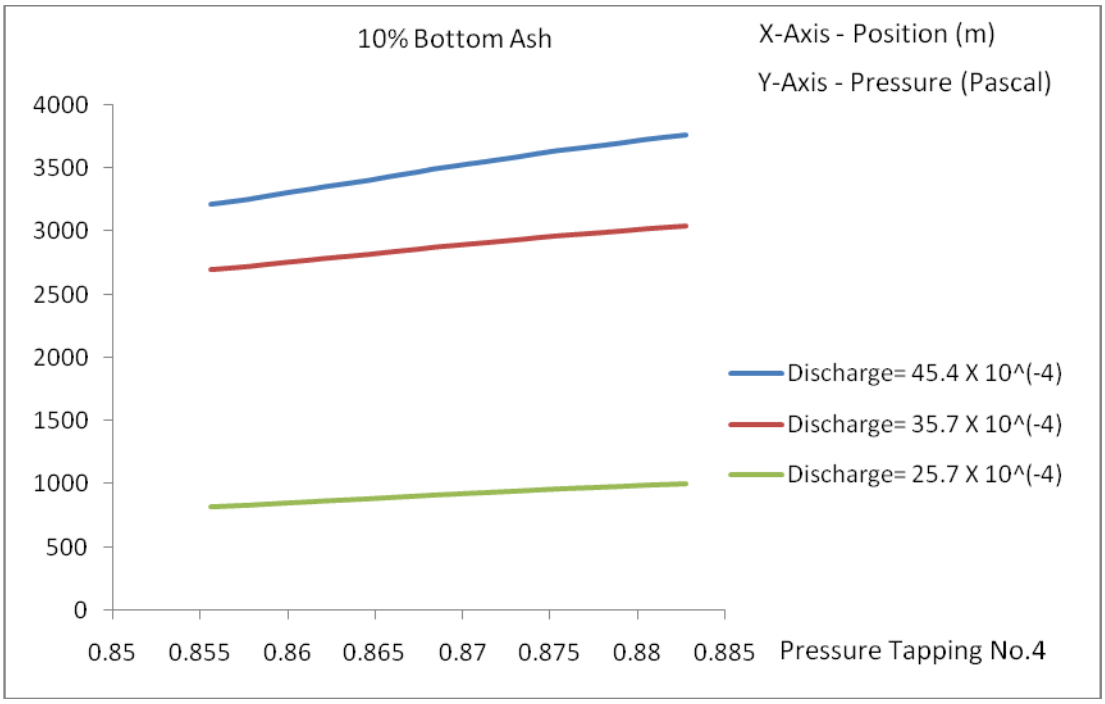

Figure No.6.9 (b): Variation of pressure at pressure tapping no.4 for different discharges with 10% bottom ash

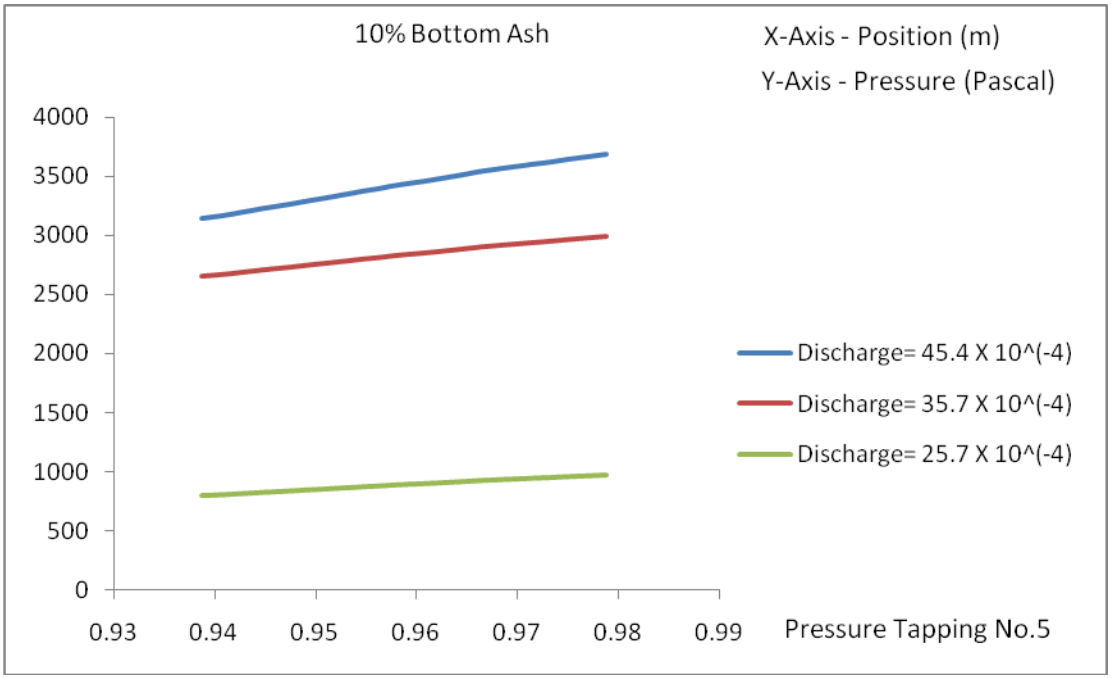

Figure No.6.9 (c): Variation of pressure at pressure tapping no.5 for different discharges with 10% bottom ash

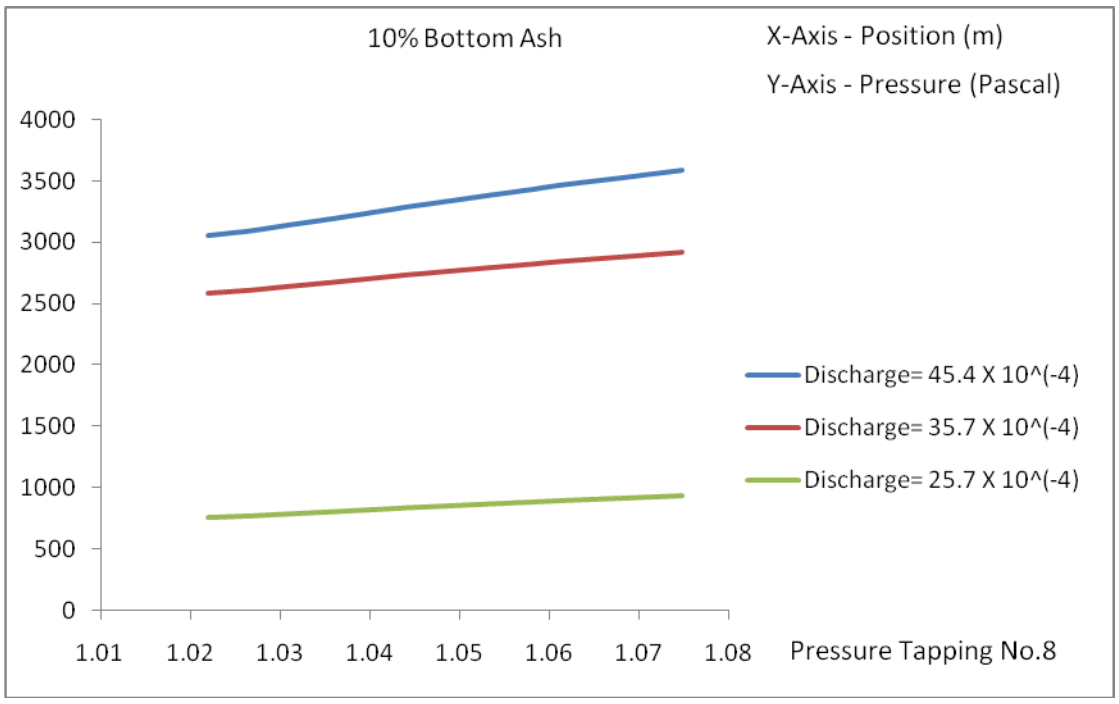

Figure No.6.9 (d): Variation of pressure at pressure tapping no.8 for different discharges with 10% bottom ash

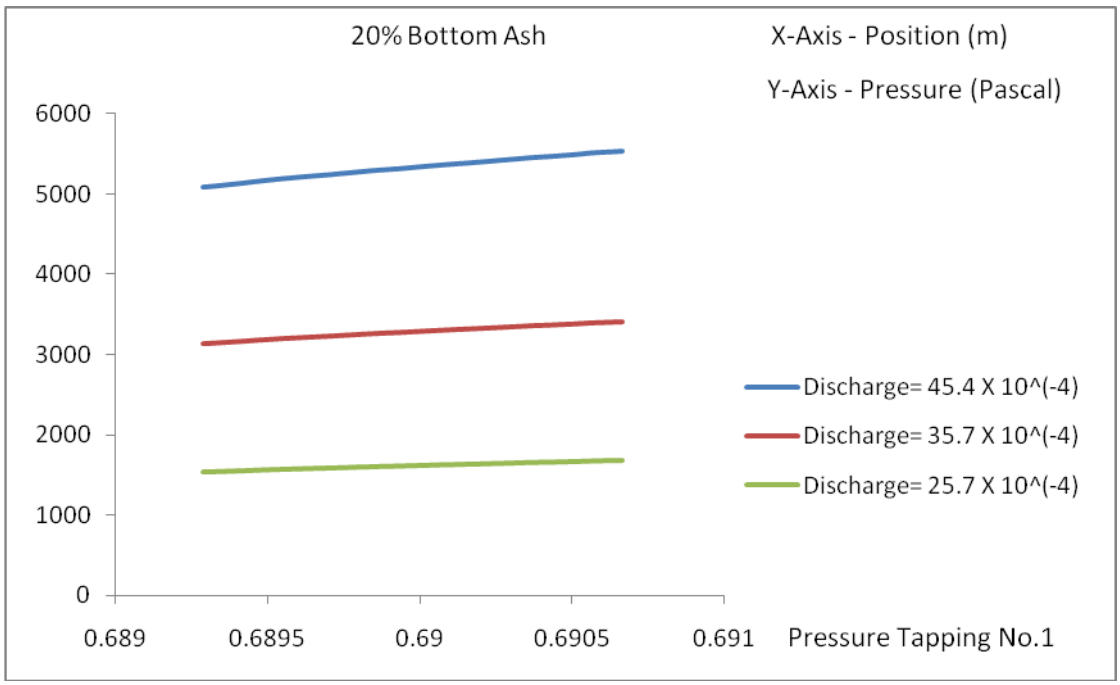

Figure No.6.10 (a): Variation of pressure at pressure tapping no.1 for different discharges with 20% bottom ash

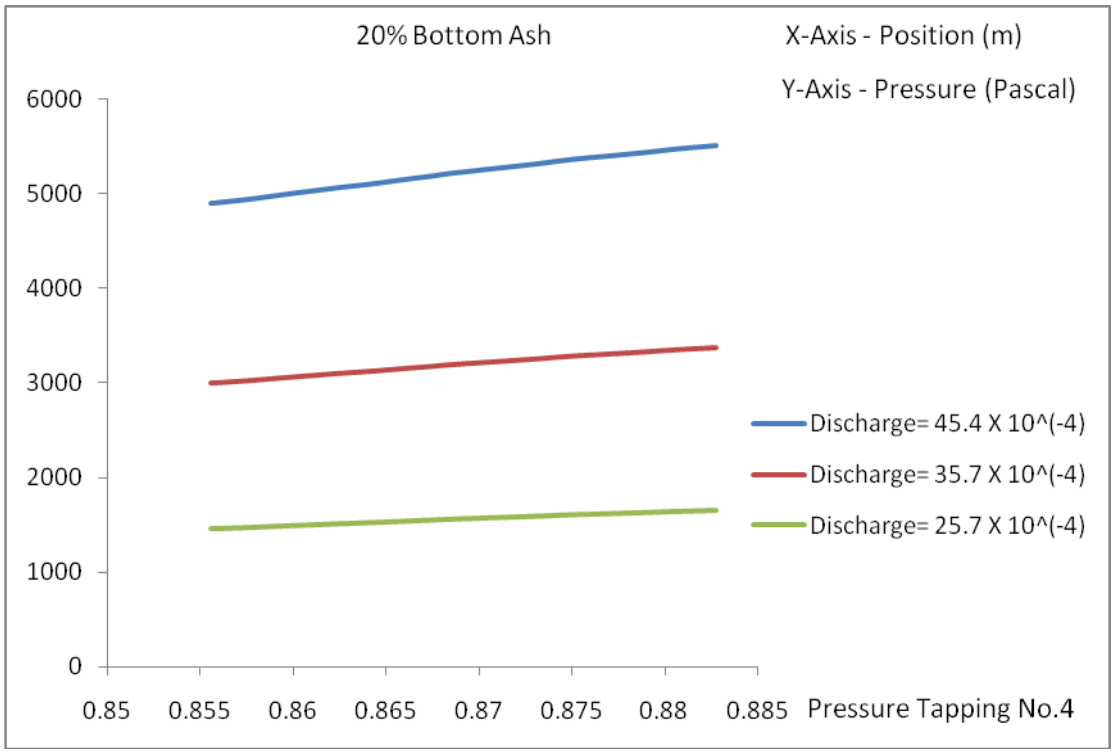

Figure No.6.10 (b): Variation of pressure at pressure tapping no.4 for different discharges with 20% bottom ash

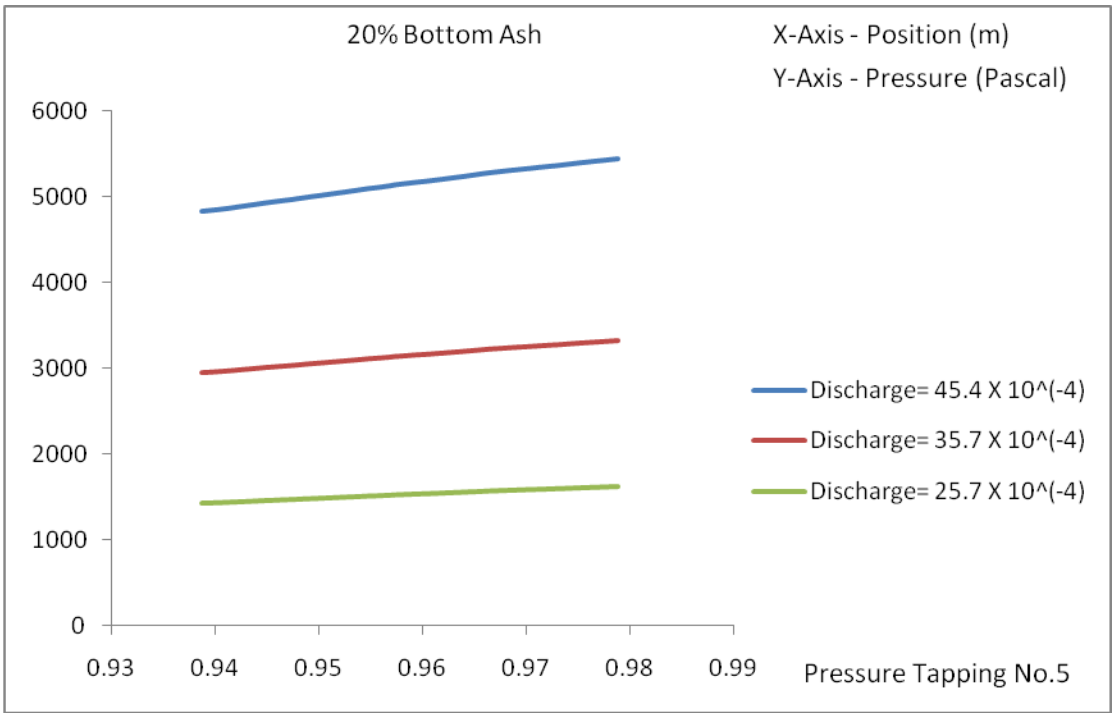

Figure No.6.10 (c): Variation of pressure at pressure tapping no.5 for different discharges with 20% bottom ash

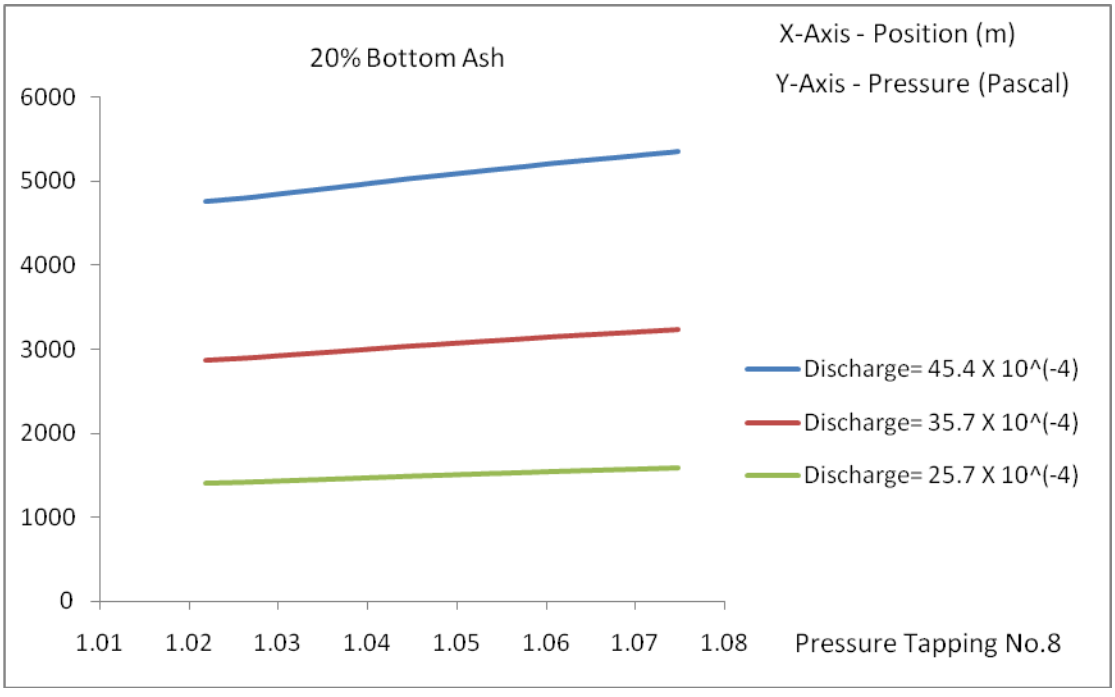

Figure No.6.10 (d): Variation of pressure at pressure tapping no.8 for different discharges with 20% bottom ash

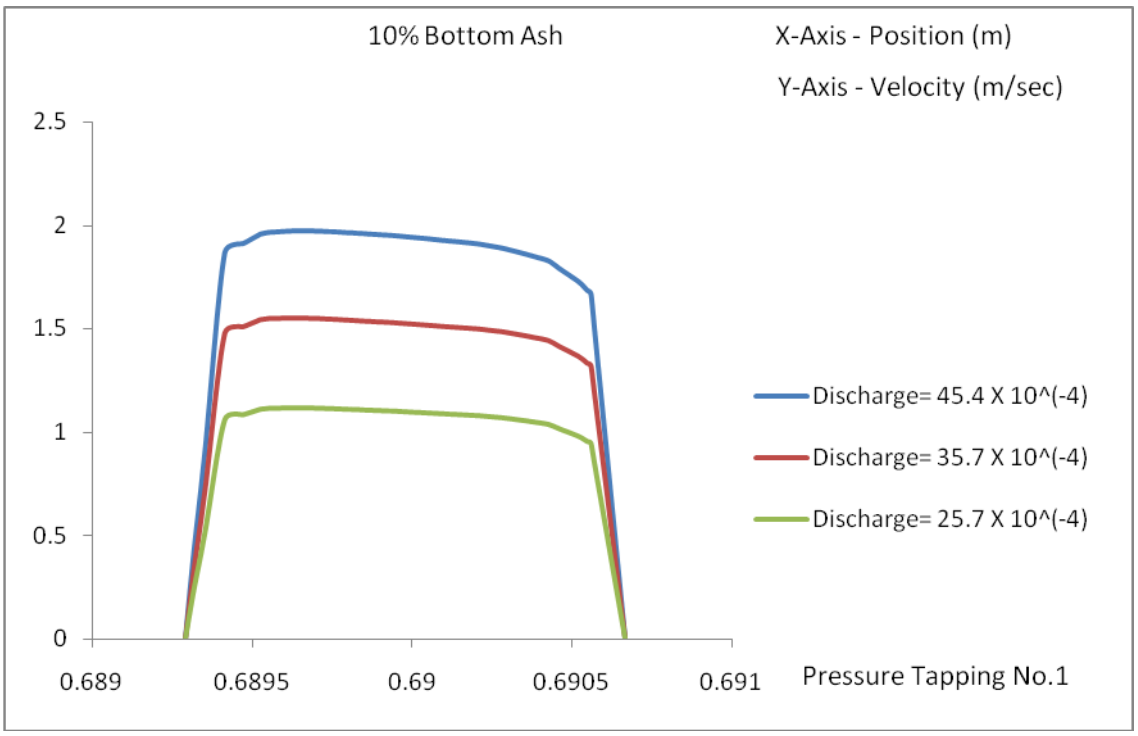

Figure No.6.11 (a): Variation of velocity at pressure tapping no.1 for different discharges with 10% bottom ash

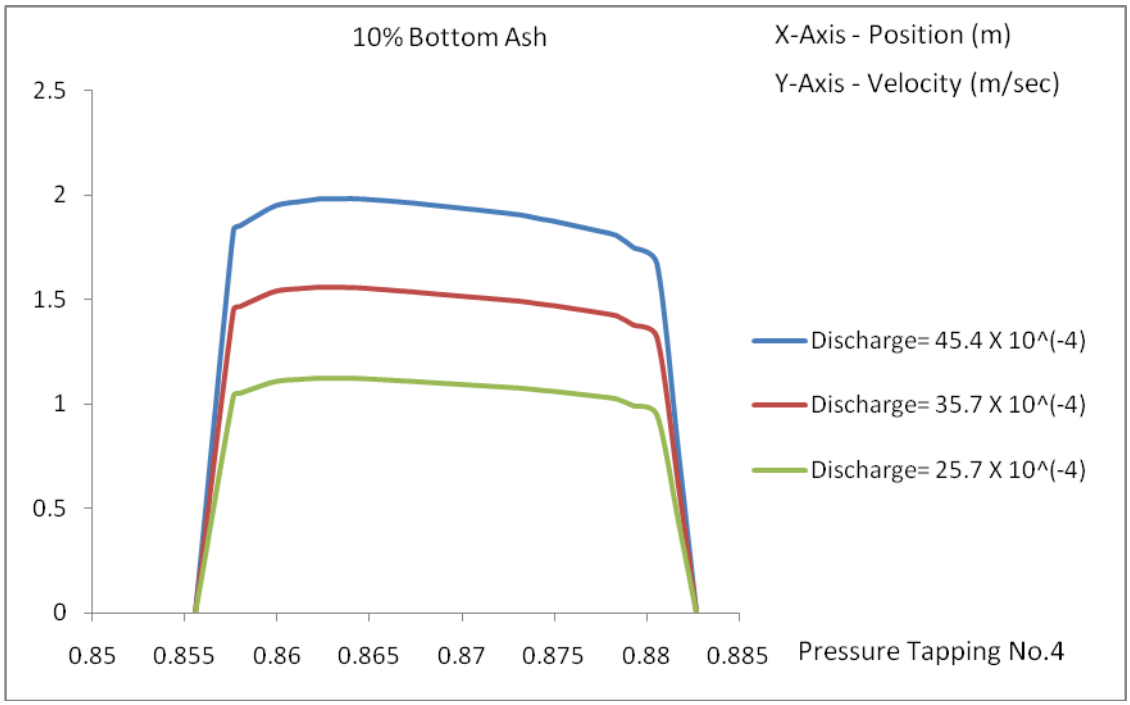

Figure No.6.11 (b): Variation of velocity at pressure tapping no.4 for different discharges with 10% bottom ash

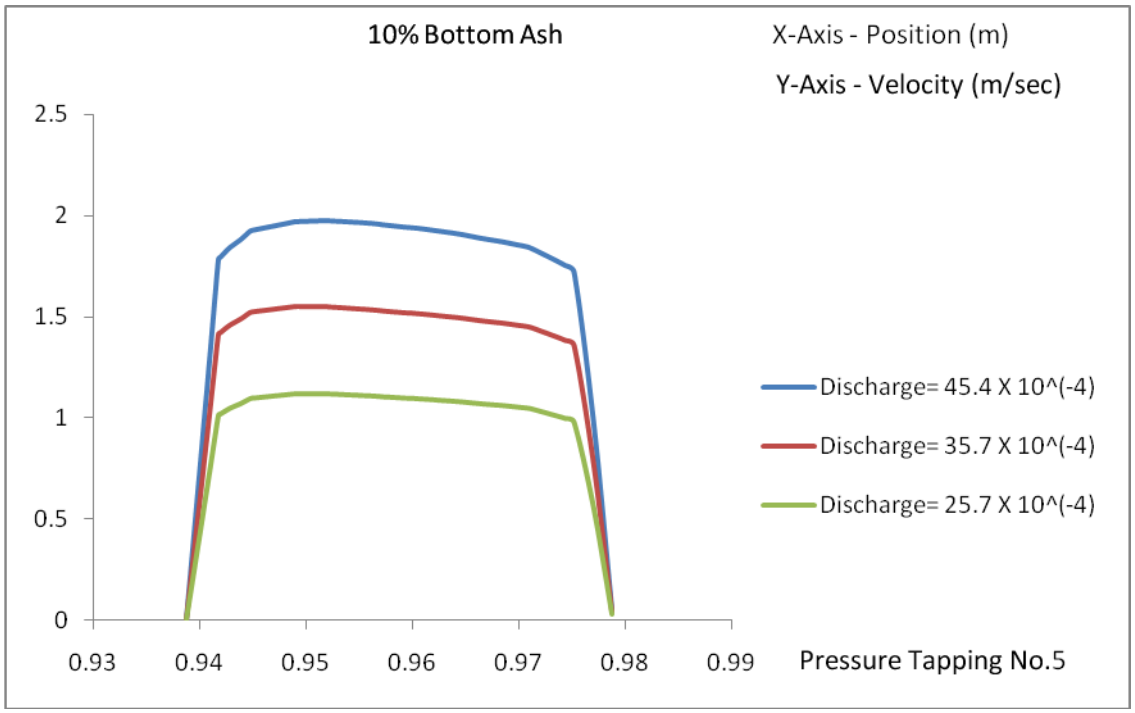

Figure No.6.11 (c): Variation of velocity at pressure tapping no.5 for different discharges with 10% bottom ash

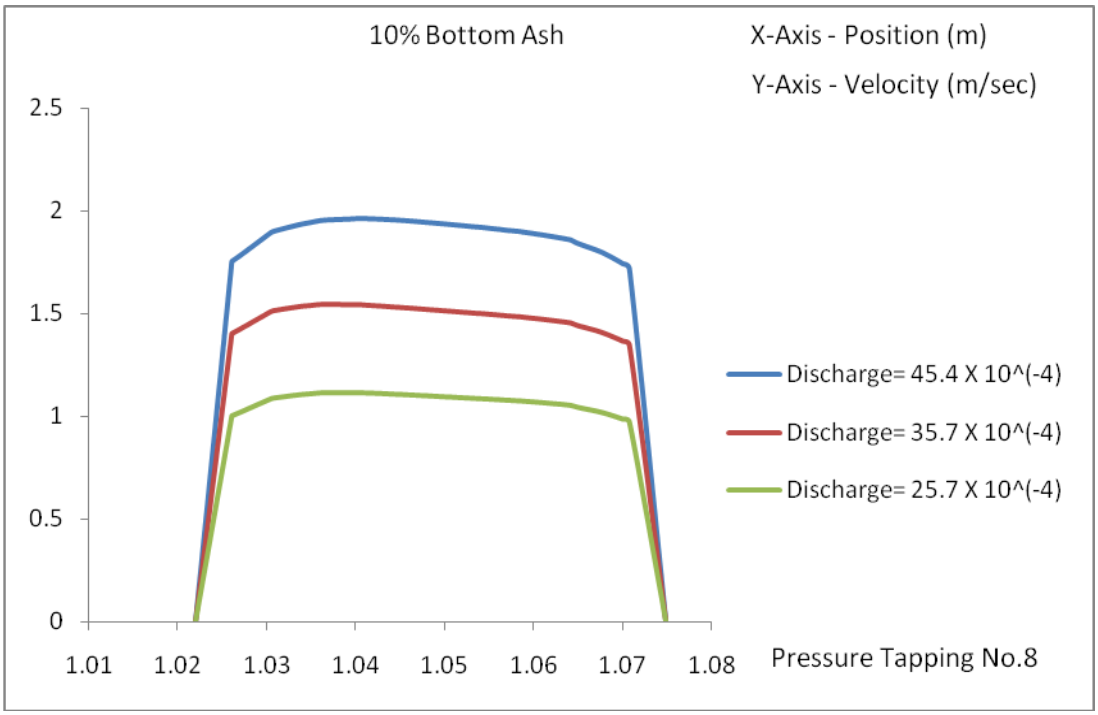

Figure No.6.11 (d): Variation of velocity at pressure tapping no.8 for different discharges with 10% bottom ash

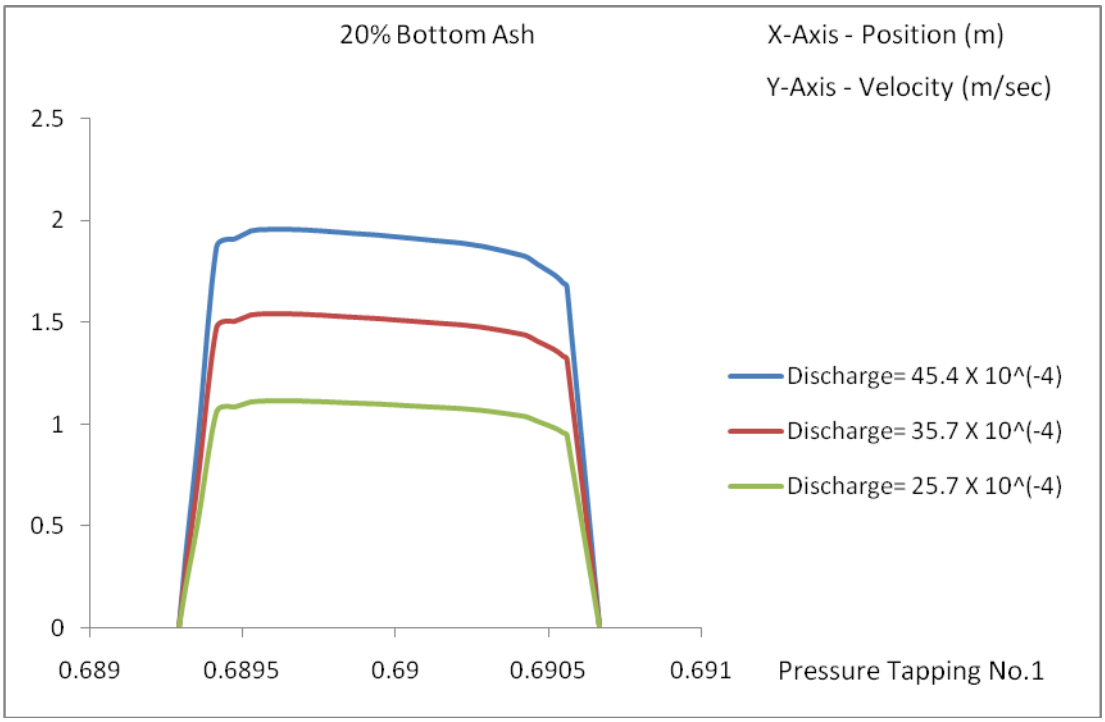

Figure No.6.12 (a): Variation of velocity at pressure tapping no.1 for different discharges with 20% bottom ash

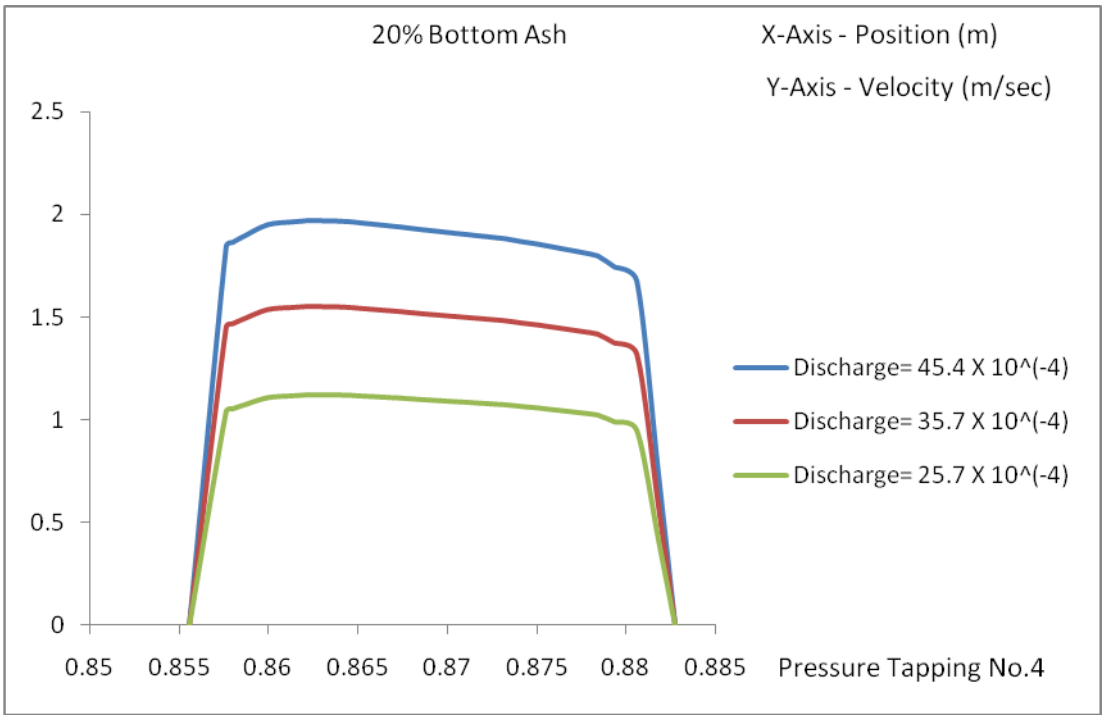

Figure No.6.12 (b): Variation of velocity at pressure tapping no.4 for different discharges with 20% bottom ash

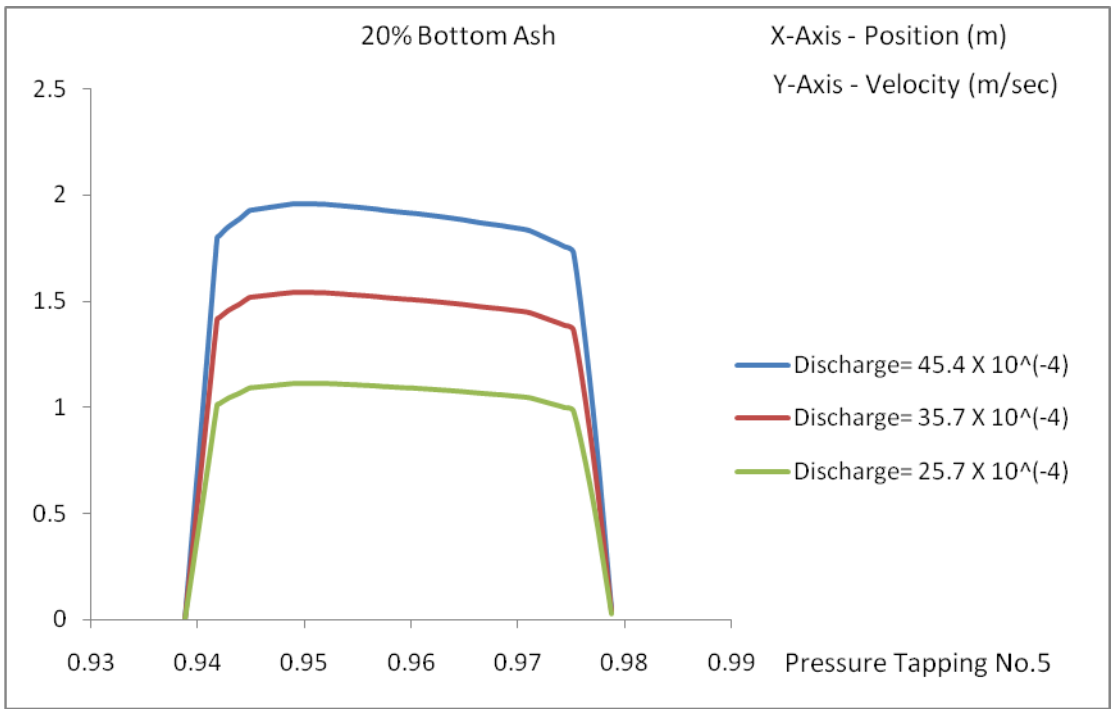

Figure No.6.12 (c): Variation of velocity at pressure tapping no.5 for different discharges with 20% bottom ash

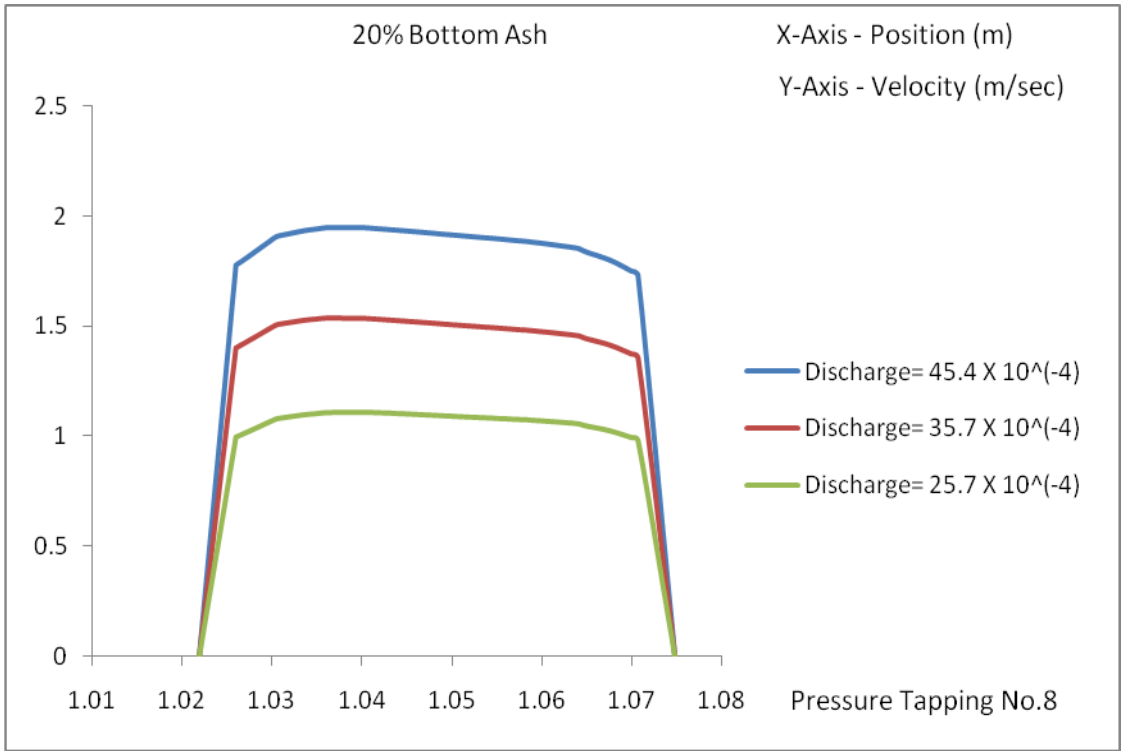

Figure No.6.12 (d): Variation of velocity at pressure tapping no.8 for different discharges with 20% bottom ash

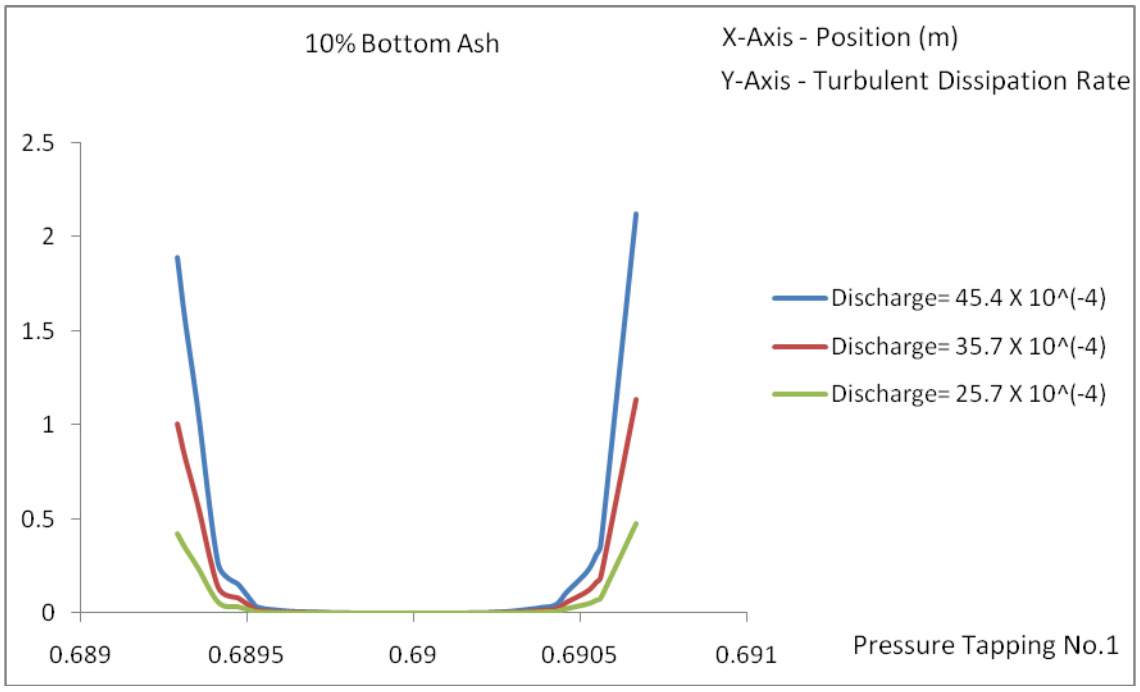

Figure No.6.13 (a): Turbulent dissipation rate at pressure tapping no.1 for different discharges with 10% bottom ash

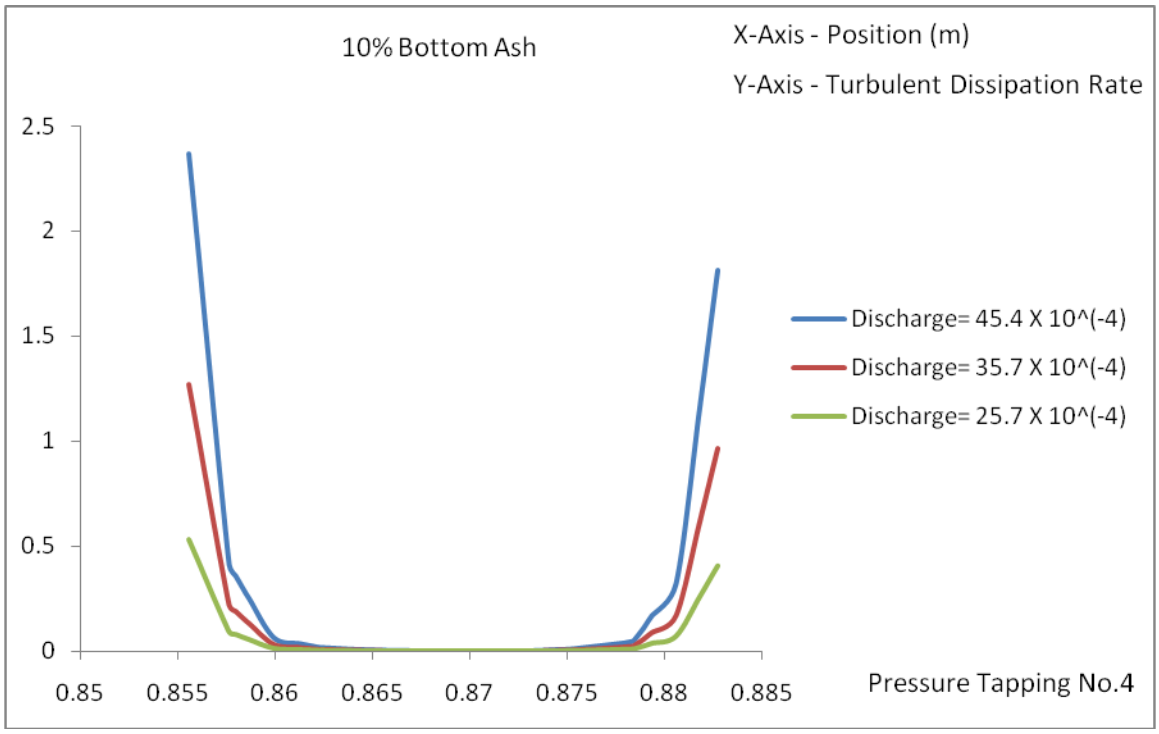

Figure No.6.13 (b): Turbulent dissipation rate at pressure tapping no.4 for different discharges with 10% bottom ash

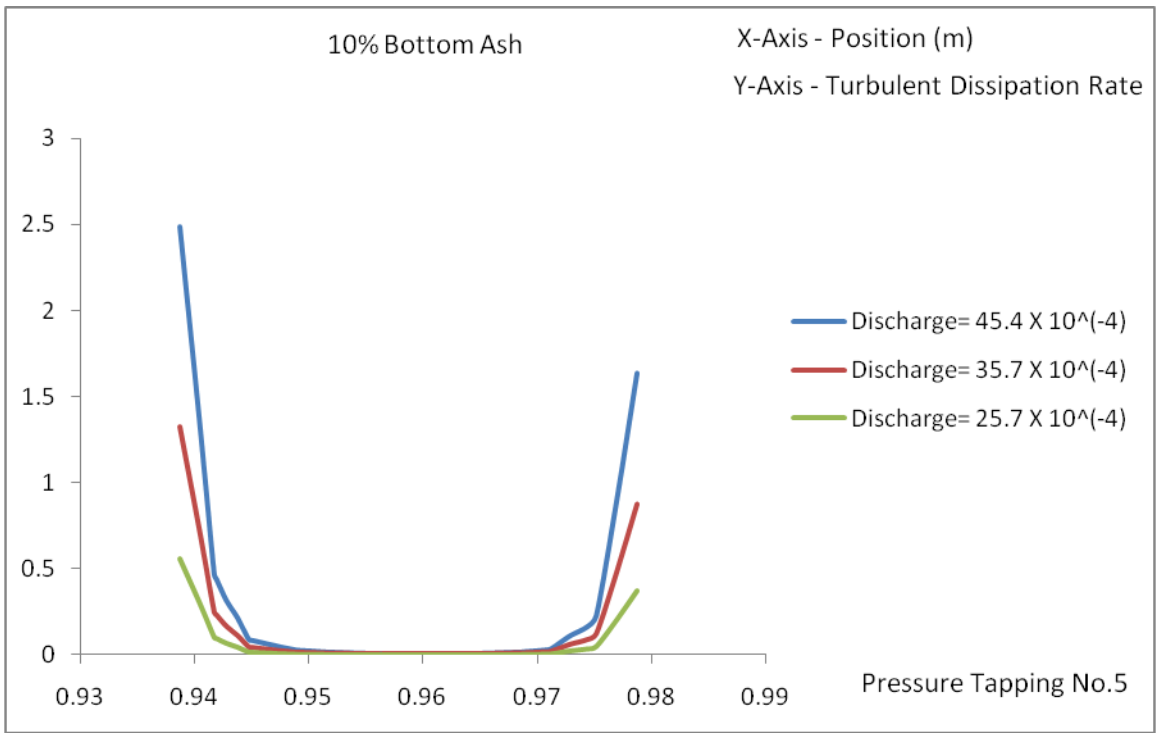

Figure No.6.13 (c): Turbulent dissipation rate at pressure tapping no.5 for different discharges with 10% bottom ash

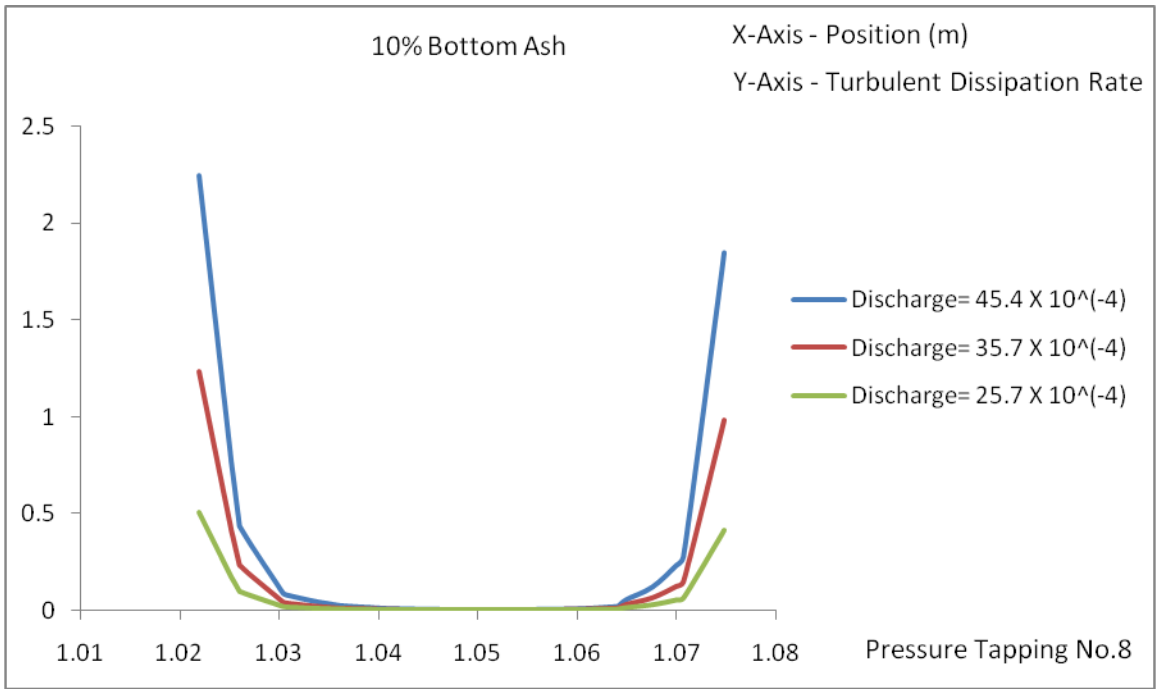

Figure No.6.13 (d): Turbulent dissipation rate at pressure tapping no.8 for different discharges with 10% bottom ash

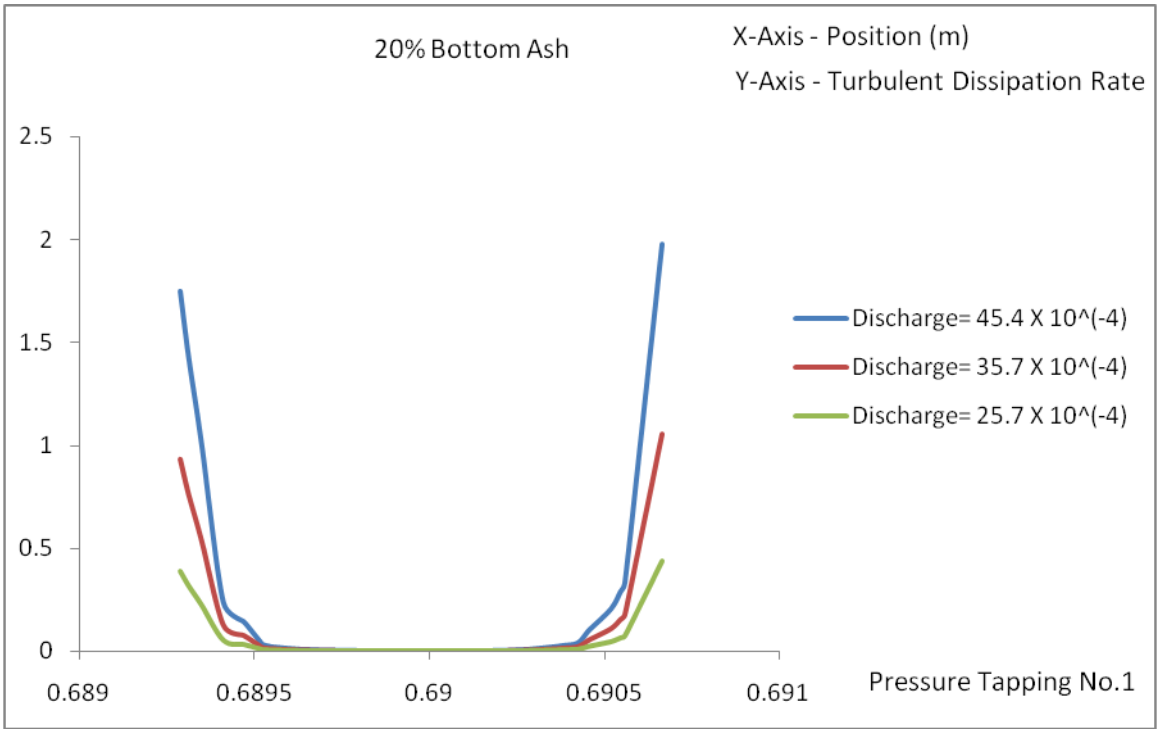

Figure No.6.14 (a): Turbulent dissipation rate at pressure tapping no.1 for different discharges with 20% bottom ash

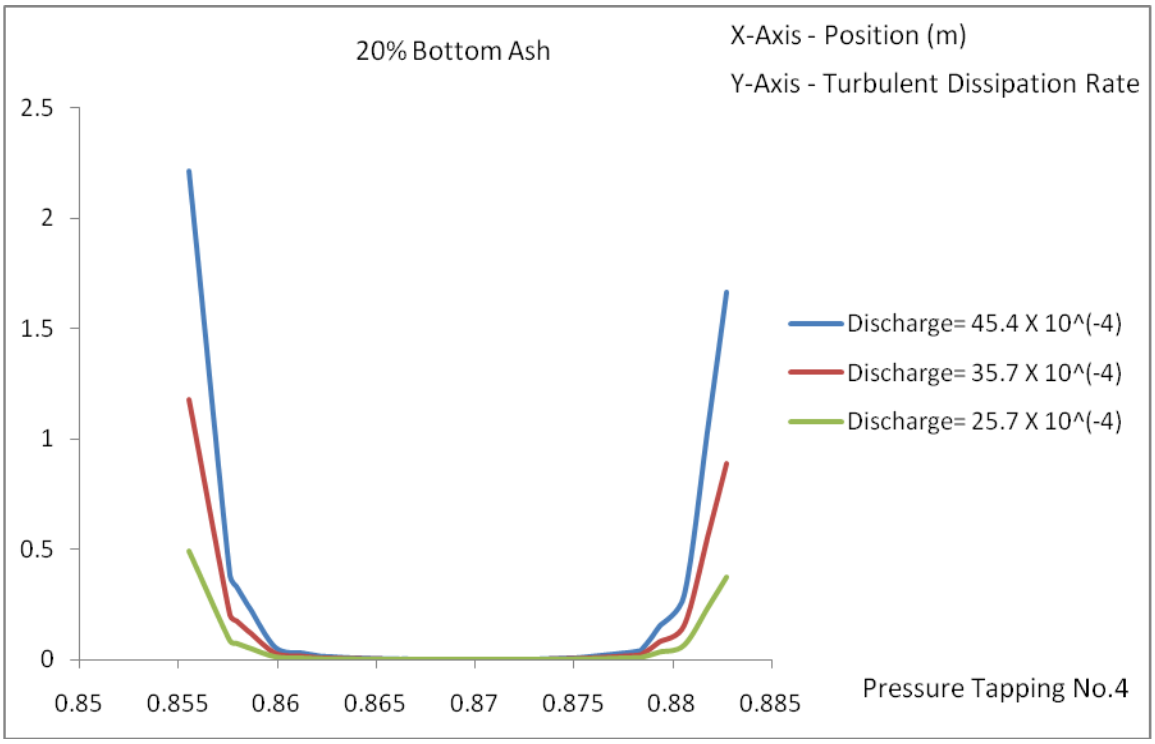

Figure No.6.14 (b): Turbulent dissipation rate at pressure tapping no.4 for different discharges with 20% bottom ash

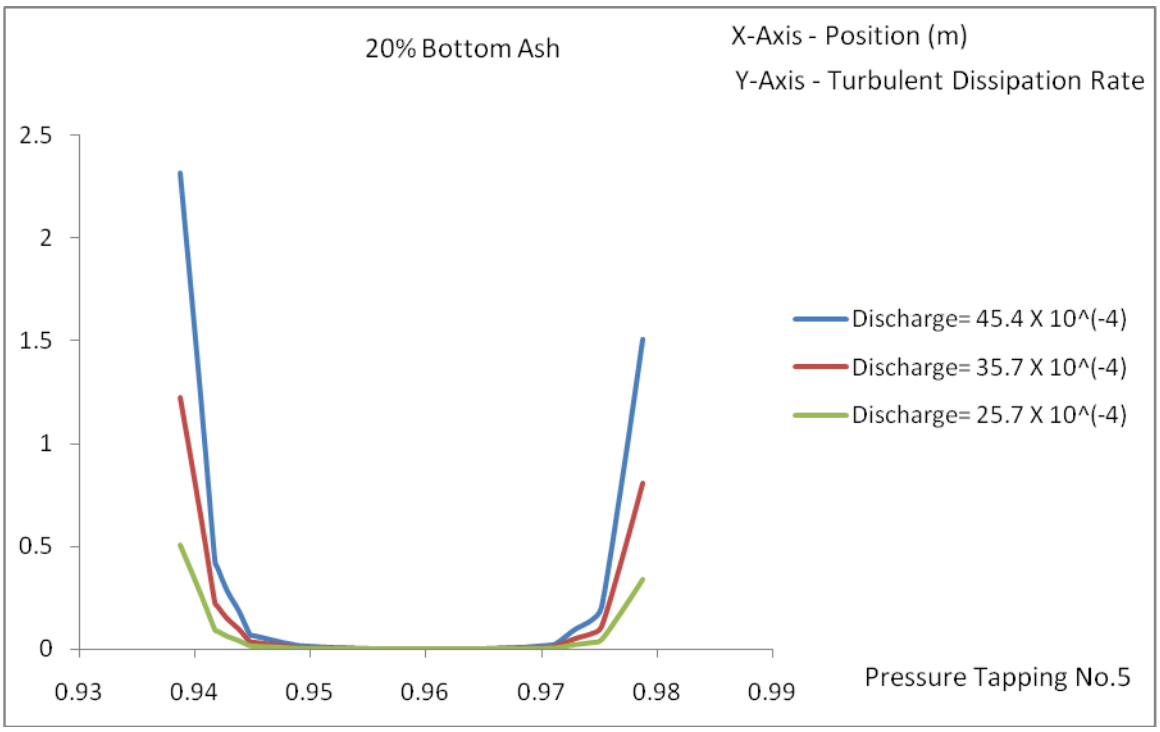

Figure No.6.14 (c): Turbulent dissipation rate at pressure tapping no.5 for different discharges with 20% bottom ash

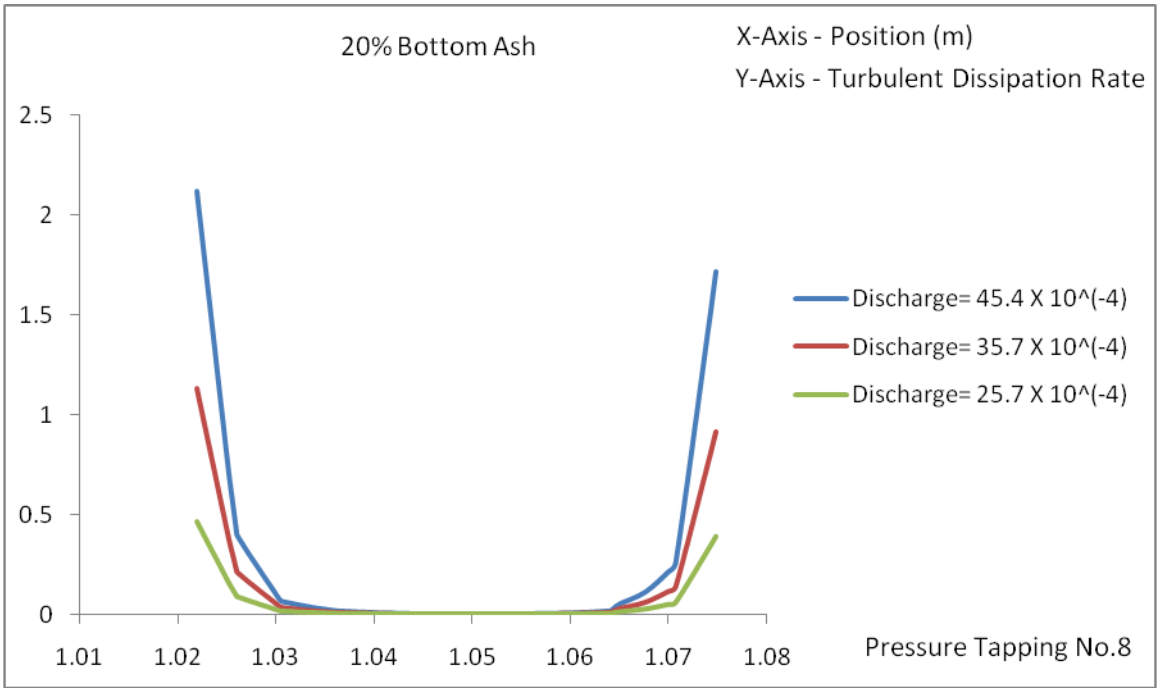

Figure No.6.14 (d): Turbulent dissipation rate at pressure tapping no.8 for different discharges with 20% bottom ash

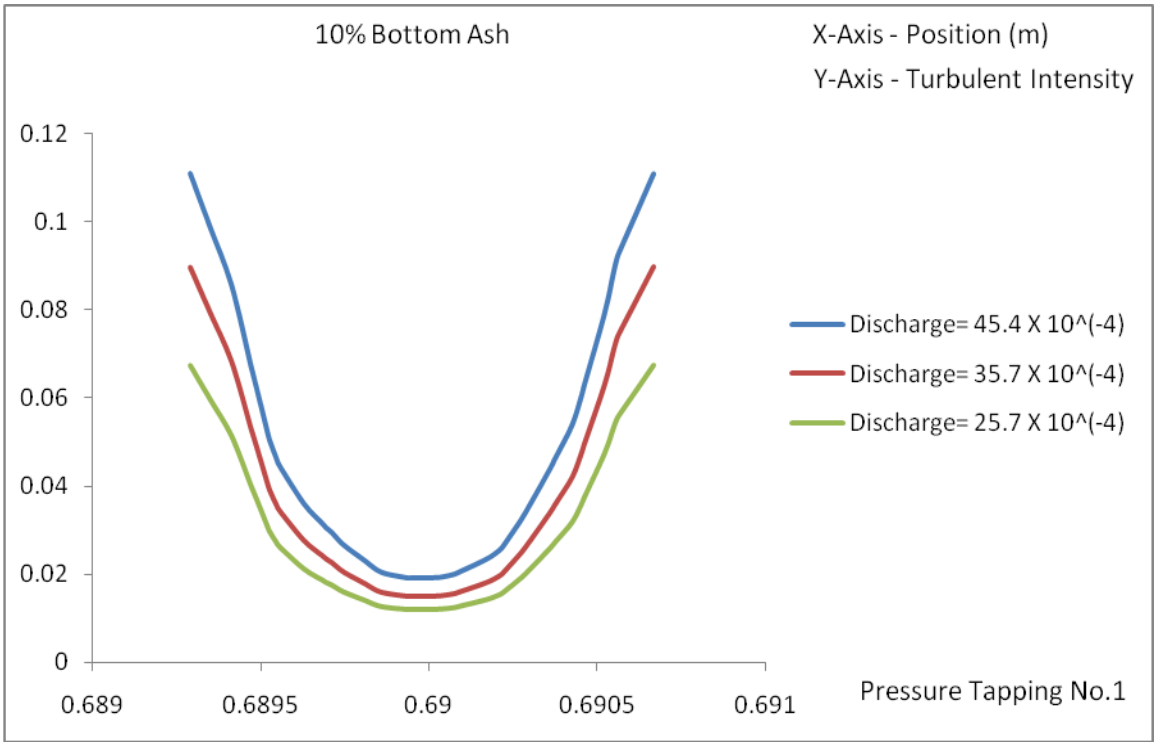

Figure No.6.15 (a): Turbulent intensity at pressure tapping no.1 for different discharges with 10% bottom ash

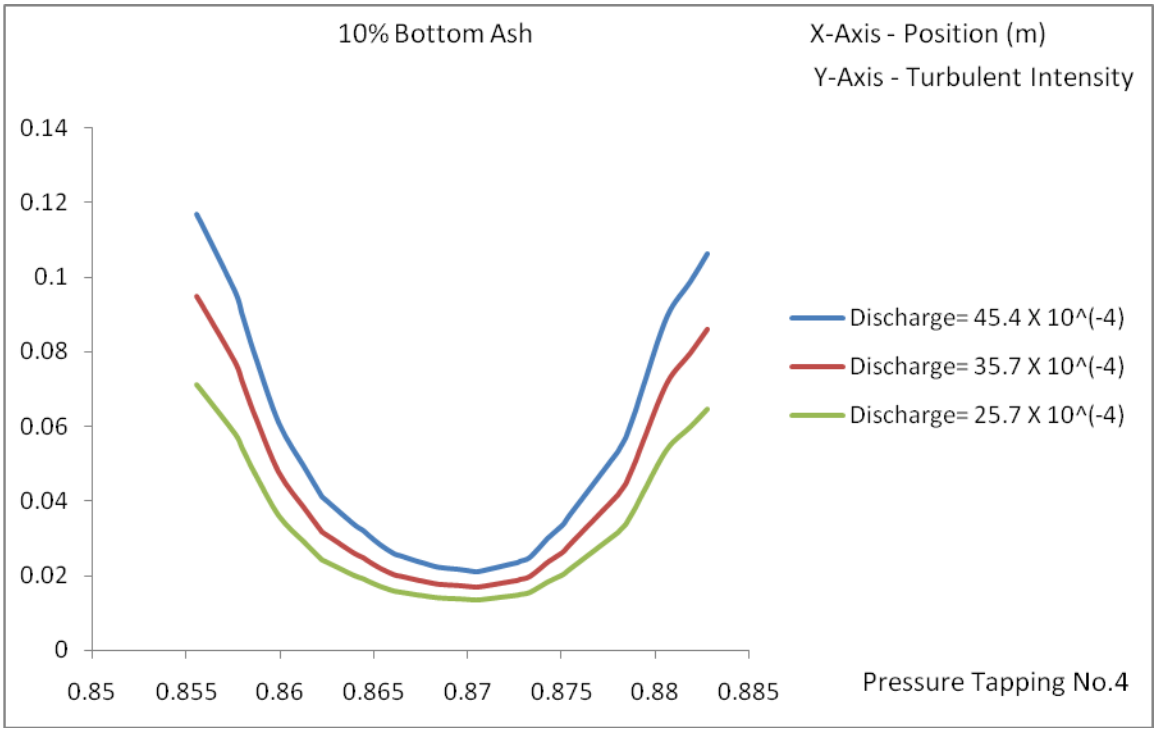

Figure No.6.15 (b): Turbulent intensity at pressure tapping no.4 for different discharges with 10% bottom ash

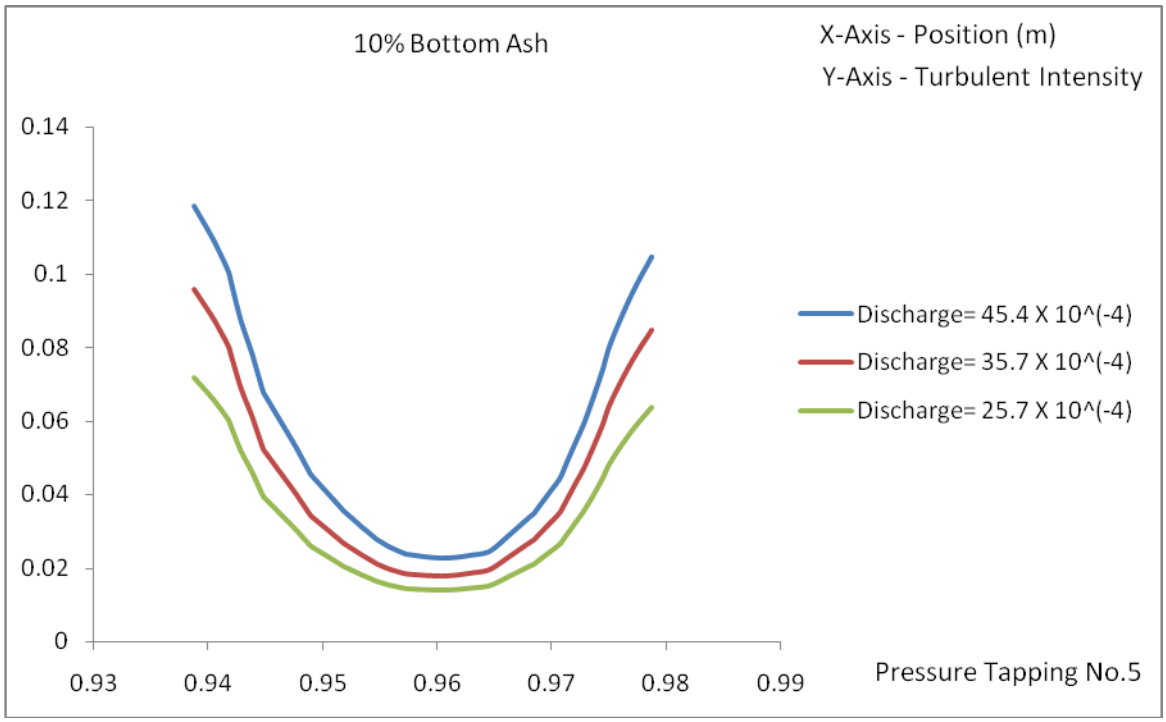

Figure No.6.15 (c): Turbulent intensity at pressure tapping no.5 for different discharges with 10% bottom ash

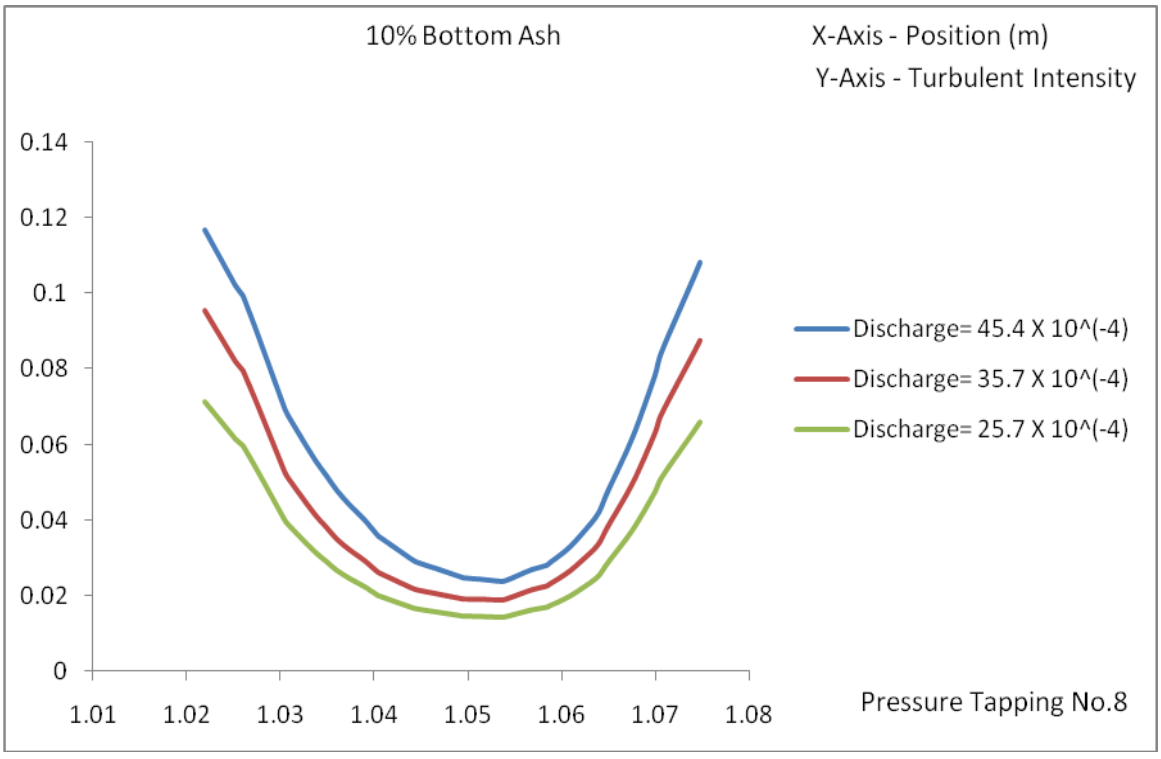

Figure No.6.15 (d): Turbulent intensity at pressure tapping no.8 for different discharges with 10% bottom ash

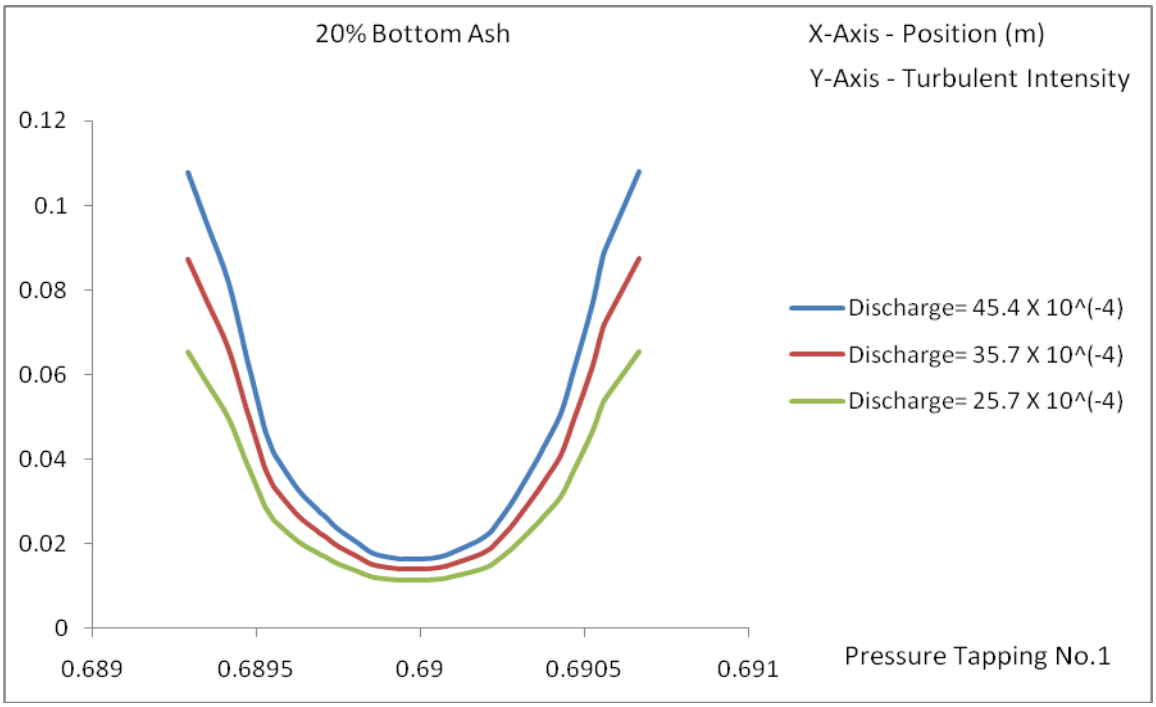

Figure No.6.16 (a): Turbulent intensity at pressure tapping no.1 for different discharges with 20% bottom ash

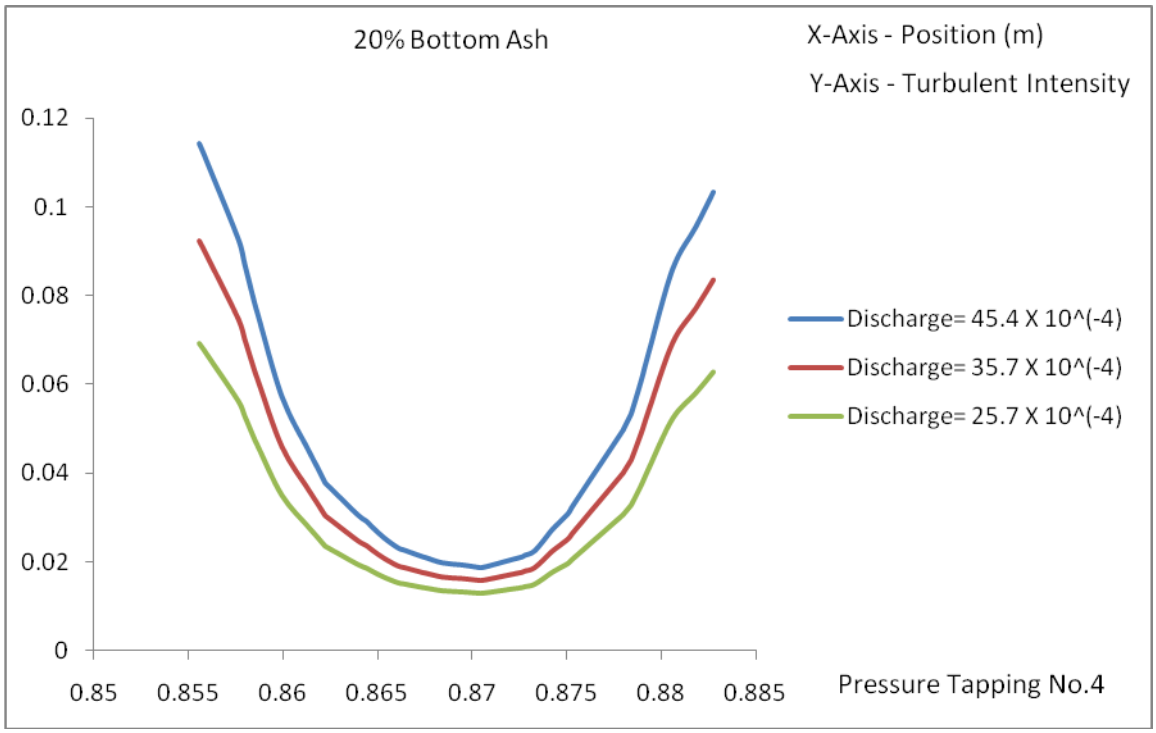

Figure No.6.16 (b): Turbulent intensity at pressure tapping no.4 for different discharges with 20% bottom ash

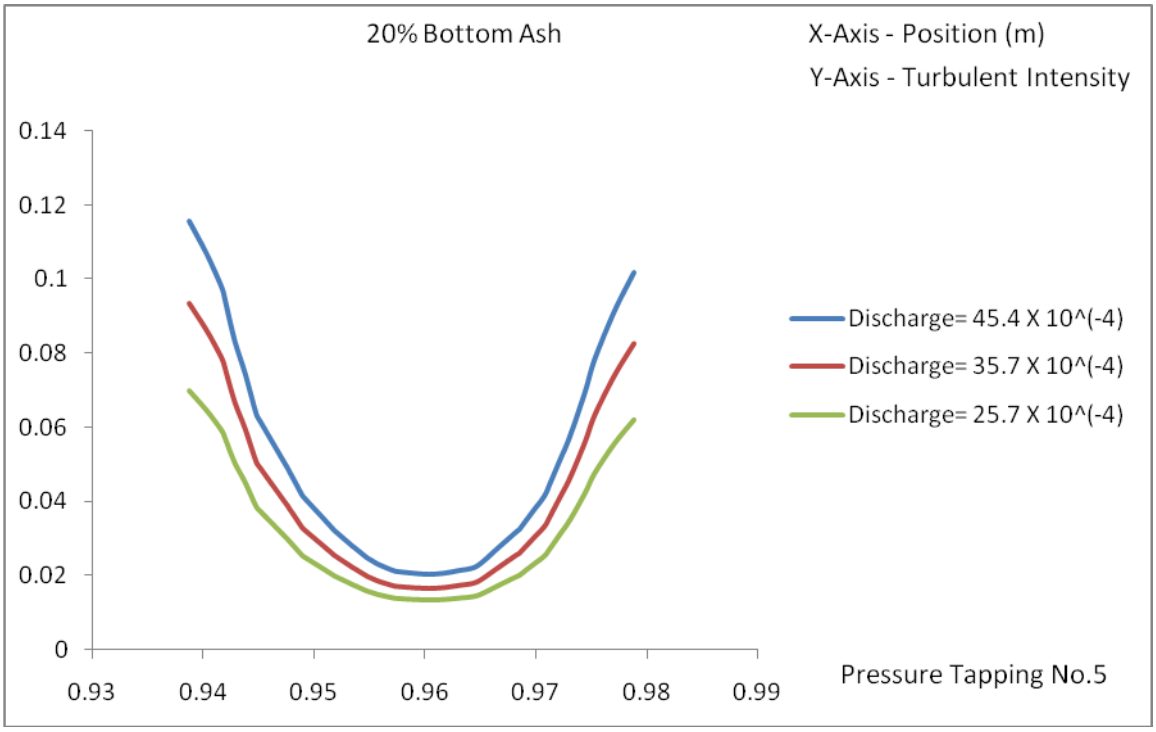

Figure No.6.16 (c): Turbulent intensity at pressure tapping no.5 for different discharges with 20% bottom ash

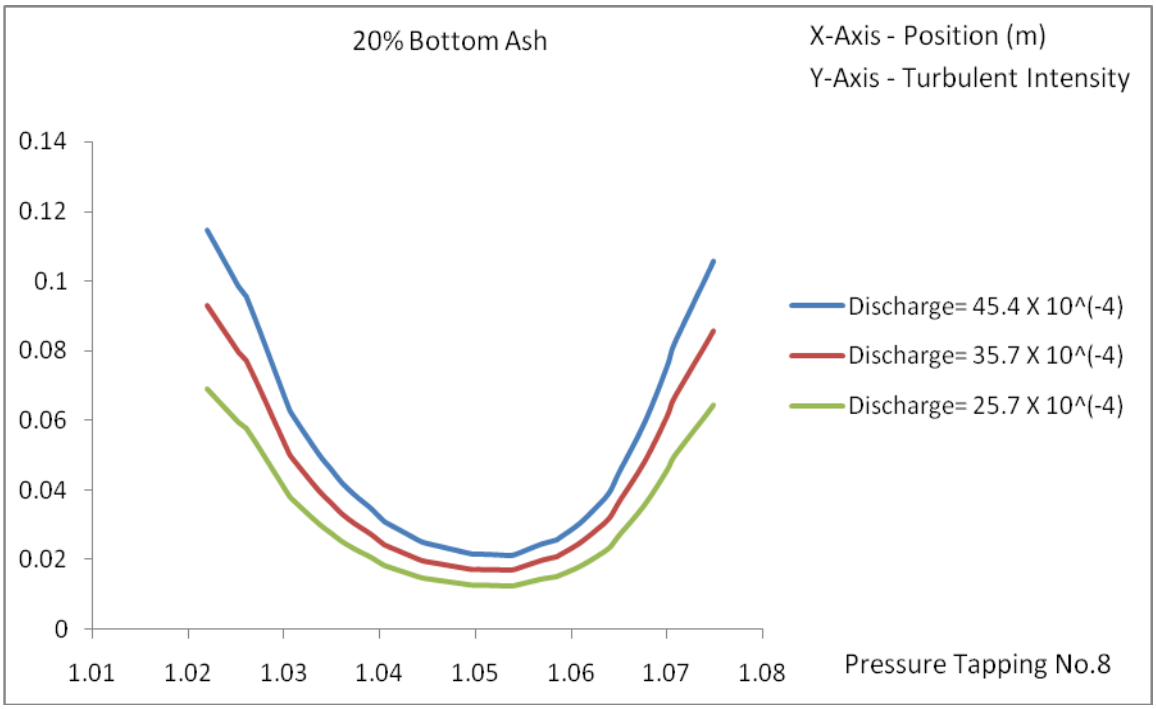

Figure No.6.16 (d): Turbulent intensity at pressure tapping no.8 for different discharges with 20% bottom ash

Pressure across the conventional bend increases with the increase in concentration of bottom ash. Figure No.6.17 shows the pressure variation for different concentrations of bottom ash and water. For all solid concentrations the pressure drop is always more than that for the single-phase water flow. The rate of pressure drop is being higher at higher slurry concentrations. This can be attributed to the change in the rheological characteristics of the slurries with efflux concentration, and the density and viscosity of the slurries also increase with increase in the efflux concentration. Figure No.6.18 shows the velocity variation for different concentrations of bottom ash and water. Pressure drop across the conventional bend is a function of flow velocity. It is observed that the pressure drop increases with increase in the flow velocity for given solid concentration. For any concentration, the rate of increase of pressure drop is higher at higher velocities. It is further seen that the pressure drop across the bend at a given flow velocity increases with increasing slurry concentrations of bottom ash. At higher concentration, there is significant increase in pressure drop even at low velocities, which could be attributed to increase in viscosity of the slurry. Figure No.6.19 shows the turbulent dissipation rate variation for different concentrations of bottom ash and water. From these figures it can also be concluded that there is no turbulent dissipation rate at the centre but at boundary dissipation rate increases with the increase in discharge and reduces with increase in concentration. Figure No.6.20 shows the turbulent intensity variation for different concentrations of bottom ash and water. It is found that the turbulence intensity is maximum at the boundary of pipe but minimum at the center of the pipe and small reduction with the increase in concentration.

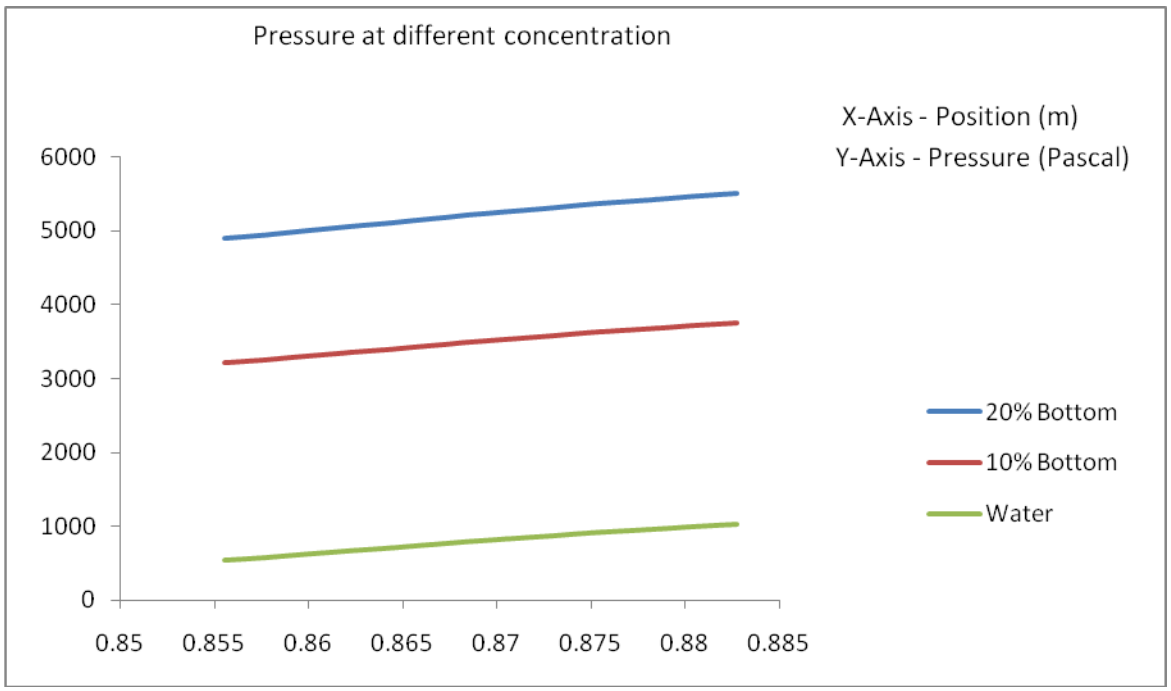

Figure No.6.17: Pressure variation at pressure tapping no.4 for different concentrations of bottom ash and water

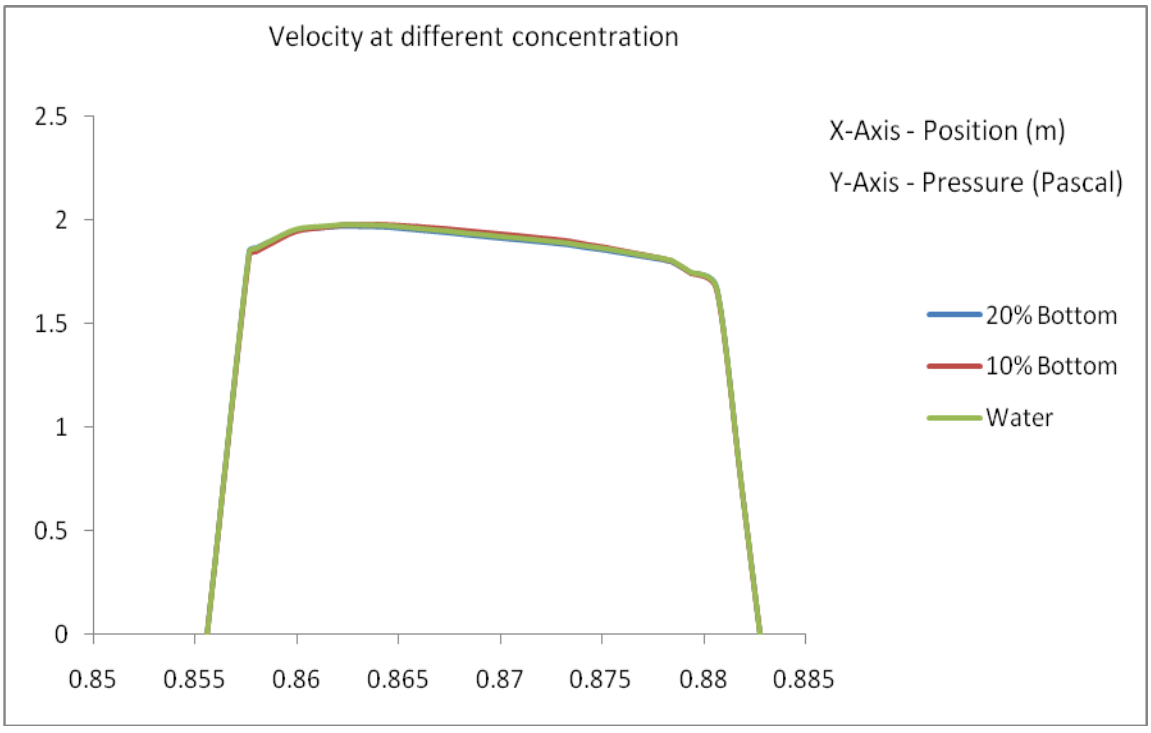

Figure No.6.18: Velocity variation at pressure tapping no.4 for different concentrations of bottom ash and water

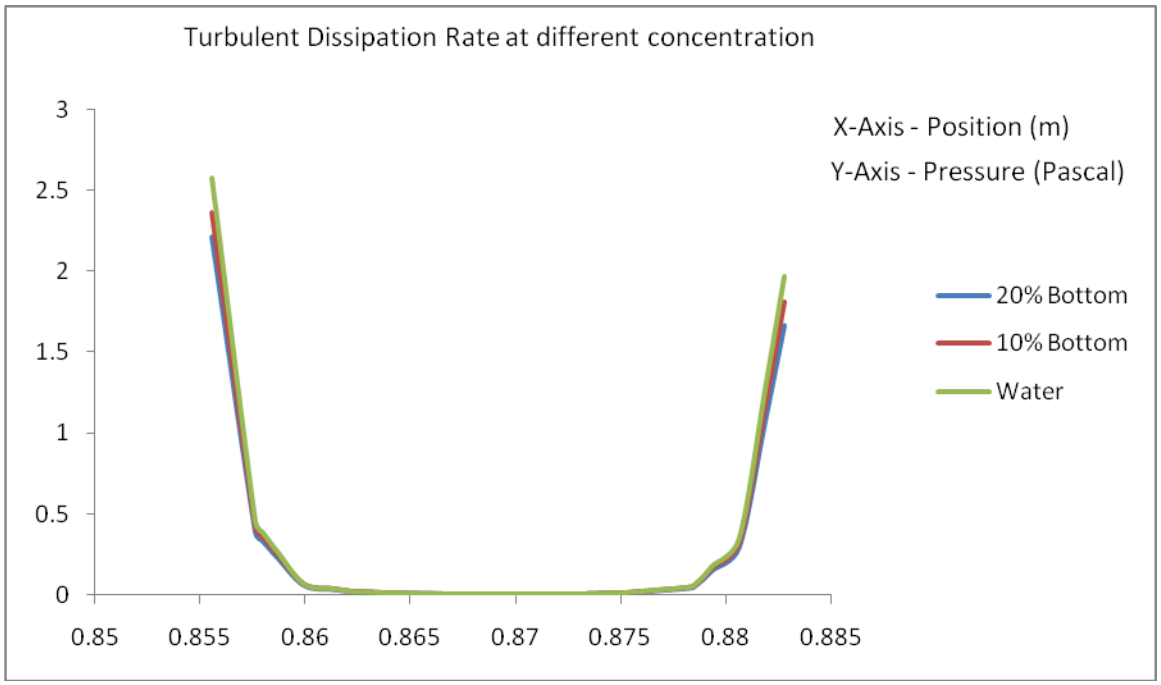

Figure No.6.19: Turbulent dissipation rate variation at pressure tapping no.4 for different concentrations of bottom ash and water

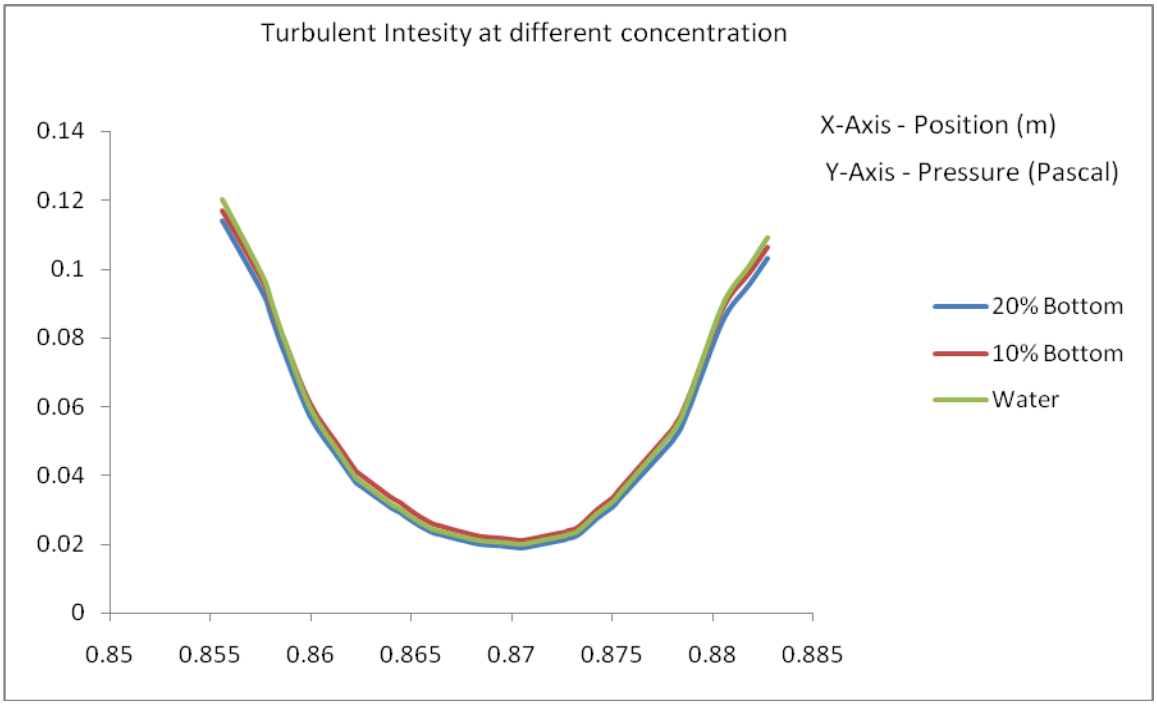

Figure No.6.20: Turbulent intensity variation at pressure tapping no.4 for different concentrations of bottom ash and water

6.2 EROSION WEAR STUDY OF SLURRY PIPELINE

Mild steel is taken for study the erosion wear of pipe material. The test is conducted for 1hour with readings taken after every 15 min interval. The contribution of mass flow rate and impact angle in erosion of mild steel is evaluated. To evaluate the erosion wear of mild steel first mild steel is cut into the size of 50mm X 45mm. Mild steel specimen is cleaned with acetone after finishing it with sand paper. Specimen is weighted before and after the experiment which is explained in chapter 3 to calculate the weight loss in given time period at different angles for different mass flow rates. Microscopic view of mild steel with lica microscope (100 X) before and after erosion is shown in figure no.6.21 (a) & (b)

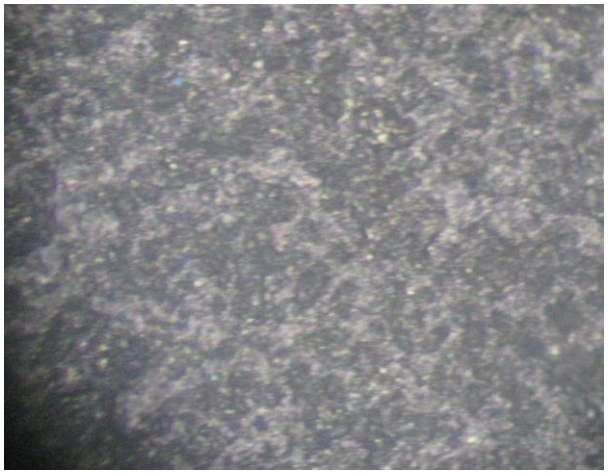

Figure no.6.21 (a): Mild steel before the erosion

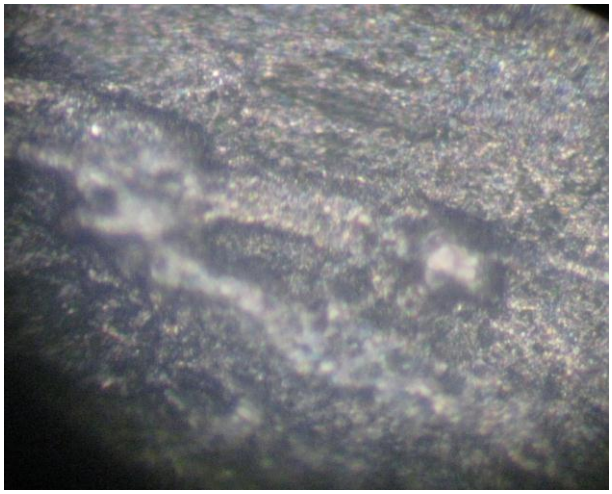

Figure no.6.21 (a): Mild steel after the erosion

6.2.1 Effect of mass flow rate

Erosion wear rate is calculated at different mass flow rates by taking the constant other parameters as well according to the design used for experiment. The effect of mass flow rate is evaluated and shown in figure no.6.22

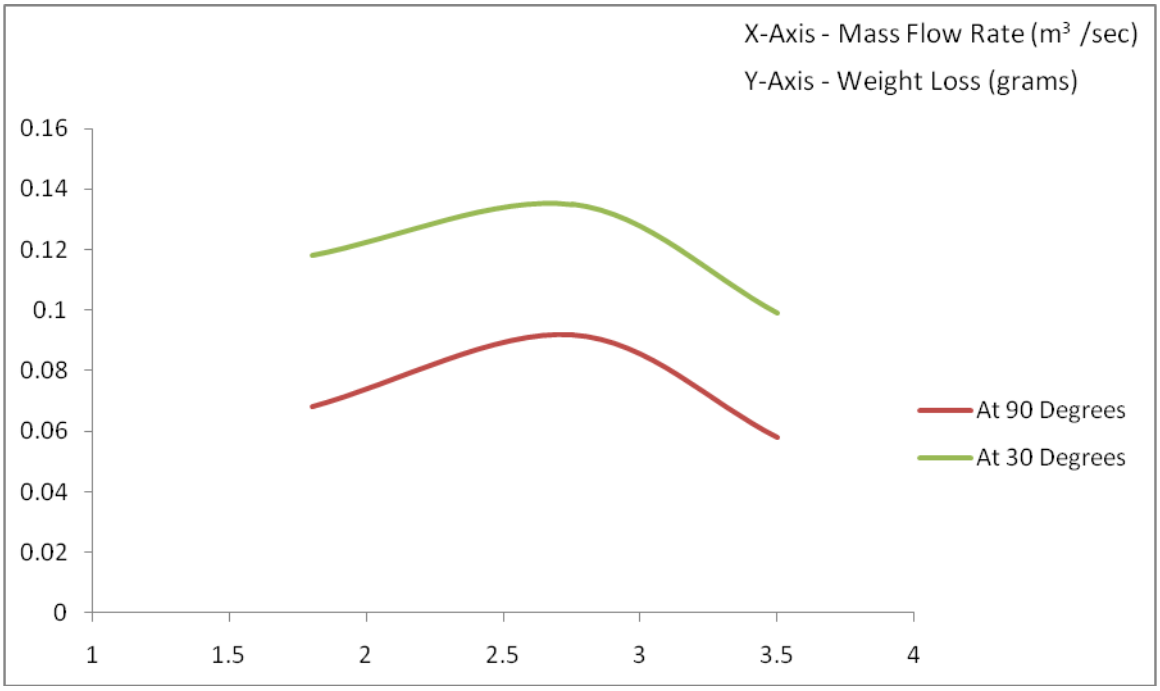

Figure No.6.22: Weight loss at different mass flow rates

It is found that the increase in mass flow rate the loss of material increases. With the increase in mass flow rate velocity increases, the kinetic energy of particles increases and thus more energy is available for the removal of material. It is also found that the increase in weight loss with the increase of mass flow rate from 1.8 m^3 /sec to 2.75 m^3 /sec is much more propound than the change in mass flow rate to 3.5 m^3 /sec. This could be due to the fact that as the mass flow rate increases, particles rebounding back will also have more rebound velocity due to which more particles move out from their path without striking the target.

6.2.2 Effect of impact angle

The study of the effect of the impact angle on the erosion is done in order to know the effect of different angles on to the erosion of mild steel. For ideal case the jet strikes the plain surface

have some impact angle as is of nozzle to specimen. Figure No.6.23 (a), (b) & (c) shows the effect of impact angle on the mild steel.

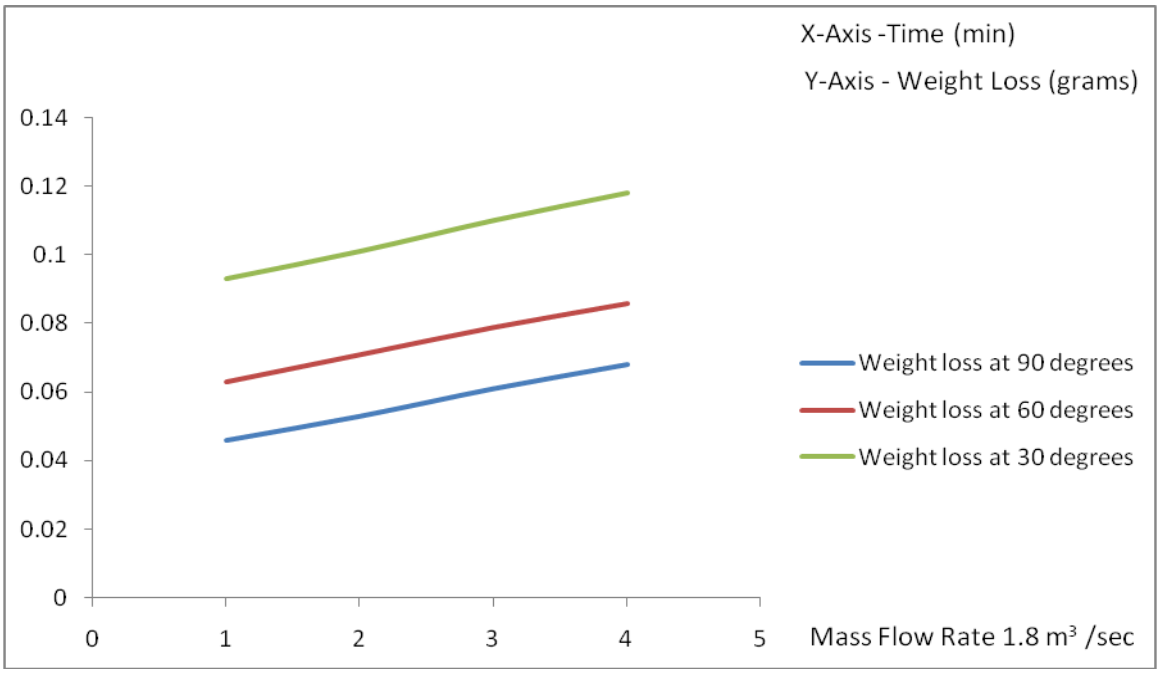

Figure No.6.23 (a): Weight loss at different angles at 1.8 m^3 /sec mass flow rate

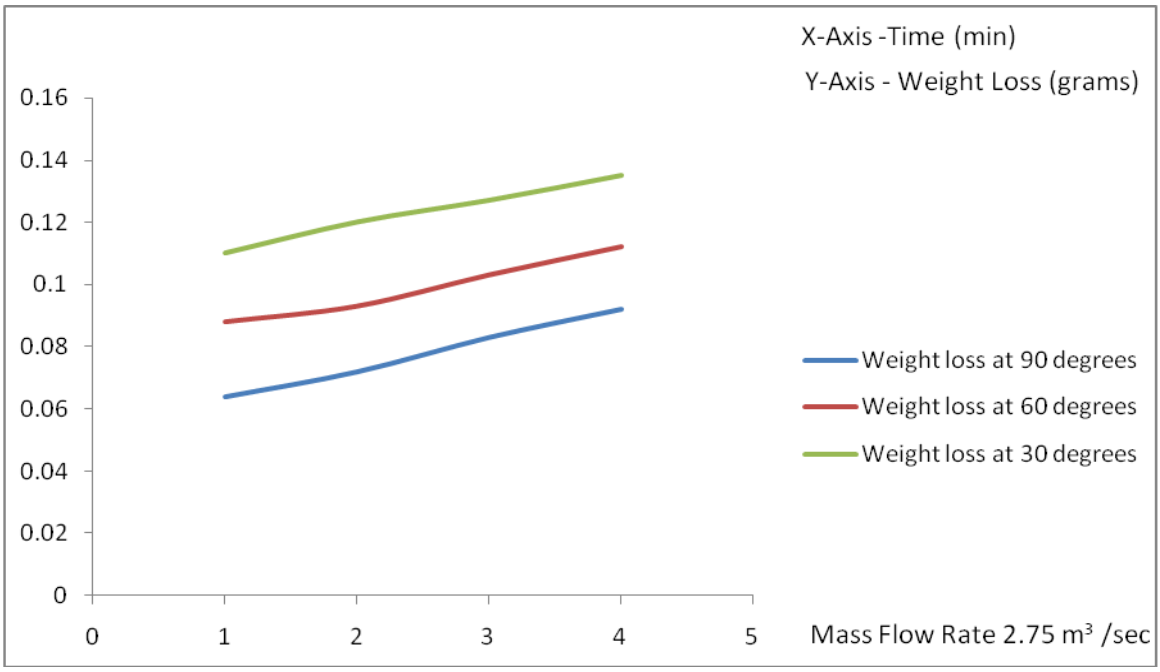

Figure No.6.23 (b): Weight loss at different angles at 2.75 m^3 /sec mass flow rate

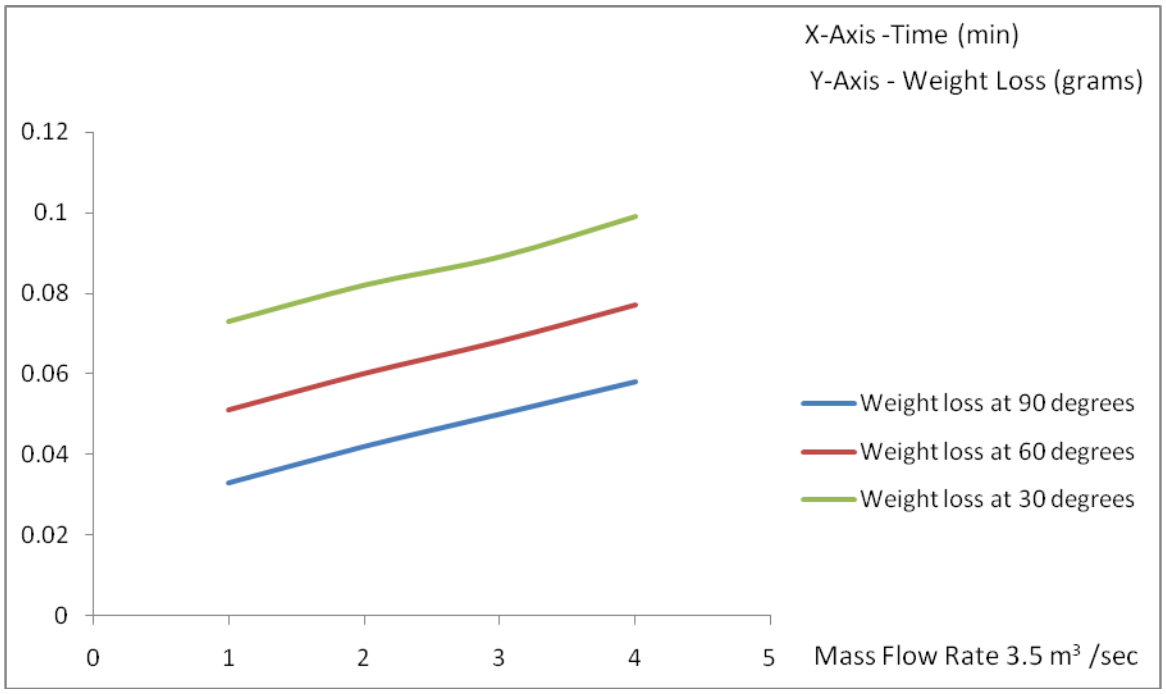

Figure No.6.23 (c): Weight loss at different angles at 3.5 m^3 /sec mass flow rate

The maximum erosion occurs at 30^0 angles and least amount at 90^0. The higher erosion at 30^0 angles shows ductile mode of failure responsible for the erosion of mild steel.

CHAPTER 7

CONCLUSIONS AND FUTURE SCOPE

CONCLUSION

The Pressure drop of the pipe bend is evaluated experimentally handling clear water. Also present work includes, study the properties of bottom ash like particle size distribution, ph value, static settled concentration, specific gravity and viscosity of bottom ash. It also includes the numerical simulation of flow through pipe bend handling 10% and 20 % (by weight) concentrated bottom ash slurry. The simulation results are obtained with different mass flow rates conditions.Based on the present investigation the following conclusions can be obtained

- The pressure drop in bends increases with the increases slurry concentration at constant mass flow rate condition.
- The pressure drop across the pipe bends increases with increase in flow velocity at given solid concentrations.
- The pressure at the outer wall is greater as compared to inner wall of the pipe bend curvature.
- FLUENT results give the good agreement with experimental results for pressure drop in pipe bend for water and different slurry concentrations of bottom ash.

Mild steel is taken for study of erosion wear as a pipe material with different impact angle and mass flow rate conditions. Based on the experimental results following conclusions are observed:

- Erosion wear rate is a function of mass flow rate.
- Erosion wear rate is maximum at 30 degree impact angle conditions and minimum at 90 degree.

FUTURE SCOPE

- The erosion wear studies can be performed with and without coatings of different materials.
- The computational approach can be used to simulate the similar work with different operating conditions.
- The effect of erosion wear of pump impeller and hydro turbine blade can be studied.

References:

1. Ahmad M, Singh S.N. and Seshadri V, (1994), "**Pressure drop in a long radius 90 degree horizontal bend for the flow of multi-sized heterogeneous slurries**", International Journal of Multiphase Flow, Vol. 21, pp 329-334.
2. Gupta R, Singh S.N and Seshadri V, (1994), "**Migration of solid particles in the heterogeneous slurry flow through a 90 degree bend**", Indian Journal of Engineering and Material Science, Vol. 4, pp. 10-20.
3. Parida A, Panda D, Mishra R.N, Senapati P.K, and Murty J.S, (1996), "**Hydraulic transportation of fly ash at higher concentration**", Ash Ponds and Ash Disposal Systems, eds, Vol 28, pp. 17-28.
4. Mishra R, Singh S.N. and Seshadri V, (1998), "**Pressure drop across conventional and diverging-converging pipe bends in the flow of multi-sized particulate slurries**", Indian Journal of Engineering and Material Science, Vol. 5, pp. 9-14.
5. Kaushal D.R. and Tomita Y, (2002), "**Solids concentration profiles and pressure drop in pipeline flow of multisized particulate slurries**", International Journal Multiphase Flow, Vol 28, pp. 1697-1717.
6. Kaushal D.R and Tomita Y, (2002), **"Solids concentration profiles and pressure drop in pipeline flow of multisized particulate slurries",** International Journal of Multiphase Flow, Vol 28, pp 1697–1717.
7. Lei L, Hiroshi S, and Hiromoto U (2002), **"The pipeline transportation of dense fly ash – water slurry",** International Journal of Coal Preparation and Utilization, Vol 22, pp 65-80.
8. Kaushal D.R. and Tomita Y, (2003), **"Comparative study of pressure drop in multisized particulate slurry flow through pipe and rectangular duct"**, International Journal of Multiphase Flow, Vol 29, pp 1473–1487.
9. Kaushal D.R., Sato K, Toyota T, Funatsu K, and Tomita Y, (2005), **"Effect of particle size distribution on pressure drop and concentration profile in pipeline flow of highly concentrated slurry"**, International Journal of Multiphase Flow, Vol 31, pp 809–823.
10. Kaushal D.R., Tomita Y, (2006), **"Experimental investigation for near-wall lift of coarser particles in slurry pipeline using γ-ray densitometer"**, Powder Technology, Vol 172, pp 177–187.

11. Cartigny M.J.B, Talmon A.M., Delfos R, Vlasblom W.J and Rosenbrand W.F, (2007), **"On the relation between hydraulic losses due to bends and mixture stratification".**

12. Knezevic D, (2008), **"The influence of ash concentration on change of flow and pressure in slurry transportation",** International Journal of Mining and Mineral Engineering, Vol 1, pp. 104-112.

13. Lahiri S.K. and. Ghanta K.C, (2008), "**Prediction of Pressure Drop of Slurry Flow in Pipeline by Hybrid Support Vector Regression and Genetic Algorithm Model",** Chinese Journal of Chemical Engineering, Vol 16, pp 841-848.

14. Ni (1996) **"The effect of high delivered volumetric concentration (c_{vd}) on characteristics of slurry" Department Of chemical science and technology, Kobe university, Japan".**

15. Clark H. McI., and Llewellyn R.J., (2001), "**Assessment of the erosion resistance of steels used for slurry handling and transport in mineral processing applications**" International Conference on Wear of Materials, Vol 250, pp 32-44.

16. Clark H. McI. (2002), "**Particle velocity and size effects in laboratory slurry erosion measurements or do you know what your particles are doing**", Tribology International, Vol 35, pp 617–624

17. Ghanta K.C. and Purohit N.K, (2002), "**Effect of Particle Size Distribution (PSD) on the Viscosity of Suspension of bi-dispersed Particles**", Proc. Hydrotransport 15, BHR Group, Fluid Engineering, Cranfield, Bedfor, England, pp. 299-313.

18. Heywood N. I, (2002), "**A Review of Techniques For Reducing Energy Consumption in Slurry Pipelines**", Proc. Hydrotransport 10, BHRA Fluid Engineering Cranfield, Bedford, England, Paper K3, pp. 319-331.

19. Korving A.C., (2002), "**High concentration fine sand slurry flow in pipelines: experimental study**", Proceeding Hydrotansport 15, BHR Group, Cranfield, Bedford, England, pp. 769-776.

20. Kumar U., Singh S.N. and Seshadri V., (2002), "**Concentration Distribution Downstream of a Bend in the Flow of Equi-Sized Particulate Slurries in Pipeline**", Hydrotransport 15, BHR group, Cranefield, Bedford, England, pp. 469-476.

21. Rudman M., Graham L.J., Blackburn H.M. and Pullum L., (2002), "**Non-Newtonian turbulent and transitional pipe flow**", Proc. Hydrotansport 15, BHR Group, Cranfield, Bedford, England, pp. 271-286.

22. Clark H.McI., (2004), "**The influence of the squeeze film in slurry erosion**", Journal of Wear, Vol 256, pp 918–926.

23. Eskin D, Leonenko Y and Vinogradov O, (2004), "**On a turbulence model for slurry flow in pipelines",** Chemical Engineering Science, Vol 59, pp 557 – 565.

24. Gandhi B K., Borse Satish V., (2004), "**Nominal particle size of multi-sized particulate slurries for evaluation of erosion wear and effect of fine particles**", Journal of Wear, Vol 257, pp 73-79.

25. Wood R.J.K, Jones T.F, Ganeshalingam J, Miles N.J, (2004), "**Comparison of predicted and experimental erosion estimates in slurry ducts**", Journal of Wear, Vol 256, pp 937-947.

26. Badr H.M., Habib M.A., Ben-Mansour R., Said S.A.M., (2005), "**Numerical investigation of erosion threshold velocity in a pipe with sudden contraction**"**,** Sam pergamon-elsevier science ltd, computers fluids, Vol 34, pp 721-742.

27. Das S.K, Godiwalia K.M, Mehrotra S P, Sastry K.K.M and Dey P.K, (2006), "**Analytical model for erosion behaviour of impacted fly-ash particles on coal-fired boiler components**", Sadhana, Vol 31, pp 583–595.

28. Desale G.R, Gandhi B.K, Jain S.C, (2007), "**Slurry erosion of ductile materials under normal impact condition**", Journal of Wear, Vol 264, pp 322–330.

29. Habib M.A, Badr H.M, Ben-Mansour R, Kabir M.E, (2007) "**Erosion rate correlations of a pipe protruded in an abrupt pipe contraction**", International journal of impact engineering, Vol 34, pp 1350-1369.

30. Huang C, Minev P, Luo J, Nandakumar K, (2008), "**A phenomenological model for erosion of material in a horizontal slurry pipeline flow**" Journal of Wear, Vol 269, pp 190-196.

31. Giguère R, Fradette L, Mignon D, Tanguy P.A, (2009), "**Analysis of slurry flow regimes downstream of a pipe bend**" Chemical Engineering Research and Design Vol 87, pp 943-950.

32. Steward N.R and Slatter P, (2009), " **The pipe flow behavior of fly ash and water mixtures in a closed loop pipe system at solids concentrations ranging from 51% to 74% by mass, in three different pipe sizes, 40, 50 and 65 nominal bore",** Australian Bulk Handling Review, Vol 4, pp 1-8.

33. Tian H.H, Addie G.R, Visintainer R.J, (2009), "**Erosion–corrosion performance of high-Cr cast iron alloys in flowing liquid–solid slurries**" Journal of Wear Vol 267, pp 2039-2047.

34. Shah S.N, and Jain S, (2007), "**Coiled tubing erosion during hydraulic fracturing slurry flow**", Journal of Wear, Vol 264 , pp 279–290.

35. Kumar A, Kaushal D.R, and Kumar U, (2008), **"Bend pressure drop experiments compared with fluent"**, Proceedings of the Institution of Civil Engineers, Engineering and Computational Mechanics, Vol 161, pp 35–42.

36. Lahiri S.K and Ghanta K.C, (2008)," **Computational Fluid Dynamics Simulation of the Solid Liquid Slurry Flow in a Pipeline",** Chemcon, http://works.bepress.com/sandip_lahiri/14.

37. L.J.W. Graham, D. Lester and J. Wu, (2009), **"Slurry erosion in complex flows: Experiment and CFD"**, CSIRO Materials Science and Engineering, Highett, Victoria 3190, Seventh International Conference on CFD in the Minerals and Process Industries, pp 1-6.